LIÈGE université
Gembloux
Agro-Bio Tech

PONTIFICIA
UNIVERSIDAD
CATÓLICA DE
VALPARAÍSO

UNIVERSIDAD TECNICA
FEDERICO SANTA MARIA

Development of a production strategy based on the modification of metabolic regulation processes in *Komagataella phaffii.*

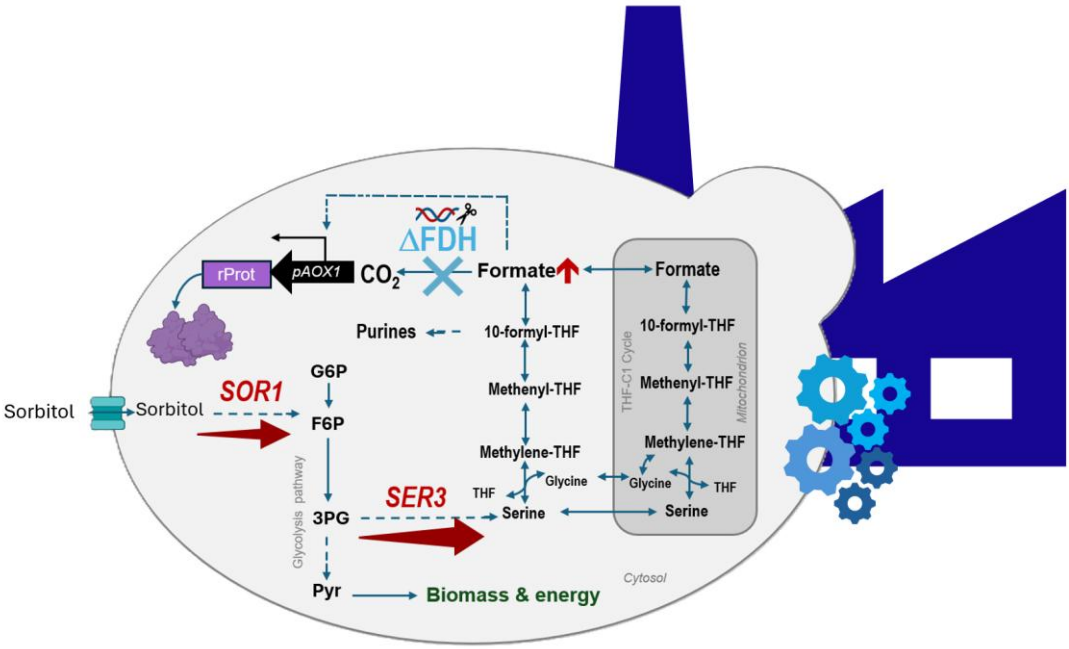

Author: Rocío Celeste Cozmar Quezada

Supervisors: Prof. Patrick FICKERS and Prof. Dr. Julio BERRÍOS.

Year 2026

CONSTANCIA DE VALIDACIÓN Y CONFIDENCIALIDAD DE MONOGRAFÍA A REPOSITORIO ACADÉMICO

1.- IDENTIFICACIÓN DEL TRABAJO ACADÉMICO

Tipo de monografía (marcar una opción): ☐ Memoria o trabajo de título ☒ Tesis de Postgrado

Título del trabajo: Development of a production strategy based on the modification of metabolic regulation processes in *Komagataella phaffii*

Nombre del candidato(a): Rocio Celeste Cozmar Quezada

Carrera / Grado: Doctorado en Biotecnología

Campus: Valparaíso **Departamento:** Tesis desarrollada en el programa doctorado en Biotecnología PUCV-USM en la escuela de ingeniería bioquímica PUCV en modalidad cotutela con la ULiege.

2.- VALIDACIÓN DEL PROFESOR GUÍA/DIRECTOR DE TESIS

Yo, Julio Andrés Berríos Araya, en mi calidad de profesor(a) guía/director(a) del trabajo académico mencionado anteriormente **DEJO CONSTANCIA** que:

- He revisado esta versión del documento y corresponde a la versión final aprobada del trabajo.
- El trabajo cumple con los requisitos académicos y de formato establecidos por la institución.

3.- EVALUACIÓN DE CONFIDENCIALIDAD POR PROPIEDAD INDUSTRIAL (marcar una opción)

☒ El trabajo **NO contiene** información que amerite confidencialidad y puede ser publicado de inmediato en repositorio con acceso abierto.

☐ El trabajo **CONTIENE** información con potenciales implicancias de propiedad industrial o intelectual y requiere un periodo de confidencialidad (**embargo**) por **(marcar una opción)**:

☐ 6 meses ☐ 12 meses ☐ 2 años ☐ 3 años ☐ 5 años ☐ 10 años

Fundamentación de la necesidad de confidencialidad (obligatorio si se solicita embargo):

4.- FIRMAS

Profesor(a) guía o director(a) de memoria o tesis:

Fecha: 03.08.2026 **Firma:** _____

Estudiante o Candidato(a):

Fecha:03.08.2026 **Firma:** _____

Este formulario debe ser insertado como página 2 de la memoria o tesis, completado y firmado por estudiante y profesor(a) antes de la entrega en portal PRISMA de Biblioteca USM.

COMMUNAUTÉ FRANÇAISE DE BELGIQUE
UNIVERSITÉ DE LIÈGE – GEMBLOUX AGRO-BIO TECH
PONTIFICIA UNIVERSIDAD CATÓLICA DE VALPARAÍSO
UNIVERSIDAD TÉCNICA FEDERICO SANTA MARÍA

Development of a production strategy based on the modification of metabolic regulation processes in *Komagataella phaffii.*

Rocío Celeste COZMAR QUEZADA

Dissertation submitted in fulfillment of the requirements for the degree of Doctor of Philosophy in Agronomic Sciences and Biological Engineering - University of Liège
&
Doctor in Biotechnology – PUCV-UTFSM

Supervisors: Prof. Dr. Patrick FICKERS and Prof. Dr. Julio BERRIOS

Year: 2026

Abstract

Rocío Celeste Cozmar Quezada (2026). "Development of a production strategy based on the modification of metabolic regulation processes in *Komagataella phaffii*" (PhD dissertation in English). Gembloux, Belgium, Gembloux Agro-Bio Tech, University of Liege. 183 pages, 54 figures, 22 tables.

Komagataella phaffii is one of the most widely used yeast cell factories for recombinant protein (rProt) production in the industry. Its success has been largely attributed to the strong alcohol oxidase 1 promoter (p*AOX1*), which is traditionally induced by methanol. However, the toxicity and handling constraints of methanol limit its industrial applicability. Recently, formate dehydrogenase (FDH) deficient strain of *K. phaffii* has been reported that formate as a key metabolite for p*AOX1* induction in sorbitol media. This doctoral research has been focused on developing methanol-free induction strategies for p*AOX1* in this FDH-deficient strain, to improve rProt production.

These results showed that sorbitol dehydrogenase (*SOR1*) overexpression gene, based on the slow sorbitol uptake limitation, enhanced sorbitol metabolism and growth rate. However, it also decreased intracellular formate accumulation, a key metabolite involved in p*AOX1* induction in this strain. Thereby, this effect reduced p*AOX1* induction and the synthesis of model rProt, such as enhanced green fluorescent protein (eGFP) and *Candida antarctica* lipase (CalB). Oxygen transfer conditions (OTC) were also found to play a critical role in p*AOX1* regulation, formate accumulation, and increased eGFP production.

Furthermore, engineering of the L-serine biosynthesis pathway through overexpression of 3-phosphoglycerate dehydrogenase (*SER3*) gene, based on previous results obtained in serine-sorbitol media, enhanced intracellular formate levels and improved the balance between growth and rProt production, SER3 strains exhibited up to 48% higher specific eGFP fluorescence and 30% higher glucose oxidase (Gox) activity compared to the parental strain. These findings highlight serine metabolism as a potential contributor to the link between central carbon metabolism and p*AOX1* induction.

In addition, signal peptide engineering was investigated as an independent approach to improve recombinant protein secretion efficiency based on different composition of pre- and pro-regions of signal peptides (SPs) of *Yarrowia lipolytica*. Yps3Pre-Lip2Pro construct yielded the highest laccase activity, highlighting the importance of secretion signal composition and design in overall rProt production performance and secretion efficiency.

These findings expand current knowledge on the molecular mechanisms underlying *pAOX1* activation and provide a foundation for designing safer, more sustainable, and efficient recombinant protein production systems in *K. phaffii*.

Keywords: *Komagataella phaffii*, recombinant proteins, *AOX1* promoter, methanol, formate, sorbitol dehydrogenase, sorbitol, oxygen transfer conditions, serine, 3-phosphoglycerate dehydrogenase, metabolic engineering, signal peptide.

Résumé

Rocío Celeste Cozmar Quezada (2026). "Développement d'une stratégie de production basée sur la modification des processus de régulation métabolique chez *Komagataella phaffii*" » (Thèse de doctorat en anglais). Gembloux, Belgique, Gembloux Agro-Bio Tech, Université de Liège. 183 pages, 54 figures, 22 tableaux.

Komagataella phaffii est l'une des plateformes cellulaires de levure les plus largement utilisées dans l'industrie pour la production de protéines recombinantes (rProt). Son succès est principalement attribué au puissant promoteur de l'alcool oxydase 1 (p*AOX1*), traditionnellement induit par le méthanol. Cependant, la toxicité et les contraintes de manipulation du méthanol limitent son applicabilité industrielle. Récemment, une souche déficiente en formiate déshydrogénase (FDH) de *K. phaffii* a été décrite, utilisant le formiate comme métabolite clé pour l'induction de p*AOX1* en milieu sorbitol. Cette recherche doctorale s'est concentrée sur le développement de stratégies d'induction sans méthanol pour p*AOX1* dans cette souche déficiente en FDH, afin d'améliorer la production de rProt.

Ces résultats ont montré que la surexpression du gène de la sorbitol déshydrogénase (*SOR1*), basée sur la limitation de l'absorption lente du sorbitol, a amélioré le métabolisme du sorbitol et le taux de croissance. Cependant, l'accumulation intracellulaire de formiate, un métabolite clé impliqué dans l'induction de p*AOX1* chez cette souche, a diminué. Par conséquent, cet effet a diminué l'induction de p*AOX1* et la synthèse de protéines recombinantes modèles, telles que la protéine fluorescente verte améliorée (eGFP) et la lipase de Candida antarctica (CalB). Les conditions de transfert d'oxygène (OTC) ont également joué un rôle critique dans la régulation de p*AOX1*, l'accumulation de formiate et l'augmentation de la production d'eGFP. En outre, l'ingénierie de la voie de biosynthèse de la L-sérine via la surexpression du gène de la 3-phosphoglycérate déshydrogénase (*SER3*), basée sur des résultats précédents obtenus en milieu sérine-sorbitol, a augmenté les niveaux intracellulaires de formiate et amélioré l'équilibre entre croissance et production de rProt. Les souches SER3 ont présenté jusqu'à 48 % de fluorescence spécifique d'eGFP en plus et 30 % d'activité supplémentaire de glucose oxydase (Gox) par rapport à la souche parentale. Ces résultats mettent en évidence le rôle du métabolisme de la sérine comme facteur susceptible de contribuer au lien entre le métabolisme central du carbone et l'induction de p*AOX1*. De plus, la modification des peptides signaux a été étudiée comme stratégie indépendante visant à améliorer l'efficacité de la sécrétion des protéines recombinantes en fonction de leurs compositions des régions pré et pro des peptides signal (SPs) de *Yarrowia lipolytica*. Le construct Yps3Pre-Lip2Pro a présenté la plus forte activité de laccase, soulignant l'importance de la composition et de la conception des signaux de sécrétion dans la performance globale de production de rProt et l'efficacité de sécrétion. Ces résultats élargissent les connaissances actuelles sur les mécanismes moléculaires sous-jacents à l'activation de p*AOX1* et fournissent une base pour concevoir des systèmes de production de protéines recombinantes plus sûrs, plus durables et plus efficaces chez *K. phaffii.*

Mots-clés : *Komagataella phaffii*, Protéines recombinantes, Promoteur *AOX1*, Méthanol, Formate, Sorbitol déshydrogénase, Sorbitol, conditions de transfert d'oxygène, Sérine, 3-phosphoglycérate déshydrogénase, ingénieure métabolique, peptides signal.

Resumen

Rocío Celeste Cozmar Quezada (2026). "Desarrollo de una estrategia de producción basada en la modificación de los procesos de regulación metabólica en *Komagataella phaffii*" (Tesis doctoral en inglés). Gembloux, Bélgica, Gembloux Agro-Bio Tech, Universidad de Lieja. 183 páginas, 54 figuras, 22 tablas.

Komagataella phaffii es una de las fábricas celulares de levadura más utilizadas en la industria para la producción de proteínas recombinantes (rProt). Su éxito se ha atribuido en gran medida al fuerte promotor alcohol oxidasa 1 (p*AOX1*), que tradicionalmente se induce con metanol. Sin embargo, la toxicidad y las limitaciones de manejo del metanol restringen su aplicabilidad industrial. Recientemente, se ha descrito una cepa deficiente en formiato deshidrogenasa (FDH) de *K. phaffii* que utiliza el formiato como metabolito clave para la inducción de p*AOX1* en medios con sorbitol. Esta investigación doctoral se ha centrado en el desarrollo de estrategias de inducción libres de metanol para p*AOX1* en esta cepa deficiente en FDH, con el objetivo de mejorar la producción de rProt.

Estos resultados mostraron que la sobreexpresión del gen de sorbitol deshidrogenasa (*SOR1*), basada en la limitación de la captación lenta de sorbitol, aumentó el metabolismo del sorbitol y la tasa de crecimiento. Sin embargo, disminuyó la acumulación intracelular de formiato, que es un metabolito clave relacionado con la inducción de p*AOX1* en esta cepa. En consecuencia, este efecto redujo la inducción de p*AOX1* y la síntesis de proteínas recombinantes modelo, como la proteína fluorescente verde mejorada (eGFP) y la lipasa de Candida antarctica (CalB). También se observó que las condiciones de transferencia de oxígeno (OTC) desempeñan un papel crítico en la regulación de p*AOX1*, la acumulación de formiato y el aumento de la producción de eGFP. Por otra parte, la ingeniería de la vía de biosíntesis de L-serina mediante la sobreexpresión del gen de la 3-fosfoglicerato deshidrogenasa (*SER3*), basada en resultados previos obtenidos en medios serina-sorbitol, aumentó los niveles intracelulares de formiato y mejoró el equilibrio entre crecimiento y producción de rProt. Las cepas SER3 mostraron hasta un 48% más de fluorescencia específica de eGFP y un 30% más de actividad de glucosa oxidasa (Gox) en comparación con la cepa parental. Estos hallazgos Estos hallazgos ponen de relevancia el metabolismo de la serina como posible factor que contribuye a la relación entre el metabolismo central del carbono y la inducción de p*AOX1*. Además, se estudió la ingeniería de péptidos señal como estrategia independiente para mejorar la eficiencia de la secreción de proteínas recombinantes en función de diferentes composiciones de las regiones pre y pro de péptidos señal (SPs) de *Yarrowia lipolytica*. El constructo Yps3Pre-Lip2Pro mostró la mayor actividad de lacasa, destacando la importancia de la composición y el diseño de las señales de secreción en el rendimiento global de producción de rProt y la eficiencia de secreción.

Estos hallazgos amplían el conocimiento actual sobre los mecanismos moleculares subyacentes a la activación de p*AOX1* y proporcionan una base para diseñar sistemas

de producción de proteínas recombinantes más seguros, sostenibles y eficientes en *K. phaffii*.

Palabras clave: *Komagataella phaffii*, Proteínas recombinantes, Promotor *AOX1*, Metanol, Formato, sorbitol deshidrogenasa, Sorbitol, condiciones de transferencia de oxígeno, Serina, 3-fosfoglicerato deshidrogenasa, Ingeniería metabólica, péptidos señal.

Acknowledgements

During my first visit to Europe, through a DAAD exchange scholarship during my training as a Biotechnology Engineer, I consolidated the idea of deepening my knowledge through research. This decision eventually led me to pursue a PhD, bringing me back to these lands ten years later. This journey has been profoundly challenging and transformative. I have learned countless lessons related to professional research tools and the critical thinking required to become an independent researcher, while also experiencing tremendous personal growth. Throughout the development of this research, the guidance I received from Professor Patrick Fickers was fundamental to the successful completion of this project. I would like to express my deepest gratitude to Professor Patrick Fickers for his invaluable support from the moment I arrived at TERRA, for believing in me, providing me with a space to develop and grow as a researcher, and for his unwavering commitment to every aspect of my doctoral project. Today, I am able to present my contribution to the scientific community in the field of yeast research, which would not have been possible without the support of Professor Julio Berrios in Chile. He gave me the opportunity to join his laboratory team and develop my research idea on *Komagataella phaffii* in collaboration with the Yeast Lab at TERRA. I would also like to thank the members of my thesis committee for their support and valuable guidance throughout this process.

This way of doing research has allowed me to meet extraordinary people along the way. I have had the privilege of meeting a member of the Yeast Lab team in Belgium whose impact on my life has been so significant that I believe the lessons I learned from her will stay with me forever. Fate has also granted me the gift of her incredible friendship: Cristina Bustos. I am deeply grateful to you from day one. I learned fundamental lessons by your side, and without you, the story I tell today would be different. Thank you for your advice, teachings, willingness to help, and, above all, your friendship. Vassiliki Korka, thank you for your sense of humor, charisma, and for always being there for us. You are not only a colleague but also a friend, and your valuable friendship has made this journey much more enjoyable. I would like to thank Juan Andrés Martínez for his guidance and for broadening my perspective, which helped me overcome many of the challenges I faced during this thesis. Sebastien Steels, with your support I learned in a short time what would otherwise have taken me months to understand. Your guidance was indispensable as I integrated molecular biology techniques into my work. I would also like to thank Marina Chanet, Marguerite Demi, and Danielle Duballet for their invaluable support, kindness, and constant willingness to help whenever I needed assistance. I am grateful to Samuel Telek for his guidance in my work with parallel bioreactors, and to Romain Thomas for his continuous support and availability in compound analysis and measurements.

Friends are the family we choose, the people with whom we decide to share the limited time we have, supporting one another and making life kinder, especially throughout a process like this. My sincere thanks go to Constance Keller, Andrea Menés, Darlene Duarte, Fabian Rolfs, Franchesco Roppo, Sergio Villareal, Hannah Sehrt, Marta Orero, Celeste Ruiz, Maximilian Sehrt, Tiphaine Gellette, Vincent Vandenbroucke, Aparna Padmanabhan, Sandeep Kumar, Sigrid Gorgen, Andrea Kerezsi, Arpita Chakraborty, and Andrea Chacón. I am also deeply grateful to my friends in Chile, who have been a constant source of support and motivation throughout this journey. I would especially like to thank Nataly Suid, my dear friend, who has always been there to listen and offer advice. Thank you for visiting me; I adore you. I would like to thank my parents, Marcos Cozmar and Ester Rosa Quezada, and my siblings, Nicole Cozmar, Diego Cozmar, and Fernanda Cozmar, who have always encouraged me to keep moving forward. I would also like to thank my lifelong friends who chose to start a new life in Europe and who have remained by my side throughout the years. Thank you, Giovanni Pérez and his wife Liesa Poschke, as well as Franco Pérez. Our friendship has always been strong, but it has grown even stronger in recent years. Thank you for the support you have given me throughout these years, for taking care of me when I was ill, and for making me feel part of a family during moments of vulnerability and emotional hardship. Thank you, my friends.

The invaluable support of my husband, Juan Ferrada, has been fundamental throughout this process. As both of us have been pursuing similar PhD journeys, his understanding and empathy have been essential during this experience, which has come at a significant personal cost for both of us. We have spent long periods physically apart in order to achieve our doctoral goals. Together, we have learned to face these challenges, strengthening our mutual understanding and our relationship more than ever before. Juan Ferrada, thank you for always being by my side. Your faith in me and your unwavering support make me feel that I can achieve anything. I love you. I would like to extend a special thank you to my other family members, Roños (Watito) and Betita, my beloved cats. Although pets are not always considered family members by everyone, they are an important part of my family. They have brought me comfort, companionship, and joy since they came into my life, including throughout my doctoral research journey.

Finally, I would like to thank everyone who has supported me, directly or indirectly, throughout these years, encouraging and guiding me along this path of academic, professional, and personal growth. It took courage to start over, step outside my comfort zone, and continually challenge myself to become a better version of who I am. I am profoundly grateful for your support throughout this entire journey.

Rocio Cozmar – June 2026

List of publications.

- Cozmar, R., Berrios, J. & Fickers, P. Engineering serine metabolism to enhance *AOX1* promoter self-induction in formate dehydrogenase-deficient *Komagataella phaffii*. *Microb Cell Fact* 25, 96 (2026). https://doi.org/10.1186/s12934-026-02968-1

- Keller, C., Cozmar, R., Alcalde, M., & Fickers, P. (2026). *Yarrowia lipolytica, Komagatoella phaffii* and secretory proteins: recombinant laccase as a case study. Journal of Biotechnology, 412, 1-4. https://doi.org/10.1016/j.jbiotec.2026.01.015

- Bustos, C., Cozmar, R., Berrios, J., & Fickers, P. (2025). "Sorbitol Uptake and Oxygen Transfer Shape *AOX1* Promoter Induction in Formate Dehydrogenase-Deficient. *Komagataella phaffii*". *Microbial Biotechnology*, *18*(11), e70263. https://doi.org/10.1111/1751-7915.70263

List of communications during scientific events.

- Poster:

"Engineering formate metabolism in *Komagataella phaffii* enables methanol-free recombinant protein production process based on p*AOX1* promoter". (International conference on yeast genetics and molecular biology 2025 ICYGMB32 Soborne Université, Paris, France, July 2025)

- Poster:

"Low oxygen availability favors the induction of p*AOX1* promoter of FdhKO strains in the yeast *Komagataella phaffii*" (Annual Seminar of the Belgian Society of Microbiology. Annual Symposium 2025: amAIzing Microbiology: demystifying AI for all microbiologists, February 2025)

- Poster:

"Enhancement of protein secretion by transcription factor *HAC1* in two *Komagataella phaffii* strains metabolic modified" (Belgian Society for Microbiology. Annual Symposium 2024: Milestones in Microbiology, Belgium, March 2024)

Table of contents

List of figures.

medium, K_La 10 h^{-1}; high, K_La 100 h^{-1}), in shake-flask cultures. Culture samples were taken at the mid-exponential growth phase (i.e. after 22 h). eGFP fluorescence was quantified by flow cytometry on 20,000 cells and expressed as TFU (total fluorescence, see materials and method for calculation details). Data are means and standard deviations of triplicate cultures.

Figure 3-8. Specific formate concentration (panel A), biomass-substrate yield coefficient ($Y_{x/s}$, panel B) and product-to-substrate yield coefficient ($Y_{p/s}$, panel C) for FdhKO eGfp (blue bars) and FdhKO-SdOE eGfp (orange bars) strains grown under different OTC, benchmarked by K_La, in shake-flask cultures. Culture samples were taken at the mid-exponential growth phase (*i.e*. after 22 h). Data are means and standard deviations of biological triplicate.

Figure A3-3. Methanol utilization pathway in *Komagataella phaffii*. Aox1, 2: alcohol oxidase1 and 2; Cat: catalase; Das1, 2: dihydroxyacetone synthase; Fld: formaldehyde dehydrogenase; Fgh: S-formylglutathione hydrolase; Fdh: formate dehydrogenase; Dak: dihydroxyacetone kinase; Tpi: triose phosphate isomerase; Fba: fructose-1,6-bisphosphate aldolase; Fbp: fructose-1,6-bisphosphatase; GS(H): glutathione; DHA: dihydroxyacetone; DHAP: dihydroxyacetone phosphate; GAP: glyceraldehyde-3-phosphate; F1,6BP: fructose-1,6-bisphosphate; F6P: fructose-6-phosphate; Xu5P: xylulose 5-phosphate.

Figure A3-4. Tetrahydrofolate (THF) mediated one-carbon (THF-C1) metabolism in yeast. Fdh, formate dehydrogenase; Shm1, mitochondrial serine hydroxymethyltransferase; Shm2, cytosolic serine hydroxymethyltransferase; Mis1-2, formate-tetrahydrofolate ligase; Mis1-3, methylenetetrahydrofolate dehydrogenase & methenyltetrahydrofolate cyclohydrolase; Mis1-1, trifunctional enzyme: formate-tetrahydrofolate ligase, methenyltetrahydrofolate cyclohydrolase and methylenetetrahydrofolate reductase; THF, tetrahydrofolate. Figure adapted from (Bustos et al., 2024).

Figure A3-5. Sorbitol Dehydrogenase enzyme. Protein alignment. XP_002489933.1 corresponds to (gene PAS_chr1-1_0490) protein sequence Komagataella phaffii, and XKU26523.1 corresponds to Saccharomyces cerevisiae.

Figure A3-6. Hexose transporter protein. Protein alignment. XP_002490706.1 corresponds to (gene PAS_chr1-4_0570) protein sequence *Komagataella phaffii*, and CAA98825.1 corresponds to *Saccharomyces cerevisiae*.

Figure A3-7. Schematic representation of the genotype of yeast strains used in 3rd chapter.

Figure A3-8. Glycerol and sorbitol concentration during the growth of FdhKO eGfp strain (blue colors, Panel A) and FdhKO SdOE eGfp strain (orange colors, Panel B)

in YNB minimal medium containing different mixtures of glycerol and sorbitol (YNBG0, 1.75 g L^{-1} glycerol; YNBGS2, 1.75 g L^{-1} glycerol and 1.75 g L^{-1} sorbitol; YNBGS4, 1.75 g L^{-1} glycerol and 3.5 L^{-1} sorbitol). The data show one representative culture.

Figure A3-9. Sorbitol concentration after 22 h of growth of strains SdhKO eGfp (blue) and SdhKO SdOE eGfp (orange) in the YNBS2 medium under different OTC (low, K_La 10 h^{-1}; medium, K_La 10 h^{-1}; high, K_La 100 h^{-1}). Data are the mean and standard deviation of triplicate cultures conducted in in shake flasks.

Figure A3-10. e*GFP* gene expression level for FdhKO eGfp and FdhKO-SdOE eGfp strains cultured strains grown under different OTC (low, K_La 10 h^{-1}; high, K_La 100 h^{-1}), in shake-flask cultures. Culture samples were taken at the mid-exponential growth phase (i.e. after 22 h). Data are means and standard deviations of triplicate cultures. Gene expression levels were normalized according to that of actin gene.

Figure 4-1. Schematic diagram illustrating the targeting serine biosynthesis pathway in a formate dehydrogenase-deficient *Komagataella phaffii.* Formate from THF-C1 metabolism induces the p*AOX1* promoter.

Figure 4-2. Serine biosynthesis pathway in *Komagataella phaffii.* Abbreviation are as follows: PGADH, 3-phophoglicerate dehydrogenase; PSAT1, phosphoserine aminotransferase encoded; PSPH, phosphoserine phosphatase; G6P, glucose-6-phosphate; G3P, 3-phosphoglycerate; NAD^+, nicotinamide adenine dinucleotide oxidized; NADH, nicotinamide adenine dinucleotide reduced; Glu, glutamate; αKG, alfa-ketoglutarate; Pyr, pyruvate; P, phosphate.

Figure 4-3. Strategy proposal overview focused on enhancing serine pathway in FDH-deficient strain.

Figure 4-4. General overview of plasmids construction by NEBuilder HiFi DNA assembly kit of different gene fragments. Z: Zeocin selection marker; H: hygromycin selection marker; N: Nourseothricin selection marker.

Figure 4-5. Specific eGFP fluorescence for eGfp strain (FdhKO p*AOX1-eGFP*) expressing gene *SER1* (panel A), *SER2* (panel B), *SER3* (panel C) and *SER1-SER3* (panel D) under the control the p*GAP* (strains marked with *g*) and p*MDH3* (strains marked with *m*) during growth in sorbitol medium (YNBS). Cells were grown in microbioreactors in batch mode as described in Materials and Methods. Specific fluorescence is the mean value (coloured lines) and standard deviation (grey shades) of biological triplicates. sFU: Specific fluorescence unit.

Figure 4-6. Biomass for eGfp strain (FdhKO p*AOX1*-eGFP) expressing gene *SER1* (panel A), *SER2* (panel B), *SER3* (panel C) and *SER1-SER3* (panel D) under the control the p*GAP* (strains marked with g) and p*MDH3* (strains marked with m) during growth in sorbitol medium (YNBS). Cells were grown in microbioreactors in batch mode as described in Materials and Methods. Biomass is the mean value (colored lines) and standard deviation (grey shades) of biological triplicates. Arb units: arbitrary unit.

Figure 4-7. Biomass (panel A), specific eGFP (panel B) and extracellular formate concentrations (Panel C) for eGfp (fdh1Δ, p*AOX1-eGFP*, blue color) and *m*SER3-eGfp (fdh1Δ, p*AOX1-eGFP*, p*MDH3-SER3*, green color) strains grown in YNB minimal media containing glycerol and sorbitol at a 1:2 ratio (YNBGS4). Cells were grown in microbioreactors in batch mode as described in Materials and Methods in glycerol-sorbitol media (YNBGS4). The data represent the mean and standard deviation of triplicate cultures. sFU: specific fluorescence unit; a.u: arbitrary units. μM: micromolar. In panel A and B, the dotted line highlights the point at which glycerol was depleted from the medium.

Figure 4-8. Glucose oxidase activity (panel A), extracellular formate concentration (panel B), biomass (panel C) and sorbitol concentration (panel D) during growth of GOX (blue color) and GOX-SER3 (green color) strains in sorbitol media (YNBS). Data are presented as the mean and standard deviation of triplicate cultures conducted in shake flasks as described in Materials and Methods. Glucose oxidase assays were performed in triplicates.

Figure 4-9. Biomass (panel A), glycerol (filled histograms) and sorbitol (empty histograms) concentrations (panel B), dissolved oxygen (panel C), and glucose oxidase-specific activity (panel D) during the growth of the GOX (blue colour) and GOX-SER3 (green colour) strains in a stirred-tank bioreactor in batch mode as described in Materials and Methods in glycerol-sorbitol media (YNBGS). Cultures were performed in duplicate. In panels A and D, the dots represent all the measurements, while the lines connect the mean values.

Figure A4-5. Codon optimized sequence of the alfa mating factor (*α*MF) from *Saccharomyces cerevisiae* (NM_001184001.1). Modified codons are in red, *Bsa*I sequence is blue. Optimization was made using SnapGene software

Figure A4-6. Codon optimized sequence of the intron less glucose oxidase gene from *Aspergillus niger* (x60601.1). Modified codons are in red. *Bsa*I sequence is blue. Sequence in purple corresponds to a histidine tag fuse to the Gox protein for purification. Optimization was made using SnapGene software

Figure A4-7. Schematic representation of the strain genotype used in 4th chapter.

Figure A4-8. Specific eGFP fluorescence of the different eGFP constructed strains. Histogram color is specific for a constructed strain, each histogram bars representing one of the three transformants tested. Data represents the mean and standard deviation of triplicate cultures. sFU: specific fluorescence unit.

Figure A4-9. Specific glucose oxidase activity of the different GOX constructed strains. Histogram color is specific for a constructed strain, each histogram bars representing one of the three transformants tested. Data represents the mean and standard deviation of triplicate cultures.

Figure A4-10. Biomass for eGfp strain (FdhKO p*AOX1*-eGFP) expressing gene *SER1* (panel A), *SER2* (panel B), *SER3* (panel C) and *SER1*-*SER3* (panel D) under the control the p*GAP* (strains marked with g) and pMDH3 (strains marked with m) during growth in sorbitol medium (YNBS). Cells were grown in microbioreactors in batch mode as described in Materials and Methods. Biomass is the mean value (colored lines) and standard deviation (grey shades) of biological triplicates. Arb units: arbitrary unit.

Figure 5-1. Schematic representation of the constructed expression systems obtained by Golden Gate (GG) assembly (Supporting information A). Abbreviations are as follow: p*TEF*, promoter p*TEF*-4UA (GGE146); Pre, presequence of α factor (αPre); Yps3 protease, (Yps3Pre); *LIP2* lipase, (Lip2Pre); SoAmy α-amylase (SoAmyPre); Lacc, LacVader laccase encoding gene; LIP2tt; *LIP2* transcriptional terminator. All constructs were integrated at the *LIP2* locus of *Y. lipolytica* strain RIY146.

Figure 5-2. Laccase specific activity after 60 h and 72 h of growth in BMD1 medium for *K. phaffii* and YNBG-Cu for *Y. lipolytica* strains. Data are for biological triplicate cultures and technical duplicate of enzyme assays.

Figure 5-3. LacVader expression level for *Y. lipolytica* Yps3Pre, Yps3Pre-αPro and Yps3Pre-Lip2Pro strains grown in YNBG-Cu after 24 h and 48 h. Data are means and standard deviation of triplicate cultures. Expression levels were first normalized to that of Actin (ΔCt) and to the mean expression level of Yps3Pre (ΔΔCt).

Figure A5-1. Schematic representation of the constructed expression systems obtained by Golden Gate (GG) assembly. Abbreviations are as follow: p*TEF*, promoter p*TEF*-4UA (GGE146); Pre, presequence (αPre, Yps3Pre, Lip2Pre or SoAmyPre); Lacc, LacVader laccase encoding gene; *LIP2*tt; *LIP2* transcriptional terminator.

Figure A5-2. Assessment of gene integration consistency. For each construct, two transformants were cultivated in biological triplicates for 48h. The laccase activity was determined in triplicate and specific laccase activity calculated from the corresponding biomass. For both transformants per constructed strain, nine values are given.

Figure A5-3. Biomass after 72 of growth of the different *Y. lipolytica* strains grown in deepweel plate in YNBCu medium in triplicate. Box represents the minimal and maximal value obtained. Black dots represent the obtained values.

List of tables.

List of Abbreviations.

ABTS:	2,2'-Azino-bis (3-ethylbenzothiazoline-6-sulfonic acid)
***AOX1*:**	alcohol oxidase 1 gene
a.u:	arbitrary units
***ADH*:**	alcohol dehydrogenase gene
Aox1:	alcohol oxidase1
Aox2:	alcohol oxidase 2
BLAST:	basic local alignment search tool
BlastX	basic local alignment search tool - translated nucleotides to proteins
BMD1:	buffered minimal medium 1
CalB:	candida antarctica lipase B
Cat:	Catalase
***DAS1*:**	dihydroxyacetone synthase 1 gene
Das1:	dihydroxyacetone synthase 1
Das2:	dihydroxyacetone synthase 2
DCW:	dry cell weight
%DO	percent dissolved oxygen
eGFP:	enhanced green fluorescent protein
Fdh:	formate dehydrogenase
***FDH1*:**	formate dehydrogenase gene
***fdh1*Δ:**	formate dehydrogenase deleted gene
Fgh:	S-formylglutathione hydrolase
Fld:	formaldehyde dehydrogenase
***FLD1*:**	formaldehyde dehydrogenase gene
FU:	fluorescence units
gDCW	gram of dry cell weight
GPI:	glycosylphosphatidylinositol
Gox:	glucose oxidase
GRAS	genetic tractability and generally recognized as safe
GS(H)/ GSSG:	reduced / oxidized glutathione
K_La:	oxygen transfer coefficient (h^{-1})
HCHO:	formaldehyde
KO:	knockout gene
HPLC:	high performance liquid chromatography
LB:	luria-bertani medium

MeOH: methanol
MUT: methanol utilization pathway
OD_{600}: optical density at 600 nm
OTC: oxygen transfer conditions
OE: overexpressed gene
p*AOX1*: alcohol oxidase 1 promoter
p*CAT1*: methanol- inducible catalase promoter
p*DAS1*: dihydroxyacetone synthase promoter
p*FLD1*: formaldehyde dehydrogenase promoter
p*GAP*: 3-phophoglicerate dehydrogenase promoter
p*MDH3*: peroxisomal malate dehydrogenase 3 promoter
p*TEF*: translation elongation factor-1α promoter
p-NPB: p-nitrophenyl butyrate
Pgadh 3-phosphoglycerate dehydrogenase
Pp*HXT1:* putative protein hexose transporter 1
Pre: pre-sequence of signal peptide
Pro: pro-sequence of signal peptide
Psat1 3-phosphoserine aminotransferase
Psph phosphoserine phosphatase
qO_2 specific oxygen consumption rate
qSor specific sorbitol up-take rate
rProt: recombinant protein
rsProt: recombinant secretory protein
***SER1*:** 3-phosphoserine aminotransferase gene
***SER2*:** phosphoserine phosphatase gene
***SER3*:** 3-phosphoglycerate dehydrogenase gene
sFU: specific fluorescence units
SoAmy: α-amylase from Sitophilus oryzae
SOR1: sorbitol dehydrogenase gene
SP: signal peptide
TFU: total fluorescence unit
THF: tetrahydrofolate
THF-C1: tetrahydrofolate-mediated one-carbon metabolism
UPR: unfolded protein response
YNBG-Cu: yeast nitrogen base glucose medium supplemented with copper
YNB: yeast nitrogen base
YNBS: yeast nitrogen base – 10 $g \cdot L^{-1}$ sorbitol

YNB2S:	yeast nitrogen base – 20 $g \cdot L^{-1}$ sorbitol
YNBG0:	yeast nitrogen base – 1.75 $g \cdot L^{-1}$ glycerol
YNBGS2:	yeast nitrogen base – 1.75 $g \cdot L^{-1}$ glycerol and 1.75 $g \cdot L^{-1}$ sorbitol
YNBGS4:	yeast nitrogen base – 1.75 $g \cdot L^{-1}$ glycerol and 3.5 $g \cdot L^{-1}$ sorbitol
YPD:	yeast peptone dextrose
$Y_{S/P}$:	substrate-product conversion yield
$Y_{S/P}$:	substrate-product conversion yield
μ:	growth rate (h^{-1})

Chapter 1

General Introduction

Chapter 1: General introduction.

1. Outline.

In the 1st chapter, a general introduction of the thesis is given, focusing on the research context and objectives.

In the 2nd chapter, the current knowledge on *Komagataella phaffii* is presented, and its utilization as a cell factory to produce recombinant proteins. It also presents the recent work performed in the yeast laboratory, particularly on the ability of the benchmark expression system based on the p*AOX1* promoter to operate in a self-induced manner in an FDH-deficient mutant strain cultivated on sorbitol as the main carbon source.

In the 3rd chapter, a strategy to improve the sorbitol catabolism in the FDH-deficient mutant and evaluate its impact on rProt productivity, exemplified for three proteins, namely the intracellular eGFP and secretory proteins lipase CalB and glucose oxidase (Gox), is presented.

The 4th chapter is focused on metabolic engineering on the serine biosynthesis pathway with the aim of enhancing formate accumulation of *K. phaffii* FDH-deficient strain. The presented analysis in this chapter examines how genetic modifications influence the formate accumulation and the production of two reporter proteins: the intracellular eGFP and glucose oxidase (Gox).

As efficient protein secretion relies partly on the nature of the signal peptide used, the 5th chapter evaluates different signal peptides for laccase production in *Yarrowia lipolytica* and compares them with *K. phaffii*. Signal peptide choice strongly influences recombinant protein secretion, depending on the host and the target protein. Although it does not involve engineered metabolic pathways, this study complements the core chapters on improving yeast-based protein production. Signal peptide optimization addresses secretion-level limitations, representing an interconnected layer of the production process.

The 6th chapter provides a general discussion of the research findings presented throughout the thesis. It synthesizes key findings and integrates the insights from the previous chapters to offer a cohesive understanding of the system. The implications of these findings are discussed, highlighting the advancements achieved in the development of a methanol-free expression system.

The 7th chapter summarizes the main conclusions and outlines future research perspectives of this thesis. It emphasizes the scientific relevance and novelty of the findings while proposing directions for further optimization of the methanol-free system.

Appendix contains appendices, which include supplementary materials such as the list of primers employed in this study, additional experimental data, and details on the scientific contributions.

2. Context and objectives.

2.1 Context.

In recent years, industrial biotechnology has been transformed by the development of cell platforms capable of producing recombinant proteins with high efficiency and scalability for both pharmaceutical and industrial applications, driving the development of efficient cell platforms known as microbial cell factories (MCF). These engineered microorganisms are capable of producing valuable compounds of interest (Lv & Cai, 2025). Among these platforms, the yeast *Komagataella phaffii* (formerly known as *Pichia pastoris*) has emerged as one of the most widely used expression systems in biotechnology (Cereghino & Cregg, 2000; Gasser et al., 2013). This host has enabled the development of therapeutic products, food enzymes, and biomolecules of industrial and commercial interest. (Ahmad et al., 2014). The relevance of these applications is reflected in the sustained growth of the global markets for industrial enzymes and recombinant proteins, approximately projected to exceed USD 24.6 billion in 2033 (Enzymes Market Size and Share, 2025) and USD 8.66 billion in 2034 (*Recombinant Proteins Market*, 2025) respectively. Its increasing adoption highlights the need for continued optimization of safe, cost-effective, and sustainable production processes.

Komagataella phaffii is a methylotrophic yeast capable of using methanol as a carbon source. Reports related to this species using methanol as a carbon source were obtained in the early 1970s (Ogata et al., 1969), which enabled Phillips Petroleum Company to develop a system for high-density yeast fermentation using methanol as a sole carbon source from methane for single-cell protein production at large scale. However, the system was rendered economically unviable due to the high cost of methanol caused by the oil crisis (Cereghino & Cregg, 2000) (Figure 1-1).

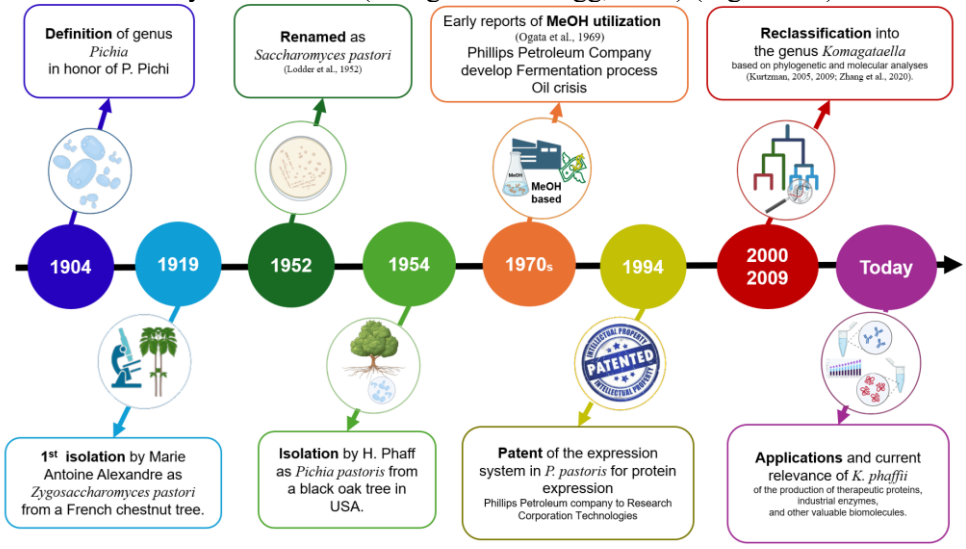

Figure 1-1. Historical timeline of *K. phaffi*: from environmental isolate to industrial expression platform.

During the following years, different authors worked on the characterization of metabolic pathways for methanol utilization in yeast. The methanol metabolism pathway is highly conserved across species capable of using methanol (MeOH) as a carbon source. It is initiated by the oxidation of methanol by alcohol oxidase (Aox) in the peroxisome, generating formaldehyde (HCHO) and hydrogen peroxide (H_2O_2), which is subsequently converted by catalase into water (H_2O) and oxygen (O_2). The formaldehyde serves as a key metabolic intermediate at the branching point in the pathway (Cregg et al., 1989). A portion of the formaldehyde enters the dissimilative pathway (represented with brown arrows in Figure 1-2), where it is further oxidized by two dehydrogenases (formaldehyde and formate dehydrogenase) to form carbon dioxide (CO_2), thereby reducing the formaldehyde's toxic effects on the cells (Berrios et al., 2022). The fraction of formaldehyde not oxidized in the dissimilative route follows the assimilative pathway (represented with light blue arrows in Figure 1-2), which is condensed with a five-carbon sugar, xyulose-5-monophosphate (XuMP), to yield two three-carbon molecules, glyceraldehyde-3-phosphate (G3P) and dihydroxyacetone phosphate (DHAP), through the action of the enzyme dihydroxyacetone synthase (Das). Subsequently, G3P exits the peroxisome and enters glycolysis, which supplies the precursors required for all cellular constituents for cell growth (Juturu & Wu, 2018) (Figure 1-2).

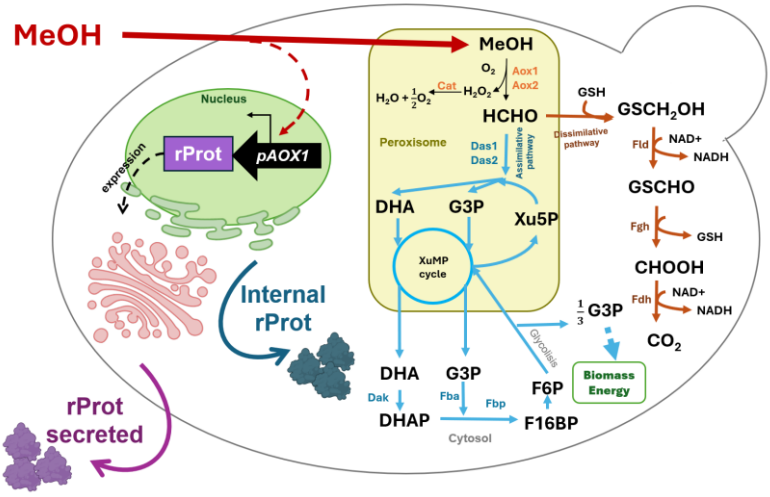

Figure 1-2. General overview of methanol metabolism and p*AOX1* induction on *Komagataella phaffii*. Figure shows the involved pathways of methanol metabolism in *K. phaffii*: Assimilative pathway (light blue arrows) and dissimilative pathway (brown arrows) and the relation of methanol with p*AOX1* induction. MeOH: methanol; Aox1, 2: alcohol oxidase1 and 2; Cat: catalase; Das1, 2: dihydroxyacetone synthase 1 and 2; Xu5P: xylulose-5-phosphate; DHA: dihydroxyacetone; DHAP: dihydroxyacetone phosphate; G3P: glyceraldehyde-3-phosphate; F6P: Fructose 1,6 biphosphate; Dak: dihydroxyacetone kinase; Fba: fructose-1,6-bisphosphate aldolase; Fbp:Fructose 1,6 bisphosphatase; Fld: formaldehyde dehydrogenase; Fgh: S-formylglutathione hydrolase; Fdh: formate dehydrogenase; GSH:

glutathione; GS-CH2OH: S-(hydroxymethyl) glutathione; GS-CHO: S-formyl glutathione; rProt: recombinant protein; p*AOX1*: alcohol axodase 1 promoter

In 1994, the patent for the protein expression system in *P. pastoris* was sold by Phillips Petroleum to Research Corporation Technologies. This change made it possible for the system to be used by any laboratory, allowing genes of interest to be expressed for academic or commercial purposes (Cereghino & Cregg, 2000).

K. phaffii is characterized by several desirable features reaching approximately 100–150 gDCW·L^{-1}, while recombinant protein production levels ranging from mg·L^{-1} to gram-per-liter scale have been achieved under optimized conditions (Cereghino & Cregg, 2000, Gu et al., 2015, Karbalaei et al., 2020). Few endogenous proteins are secreted by *K. phaffii*, resulting in a predominant fraction of total extracellular proteins being recombinant proteins, which simplifies downstream processing (Figure 1-3).(Looser et al., 2015; Meng et al., 2014).

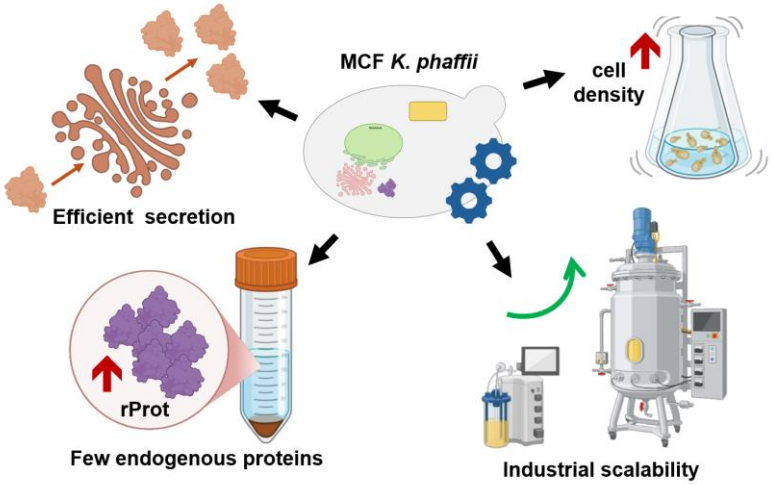

Figure 1-3. Advantages of use of *K. phaffii* as microbial cell factory. rProt: recombinant protein: MCF: Microbial cell factory.

These characteristics are largely due to *K. phaffii*'s ability to oxidize methanol to integrate it into the methanol utilization pathway (MUT). In cells and in the presence of methanol, *AOX1* gene is expressed at high level while this expression is repressed when cells are grown of glucose and glycerol. Based on these features, promoter of *AOX1* gene (p*AOX1*) has been used to develop efficient expression systems in *K. phaffii* (Figure 1-2) (Juturu & Wu, 2018,Türkanoğlu Özçelik et al., 2019; Vogl & Glieder, 2013). However, several limitations are associated with methanol use. It is highly toxic and flammable; careful handling is required, complicating large-scale industrial processes (Couderc & Baratti, 1980). Its metabolism leads to the generation of reactive oxygen species (ROS), resulting in oxidative stress, which may negatively affect protein folding, stability, and secretion efficiency (Jia et al., 2021; Vanz et al., 2012). Large amounts of oxygen are consumed during methanol oxidation, and extra

heat is generated by this process. These effects increase production costs and complicate scale-up because methanol requires high oxygen transfer rates and strict safety control during industrial fermentation processes (Cooney et al., 2000; Zavec et al., 2020) (Figure 1-4).

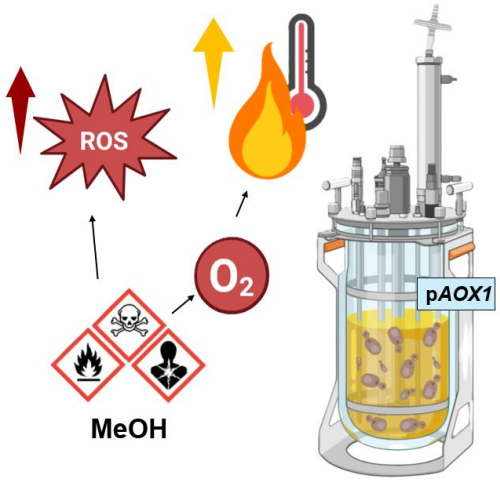

Figure 1-4. Limitations associated with the Methanol use for the p*AOX1* induction. MeOH: methanol, ROS: Reactive oxygen species; O_2: Oxygen; p*AOX1*: Acohol oxidase 1 promoter.

The limitations associated to the use of methanol for p*AOX1* induction have driven the search for alternative methanol-free expression systems in *K. phaffii.* One approach is the co-feeding of methanol with an additional carbon source, such as glucose or glycerol (Berrios et al., 2017; Žitkus et al., 2025). This strategy is widely used in industry to reduce methanol use. However, those carbon sources are known to repress p*AOX1* (Inan & Meagher, 2001; Thorpe et al., 1999; J. Wang et al., 2018), and reduce the induction level of p*AOX1*. In contrast, the co-feeding of methanol with non-repressive carbon sources has emerged as an alternative strategy that does not repress p*AOX1* (Carly et al., 2016). such as mannitol (Inan & Meagher, 2001; Vogl et al., 2016), sorbitol (Berrios et al., 2017) and lactate (Spohner et al., 2015) or formate (Jayachandran et al., 2017b; Singh & Narang, 2020).

In addition, other approaches have been developed to reduce methanol dependency for gene induction. These approaches are focused on the use of methanol-independent promoters, such as the sorbitol dehydrogenase promoter. (p*SDH*) (B. Liu et al., 2023), phosphoenolpyruvate carboxykinase promoter *PEPCK* (Rajak et al., 2024), pH-responsive promoters such as thioredoxin peroxidase promoter p*TSA1*, small heat shock protein promoter p*HSP12,* and sodium-coupled phosphate symporter promoter p*PHO89* (Albacar et al., 2024). Nevertheless, these methanol-free expression systems are based on alternative promoters and do not rely on the p*AOX1* promoter, which remains the most widely used system for recombinant protein production in industry.

Therefore, developing strategies to improve p*AOX1* induction without methanol remains a major challenge and could significantly advance both fundamental research and applied bioprocess technologies (Figure 1-5).

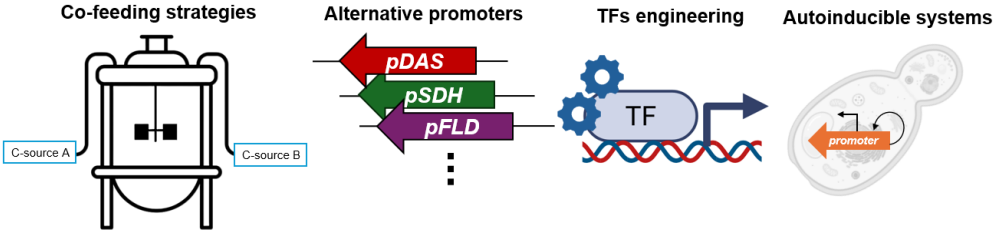

Figure 1-5. Summary of Methanol-free actual approaches. TF: transcription factor; pDAS: dihydroxyacetone synthase promoter; pSDH: sorbitol dehydrogenase promoter; pFLD: formaldehyde dehydrogenase promoter.

In this context, formate has emerged as an interesting option to induce p*AOX1* (Singh & Narang, 2020) and some studies reported the utilization of formate as an alternative inducer for p*AOX1* (Feng et al., 2022a; B. Liu, Zhao, et al., 2022). Recently, we demonstrated in our laboratory that formate generated from one-carbon metabolism mediated by tetrahydrofolate (THF-C1) can induce p*AOX1* promoter in a strain deficient in formate dehydrogenase (FDH) when grown on sorbitol as sole carbon source (Bustos et al., 2024). Nevertheless, this new FDH-deficient strain grows slowly in sorbitol compared to glycerol (0.02 $g \cdot gDCW^{-1} \cdot h^{-1}$and 0.9 $g \cdot gDCW^{-1} \cdot h^{-1}$, respectively). Furthermore, it has been reported that supplementation of the culture medium with serine increases specific fluorescence in the FDH-deficient mutant strain grown on sorbitol media (Bustos et al., 2024). Since intracellular formate has been associated with p*AOX1* induction in this system, these results suggest a possible connection between serine availability, formate metabolism, and p*AOX1* induction. These limitations emphasize the potential for further improvement of the autoinducer system.

Given the current approaches to minimize methanol use, this work investigates strategies on FDH-deficient strain *K. phaffii* to improve p*AOX1* induction. Additionally, it provides a detailed explanation of the underlying mechanisms involved in these advancements.

2.2 Objectives

The main objective of this thesis is developing strategies to enhance formate accumulation in *K. phaffii* FDH-deficient strain, through metabolic engineering, using sorbitol as a carbon source, in order to improve the *AOX1* promoter induction and the recombinant protein production.

To achieve this objective, two main strategies were implemented: The first strategy consisted of enhancing sorbitol assimilation, while the second strategy aimed to enhance serine biosynthesis to increase intracellular formate and further enhance *AOX1* promoter activity. The effects of these modifications were evaluated using intracellular enhanced green fluorescence protein (eGFP) as a reporter for p*AOX1* induction, and extracellular *Candida antarctica* lipase B (CalB), and secreted *Aspergillus niger* glucose oxidase (Gox) as model secreted proteins.

The scheme followed in order to accomplish these objectives is illustrated in Figure 1-6: Based on the slow growth of the FDH-deficient strain on sorbitol reported by Bustos et al. (2024), the strain was metabolically engineered to overexpress the *PpHXT1* and/or *SOR1* genes. These modifications aimed to enhance sorbitol metabolism. In addition, based on the serine supplementation, which has been shown to improve fluorescence in this strain when grown on sorbitol media (Bustos et al., 2024), the serine biosynthesis pathway flux was enhanced through the overexpression of *SER3, SER1,* and *SER2* under selected promoters. The resulting mutants were evaluated in terms of specific fluorescence, biomass, growth rate, carbon source consumption, formate accumulation, and recombinant protein production.

A side research project, we focused on the optimization of protein secretion in the yeast *Yarrowia lypolitica*. For that purpose, protein secretion efficiency, using CalB as a model protein, was determined for different combinations of pre- and pro-sequence. The summary scheme of complete work is described in Figure 1-6 as follows:

A: Description of Background and Conceptual framework of using methanol in *Komagataella phaffii* for recombinant protein production and the developed methanol-free system **B**: Develop of strategies for enhancement of sorbitol uptake through metabolic engineering of the sorbitol pathway in FdhKO strain **C:** Evaluation of kinetics in cultures of engineered strains decreases p*AOX1* induction and low O_2 improves it **D:** Develop of strategies for enhancement of formate accumulation through metabolic engineering of the biosynthesis serine pathway **E:** Comparative analysis of overexpressed enzymes: *SER3* bottleneck of biosynthesis serine pathway **F**: Evaluation of constructed strains in operational conditions **G**: Testing the increase of the synthesis of secreted protein in bioprocess conditions.

Abbreviations: rProt: specific recombinant protein ; s.r.prot: specific recombinant protein FdhKO: formate dehydrogenase deficient strain; Δ*FDH1*: formate dehydrogenase gene deleted; μ: growth rate; p*AOX1*: alcohol oxidase 1 promoter; p*GAP*; 3-phophoglicerate dehydrogenase promoter; p*MDH3*: peroxisomal malate dehydrogenase promoter; P*pHXT1*: hexose transporter gene; *SOR1*: sorbitol dehydrogenase gene; Sor1: sorbitol dehydrogenase; FdhKO SdOE: formate dehydrogenase deficient overexpress *SOR1* strain; K_La: oxygen transfer coefficient; Pgadh: 3-phophoglicerate dehydrogenase; Psat1: phosphoserine aminotransferase; Psph: phosphoserine phosphatase; G6P: glucose-6-phosphate; 3PG: 3-phosphoglycerate; NAD^+: nicotinamide adenine dinucleotide oxidized; NADH: nicotinamide adenine dinucleotide reduced; Glu: glutamate; αKG: alfa-ketoglutarate; Pyr: pyruvate; P: phosphate *SER3*: 3-phophoglicerate dehydrogenase gene; *SER1*: phosphoserine aminotransferase gene; *SER2*: phosphoserine phosphatase gene; *m*SER3: formate dehydrogenase deficient strain overexpress *SER3*; GOX; formate dehydrogenase deficient strain with Gox as model secreted protein SER3-GOX: formate dehydrogenase deficient strain overexpress

SER3 with Gox as model secreted protein eGFP: enhanced green fluorescent protein; CalB: *Candida antarctica* lipase B, Gox: glucose oxidase.

Overall, this doctoral project aimed to develop and optimize *K. phaffii* FDH-deficient strain for recombinant protein production. Metabolic engineering strategies were implemented to improve carbon utilization and intracellular metabolite availability, while secretion efficiency was addressed through signal peptide optimization. Together, these approaches were integrated to enhance recombinant protein yield and to expand the performance of the *K. phaffii* expression system. Figure 1-7 offers a schematic overview of the thesis framework integrating carbon metabolism, metabolic engineering, and secretion optimization strategies for improved recombinant protein production.

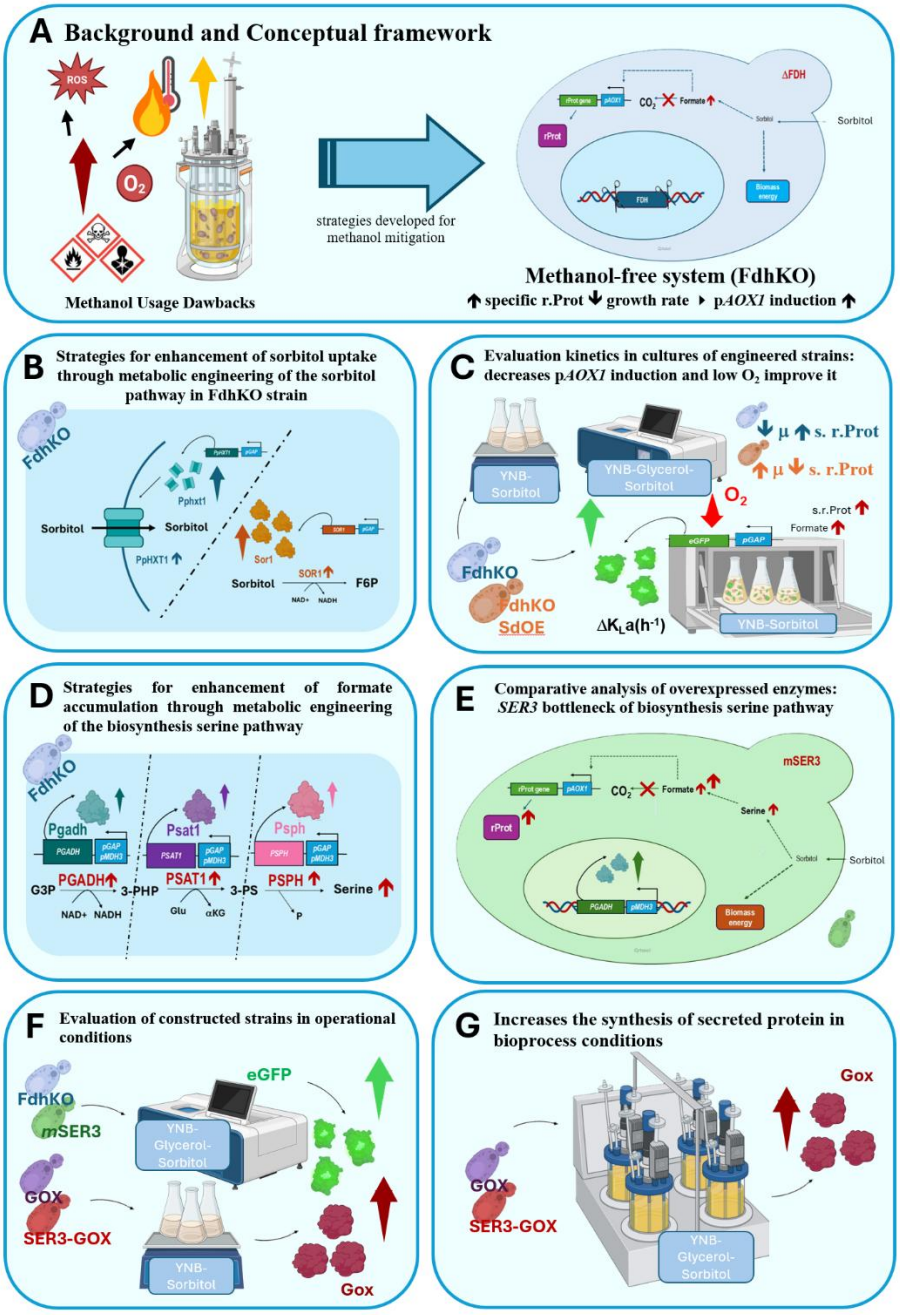

Figure 1-6. A schematic overview of the improvement of the *Komagataella phaffii* FDH-deficient strain strategies performed in this investigation.

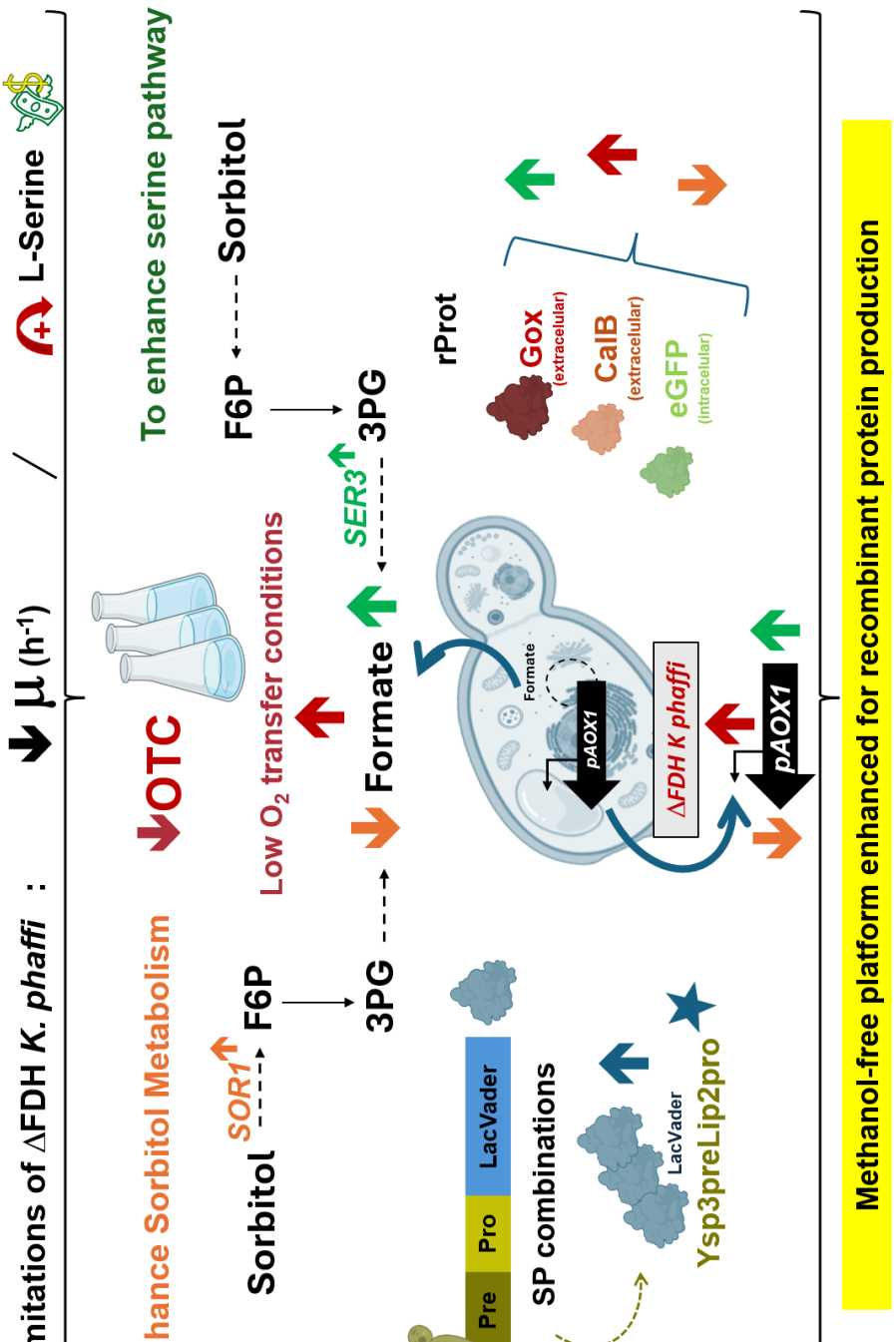

Figure 1-7: Graphical abstract of " Development of a production strategy based on the modification of metabolic regulation processes in *Komagataella phaffii*." doctoral project. The arrows in colors show the effect of implemented strategy described: to enhance sorbitol metabolism (orange), to test oxygen transfer conditions (red),to enhance serine pathway (green) and signal peptides combinations (blue).

Chapter 2

Komagataella phaffii as a Yeast Cell Factory: Methylotrophic Metabolism, Promoter Engineering, and Methanol-Free Expression Strategies.

Description of Chapter 2

This chapter provides a deep background on *K. phaffii* as a versatile yeast cell factory, emphasizing its methylotrophic metabolism and inducible promoters, particularly p*AOX1*. It reviews promoter regulation by key transcription factors and strategies for methanol-free or autoinduced expression, including alternative carbon sources, transcription factor engineering, and hybrid systems, especially focuced in the formate as inducer to establish the foundational understanding necessary for FDH-deficient strains of *K. phaffii* as an interesting model to enhance p*AOX1* induction. Based on the results of this investigation in the subsequent chapters, the insights present in this chapter will be discussed.

Chapter 2: Advances in *Komagataella phaffii* as a yeast cell factory: Methylotrophic metabolism, inducible promoter engineering and methanol-free expression Approaches.

1. Yeast-based cell factories and *Komagataella phaffii.*

In the last decades, the concept of cell factories has gained relevance in the biotechnology industry, where microbial hosts are engineered to produce a wide array of high-value compounds like biopharmaceuticals, biofuels, and fine chemicals (Nielsen & Keasling, 2016). Well-studied examples of yeast hosts include *Saccharomyces cerevisiae, Yarrowia lipolytica* and *Komagataella phaffii* (L. Liu et al., 2013). *K. phaffi*, formerly known as *Pichia pastoris*, is a non-conventional yeast that has emerged as a robust and versatile host for recombinant protein (rProt) production and has become one of the most widely used yeast cell factories (Gasser et al., 2013). Under controlled growth conditions, it can reach high cell densities, and its post-translational modifications are simplified compared with higher eukaryotic hosts, making this yeast an attractive expression system, which underpins its widespread use in heterologous protein production (Ahmad et al., 2014; Veenhuis et al., 2000).

2. Methylotrophic metabolism of *K. phaffi.*

K. phaffi is able to utilize methanol as a sole carbon and energy source (Cereghino & Cregg, 2000; J. Lin-Cereghino et al., 2005) via a dual-pathway system known as the methanol utilization pathway (MUT). The MUT pathway is regulated at the transcriptional level through promoters of genes encoding enzymes involved in this pathway, which are controlled by transcription factors (TFs). TFs are regulatory proteins that control the rate of gene transcription by binding to specific DNA sequences (Shen et al., 2023). The assimilative and dissimilative pathways are tightly regulated at the transcriptional level largely by the transcription factor Mxr1, which is the master regulator of methylotrophy in *K. phaffii*. Mxr1 controls the expression of *AOX1*, including other key genes: dihydroxyacetone synthase (*DAS1*), formaldehyde dehydrogenase gene (*FLD1*), and formate dehydrogenase gene (*FDH1*), in response to the presence of methanol and can be repressed by glucose and glycerol (J. Lin-Cereghino et al., 2005; Zhan et al., 2017).

According to the methanol-utilization pathway, there are three phenotypes: The wild-type methanol utilization phenotypes, known as methanol utilization plus (Mut^+) strains of *K. phaffi*, both *AOX1* and *AOX2* genes are active, supporting rapid methanol metabolism and high alcohol oxidase activity. Under methanol-inducing conditions, the alcohol oxidase 1 promoter (p*AOX1*) is strongly induced, leading to high levels of the enzyme alcohol oxidase (Aox) (Cámara et al., 2017). In Mut^S strains of *K. phaffi*, *AOX1* is deleted while *AOX2* remains functional. As a result of this modification, methanol metabolism is slowed, Aox activity is reduced, and oxygen consumption and heat generation are decreased, which can be advantageous under certain

cultivation conditions (Krainer et al., 2012). Nonetheless, this disruption of *AOX1* in Mut^S introduces its own drawbacks. The methanol metabolism in Mut^S is slowed, leading to intracellular methanol accumulation. As a result, methanol is erroneously used as a substrate by O-acetylhomoserine sulfhydrylase as a substrate instead of H_2S (Schotte et al., 2016). O-methyl-L-homoserine accumulation is triggered by this phenomenon, leading to oxidative stress (Barone et al., 2023; Hausjell et al., 2020; Schotte et al., 2016; Vanz et al., 2012).

Mut$^-$ phenotype is characterized by deletion of *AOX1* and *AOX2*, resulting in the inability to metabolize methanol while retaining inducibility of the p*AOX1*. rProt production is therefore decoupled from growth and is associated with reduced oxygen demand and heat generation. However, its application is constrained by the obligatory need for co-substrates, increasing the complexity of cultivation strategies (Zavec et al., 2020). Mut^S and Mut$^-$ drawbacks, such complicated production and oxidative stress, underscoring the need for methanol-free or reduced-methanol induction strategies (Figure 2-1).

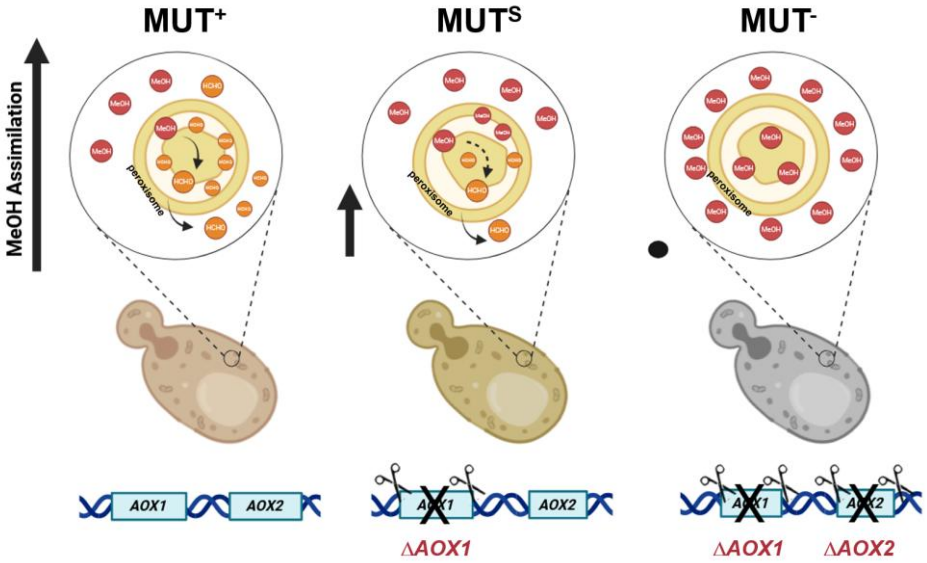

Figure 2-1. General overview of *K. phaffii* phenotypes. The Mut+ strains, both *AOX1* and *AOX2* genes are active, supporting high methanol (MeOH) assimilation. In Mut^S strains, *AOX1* is deleted while *AOX2* remains functional, with slow methanol assimilation, and Mut$^-$ have both *AOX1* and *AOX2* genes deleted, resulting in the inability to metabolize methanol.

3. Regulated promoters in *K. phaffi* expression system.

While constitutive promoters such as glyceraldehyde-3-phosphate dehydrogenase promoter (p*GAP*) provide continuous expression of rProt and allow high levels of gene expression, they offer limited control over timing and duration of gene expression. In contrast, regulated promoters of *K. phaffi* allow precise temporal control of recombinant protein gene expression. Multiple advantages are offered by

this strategy: cell growth and protein production phases can be separated, metabolic burden during growth phase is reduced, and premature expression of recombinant proteins that may negatively affect cell growth or viability can be avoided (Cereghino & Cregg, 2000; Vogl & Glieder, 2013).

The most studied regulated promoters, including the p*AOX1*, the formaldehyde dehydrogenase promoter (p*FLD1*), and the dihydroxyacetone synthase promoter (p*DAS1*) are linked to the metabolism of specific carbon sources. The p*AOX1* promoter is the most extensively studied and widely used in *K. phaffii*. It provides robust transcriptional activation in the presence of methanol and strong repression in the presence of non-inducing carbon sources such as glucose, glycerol, and ethanol. This promoter enables high-level expression of heterologous proteins and is often the preferred choice for industrial-scale processes (Cereghino & Cregg, 2000; Cregg et al., 2000; Vogl & Glieder, 2013). In contrast, the p*FLD1* promoter is regulated by methylamine and formaldehyde (Daly & Hearn, 2005), which provides methanol-free expression under certain conditions (Resina, 2004). The methanol-regulated catalase promoter (p*CAT1*) has been shown to drive expression during peroxisomal proliferation and oxidative stress (Baumann et al., 2008; Vogl et al., 2014). p*DAS1* is regulated by methanol via methanol-specific transcriptional factors Mrx1 and Mit1. Compared with p*AOX1*, it exhibits a weaker response amplitude. This response to methanol is considered advantageous in a controlled expression, reducing metabolic burden, limiting oxidative stress associated with methanol metabolism. In this context, Takagi et al., (2019) has identified a methanol-independent region in p*DAS1*, named Enhancer Sequence of p*DAS1* (ESP*DAS1*). This sequence was shown to enhance the activity of the transcription factor Prm1p. An engineered version of p*DAS1* was constructed using this regulatory element. Methanol-free phytase production was increased by 25% compared with the constitutive glyceraldehyde-3-phosphate dehydrogenase promoter (p*GAP*), known for its high response on gene expression, which is largely unaffected by the carbon source used.

Table 2-1. Main regulated promoters in *Komagataella phaffi*.

Gene name	Gene description	Regulation	Ref
AOX1	Alcohol oxidase 1	Induced by methanol Repressed by glucose and glycerol	(Cereghino & Cregg, 2000; Ellis et al., 1985; Tschopp et al., 1987)
AOX2	Alcohol oxidase 2	Induced by methanol Repressed by glucose and glycerol	(Cregg et al., 1989; Koutz et al., 1989)
DAS	Dihydroxyacetone synthase	Induced by methanol	(Ellis et al., 1985; Küberl et al., 2011; Tschopp et al., 1987)
FLD1	Formaldehyde dehydrogenase	Induced by methylamine derepressed mode in the presence of glucose or glycerol	(Duan et al., 2009; Püllmann & Weissenborn, 2021; Resina, 2004; Resina et al., 2009; S. Shen et al., 1998)
PMP20	Peroxisomal glutathione peroxidase	Induced by methanol	(J. Li et al., 2024; Vogl et al., 2016)
FDH1	Formate dehydrogenase	Induced by methanol	(Vogl et al., 2016)
ICL1	Isocitrate lyase 1	Desrepression by ethanol induction	(Menendez et al., 2003)
PEX8	Peroxisomal matrix protein	Induced by methanol and methylamine or oleate	(H. Liu et al., 1995)
PHO89	Sodium-coupled phosphate symporter	Induced by phosphate limitation. Alkaline induction	(Ahn et al., 2009; Albacar et al., 2024)
HS12	Small heat shock protein	Alkaline induction	(Albacar et al., 2024)
TSA1	Thioredoxin peroxidase	Alkaline induction	(Albacar et al., 2024)
THI11	Protein involved in thiamine biosynthesis	Repressed by thamin completely	(Stadlmayr et al., 2010)
ADH	Alcohol dehydrogenase	Induced by methanol, ethanol glycerol	(Erden-Karaoğlan et al., 2022; Karaoglan et al., 2016a, 2016b)
GTH1	Glucose transporter gene	Induced by limited glucose Induced by limited glucose *FLO8*Δ genotype	(Prielhofer et al., 2013, 2018; Rebnegger et al., 2024)
ALDH	Aldehyde dehydrogenase	Induced by limited glucose	(Prielhofer et al., 2013)
AOD	Mitocondrial alternative oxygenase	Induced by glucose, not on methanol Carbon source dependent	(Kern et al., 2007)
CUP1**a**	Cooper metallothionein	Induced by Cu^{2+}	(Koller et al., 2000; Macreadie et al., 1991)
CAT	Methanol-inducible catalase	Induced by methanol	(Huang et al., 2025; Vogl et al., 2016, 2018)

	Desrepressed by exhausted glucose, glycerol, and ethanol

Abbreviations: *AOX1*: Alcohol oxidase 1; *AOX2*: Alcohol oxidase 2; *DAS*: dihydroxyacetone synthase; *FLD1*: formaldehyde dehydrogenase 1; *ICL1*: Isocitrate synthase 1; PEX8: Proximal atrix protein; PHO89: Sodium-coupled phosphate symporter; HS12:Small heat shock protein; TSA1: Thioredoxin peroxidase; THI11: Protein involved in thiamine biosynthesis; *ADH*: alcohol dehydrogenase; *GTH1*: glucose transporter gen; *ALDH*: Aldehyde dehydrogenase; AOD: Mitocondrial alternative oxzgenase; CUP1: Cooper metallothionein ; *CAT*: methanol-inducible catalase

Other promoters, such as the peroxisomal glutathione peroxidase promoter (p*PMP20*) and formate dehydrogenase promoter (p*FDH1*), have also been characterized as methanol-regulated promoters (Vogl et al., 2016).

However, the exclusive use of methanol imposes regulatory and safety constraints. Therefore, hybrid conditions involving non-repressing co-substrates such as sorbitol, lactate, and ethanol have been characterized to optimize induction and minimize risks. (Baumann et al., 2008; Spohner et al., 2015; Vogl & Glieder, 2013).

Unlike constitutive systems, where expression level is continuous, regulated promoters allow fine-tuning of the timing, level, and duration of gene expression. They are especially useful for producing toxic, unstable proteins, or proteins prone to misfolding, aggregation, or endoplasmic reticulum (ER) stress. These promoters have also been the subject of extensive engineering efforts to tune their regulatory behavior to enhance versatility across diverse production environments (Vogl & Glieder, 2013). Among the main regulated promoters available in *K. phaffi* (Table 2-1), *pAOX1* stands out as the most extensively characterized high-level expression of recombinant proteins in this host. Its regulation is closely linked to the methanol utilization pathways

3.1 The *AOX1* promoter regulation.

Methanol has been associated with the regulation of several transcription factors (X. Wang, Wang, et al., 2016). In presence of methanol, p*AOX1* is regulated by the methanol expression regulator 1 (Mxr1), whereas repression of p*AOX1* is observed in the presence of glucose or glycerol (G. P. Lin-Cereghino et al., 2006). Derepression of p*AOX1* is mediated by Mxr1, resulting in promoter induction. Subsequently, expression of the positive regulator of methanol 1 (Prm1) is triggered, followed by induction of methanol-induced transcription factor (Mit1) expression, which is required for the regulation of p*AOX1* (Haghighi Poodeh et al., 2022) (Figure 2-2).

However, feedback inhibition of Prm1 expression by Mit1 has been reported (Sahu et al., 2014). Repression of p*AOX1* is mediated by the transcription factors Mig1 and Mig2 (N. V. Kumar & Rangarajan, 2012; J. Wang et al., 2017). The ROP repressor, known as phosphoenolpyruvate carboxykinase (PECK), has been described as a repressor of methanol-inducible expression of p*AOX1* (N. V. Kumar & Rangarajan, 2012). Additionally, repression of p*AOX1* by competition for Mxr1 binding elements under glucose and glycerol media is mediated by the transcription factor (Nrg1) (X. Wang, Cai, et al., 2016). These studies have improved the understanding of transcriptional regulatory mechanisms of p*AOX1* regulation of repression and

induction (Figure 2-2) (Parua et al., 2012; J. Wang et al., 2017; X. Wang, Cai, et al., 2016; X. Wang, Wang, et al., 2016).

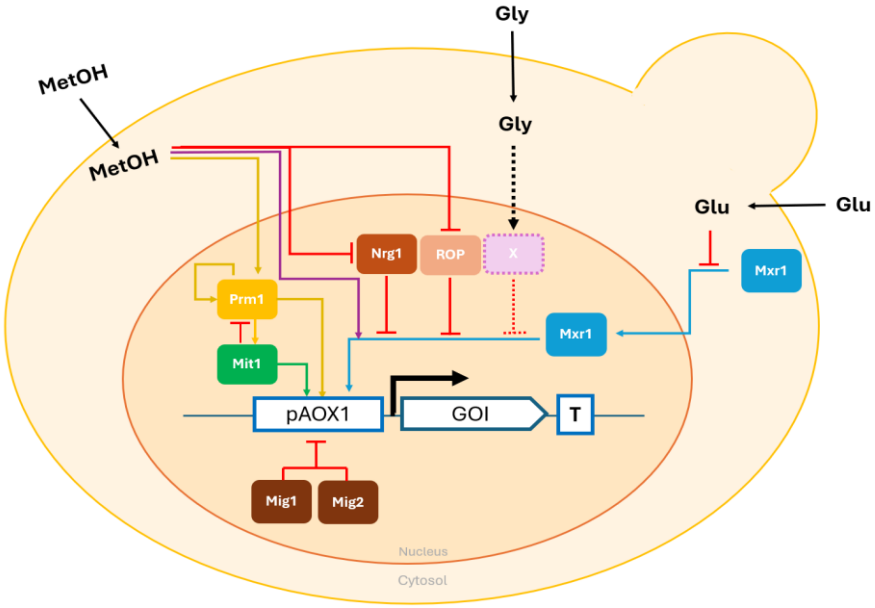

Figure 0-2. *AOX1* promoter regulation by transcription factors under different carbon sources reported in *Komagataella phaffii.* Mrx1: methanol expression regulator 1 transcription factor; Mit1: methanol-induced transcription factor 1; Mig1, 2: transcription factor repressors; Nrg1: Transcription factor repressor; ROP: Repressor of phosphoenolpyruvate carboxykinase; Prm1: positive regulator of methanol 1; MetOH: methanol; Glu: Glucose; Gly: Glycerol.

3.2 Methanol-free *AOX1* induction approaches.

Methanol is the primary and most potent inducer, leading to rapid and strong activation of *AOX1* transcription. However, methanol is inherently toxic due to the generation of formaldehyde and H_2O_2, which can cause cellular damage (Ahmad et al., 2014; Cregg et al., 2009). Additionally, methanol oxidation is highly exothermic, leading to substantial heat production that necessitates complex cooling systems to maintain optimal fermentation temperatures(G. P. Lin-Cereghino et al., 2006). The high oxygen demand during methanol metabolism also increases operational costs and requires aeration supply and agitation equipment (Prielhofer et al., 2013).

In the search for methanol-free system strategies, a study done by J. Wang et al. (2017), transcription factors were engineered to alter this natural p*AOX1* regulation, enabling promoter induction without methanol. Specifically, three transcriptional repressors were deleted (Mig1, Mig2, and Nrg1) and one activator was overexpressed (Mit1), resulting in a modified strain in which p*AOX1* can be derepressed in the presence of glycerol instead of methanol. In this engineered strain, glucose still acts as a strong repressor of p*AOX1*, whereas glycerol does not induce the promoter but allows derepressed expression under the modified transcriptional regulation. The

authors implemented a glucose-to-glycerol shift induction strategy, achieving 2.46 g/L insulin precursor production in a 5-L bioreactor, with substantially lower oxygen consumption and heat production compared to the wild-type methanol-induced process.

In other reports, deletion of the high-affinity hexose transporter (P*pHXT1*) gene was found to permit glucose- or fructose-mediated derepression of p*AOX1* in a *HXT1*-deficient strain background. (P. Zhang et al., 2010). In this mutant, initial Aox activity was detected under repressible carbon sources, but its level declined sharply during later growth phases due to peroxisome degradation by pexophagy.

Similarly, another strategy relies on transcriptional rewiring of the conventional p*AOX1*-based expression platform through derepressed overexpression of single transcription factors from the native regulatory network. In this approach, overexpression of Mit1 or Mxr1 enabled methanol-independent regulation of p*AOX1*, thereby converting the system into glucose- or glycerol-responsive expression platforms (Vogl et al., 2018).

Rebnegger et al., (2024) reported a novel fed-batch system for recombinant protein production using a *FLO8*-deficient strain under the *GHT1* promoter under glucose-limited conditions. Growth was reduced and unwanted morphological phenotypes were suppressed by the *flo8Δ* mutation, while the transcriptional activity of glucose-regulated promoters was enhanced. Under these conditions, recombinant protein yields were significantly increased with up to ~4.8-fold higher secreted product compared with the parental strain.

p*AOX1* is repressed by ethanol (Brierley et al., 1990), although the extent of repression depends on ethanol concentration and growth conditions (Cereghino & Cregg, 2000; Cregg et al., 2000). In recent years, investigations have been conducted into engineering p*AOX1,* like inducible *AOX1* hybrid-promoter by ethanol, specifically p*AOX1*/Cat8-L3 variant (integrating a single synthetic Cat8 the cis-acting element) and p*AOX1*/Adr1-L3/Cat8-L3 variant (made with single Cat8 and Adr1 cis-acting elements) were obtained by replacing specific cis-acting DNA motifs within the native p*AOX1* sequence. Using these constructs, eGFP expression increased by 74% and 85%, respectively, compared to methanol-induced p*AOX1* control. (Ergün et al., 2020).

From this perspective**,** sorbitol and lactate are considered as non-repressing carbon sources, making them suitable for co-feeding strategies in industrial bioprocesses (Spohner et al., 2015). In recent years, a methanol-independent expression system in *K. phaffii* was developed using the sorbitol dehydrogenase promoter (p*SDH*) induced by sorbitol. In this system, sorbitol was used to induce p*SDH* activity. The promoter was engineered to control the expression of Mit1. As a result, Mit1 was expressed first, and the heterologous protein xylanase, placed under p*AOX1*, was produced. Subsequently, xylanase production was enhanced by 1.7- to 2.1-fold higher activity when Mit1 expression was increased with this approach (B. Liu et al., 2023).

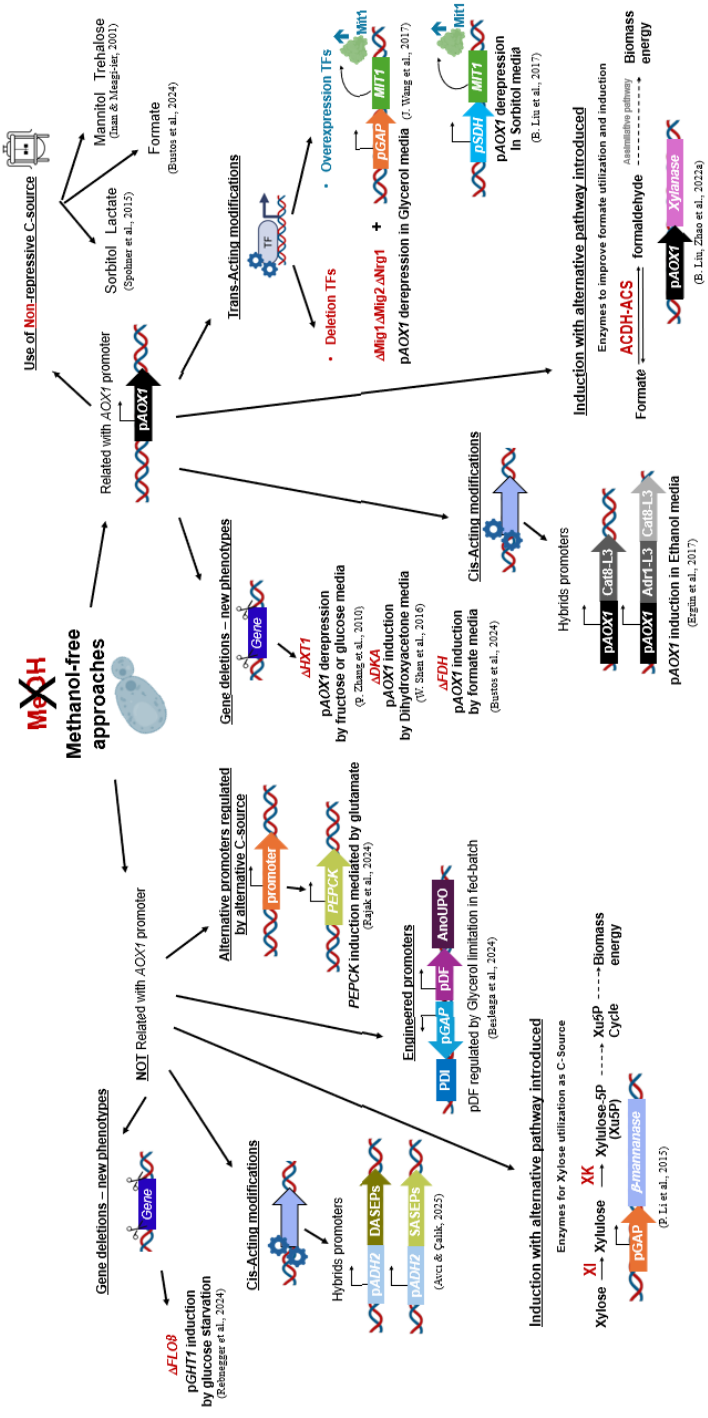

Figure 2-3. Methanol-free *AOX1* induction approaches presented in section 3.2, 2nd chapter.

Similarly, glutamate-regulated promoters such as *PEPCK* (phosphoenolpyruvate carboxykinase promoter) have been exploited for monosodium glutamate (MSG-regulated), such as the expression of recombinant proteins, including RBD domains of SARS-CoV-2 (Rajak et al., 2024). Mannitol has also been shown to provide moderate expression levels useful for toxic or folding-sensitive proteins (Inan & Meagher, 2001; Vogl et al., 2016).

In other reports, dihydroxyacetone (DHA) can induce p*AOX1* in dihydroxyacetone kinase Dak-deficient strain in the presence of DHA without methanol, a *dak*Δ-DHA methanol-free system (W. Shen et al., 2016). This system can reach gene expression levels that surpass those of the p*GAP* system, with values around 50-60% higher than the traditional methanol-induced system. Other compounds from the dissimilative pathway, such as formate, have been shown to induce the p*AOX1* promoter in FDH-deficient strains, enabling C1 metabolism-based induction without the use of methanol in sorbitol-containing media (Bustos et al., 2024).

Synthetic biology has also enabled the development of hybrid promoters combining engineered regulatory elements that respond to signals such as suitable carbon sources (SCSs). These promoters were constructed based on a p*ADH2* hybrid architecture, and synthetic transcription factor binding sites (TFBS) were predicted and selected to target transcription factors involved in carbon-source regulation, including Cat8 and Hap1 or Hap2/3/4/5 complexes to create dual-acting single-engineered promoters (DASEPs) (Avcı & Çalık, 2025). Conditional transcriptional activation in response to SCSs was enabled by these promoters. Two variants were tested: DASEP1, constructed with the dual-acting Cat8- and Hap1-transcriptional switches, and (ii) DASEP2, constructed with the dual-acting Cat8- and Hap2/3/4/5-transcriptional switches. eGFP expression was measured under these promoters in ethanol, glycerol, acetate, and methanol. Expression levels under DASEPs were increased compared to single-acting single-engineered promoters (SASEPs), with fold-increases as follows: 8.2- and 6.5-fold on glycerol, 2.7- and 2.6-fold on 2 % (v/v) ethanol, 3.9- and 4.0-fold on 1 % (v/v) ethanol, 3.6- and 4.2-fold on 1 % (v/v) methanol, and 3.7- and 2.8-fold on acetate. These tunable promoters provide customizable control over expression kinetics and improve product quality.

A methanol-free expression system was designed to co-express peroxygenases that are difficult to produce recombinantly. Promoters were arranged so that two genes were transcribed in opposite directions. This system is activated under derepressed conditions, enabling controlled expression without methanol (Besleaga et al., 2024). Their system is arranged in opposite directions: One direction is the protein disulfide isomerase (PDI) under standard promoters (pHHT1, pDC or pDC19), and in the opposite direction an unspecific peroxygenase (AnoUPO) under the desrrepresible promoter pDF, which responds efficiently during carbon source shifts without requiring methanol to produce peroxydases. This design offers a scalable, tightly regulated solution for industrial biocatalysis, minimizing safety concerns and simplifying downstream processing.

In this context, focused on methanol-free strategies, xylose has been reported as a non-utilizable carbon source for *K. phaffii* (Inan & Meagher, 2001). To enable xylose metabolism, the wild-type *K. phaffii* strain was genetically modified. The xylose isomerase gene from *Orpinomyces* spp. and the endogenous xylulokinase gene were introduced. Sequential batch cultivation for approximately 50 generations was applied to select strains with improved xylose utilization. In the resulting strains, β-mannanase production was significantly enhanced in xylose-based media (P. Li et al., 2015). Fructose can act similarly to glucose in repressing p*AOX1* through carbon catabolite repression mechanisms (Cereghino & Cregg, 2000; Cregg et al., 2000). Moreover, amino acids such as alanine and disaccharides like trehalose have been reported to influence p*AOX1* regulation, although their mechanisms are not fully understood and may involve indirect effects on central carbon metabolism. Trehalose has no catabolite repression effect on p*AOX1*, but methanol is required for expression (Inan & Meagher, 2001). Figure 2-3 presents a summary scheme of the different approaches presented in this section.

4. Advances in autoinduced methanol-free expression systems in *K. phaffi.*

Autoinduced systems in *K. phaffii* represent an important technological development aimed at reducing dependency on methanol while maintaining high expression levels of recombinant proteins. These systems increase the internal metabolic or environmental cues of the host to regulate expression, thus eliminating the need for external inducers, using metabolites present in the medium or generated by the cells themselves, and simplifying process control.

In recent years, alkaline pH-responsive promoters (p*TSA1*, p*HSP12,* and p*PHO89*) have also been characterized for use in methanol-free fermentation environments, providing tunable expression responsive to extracellular pH shifts (Albacar et al., 2024). Based on transcriptional profiles, genes inducible under carbon-limited conditions have been identified. A methanol-free alternative has been developed using glycerol as the sole carbon source and a heat shock-associated promoter (p*DH*). The promoter is induced under carbon starvation, when carbon availability is low, and growth is slowed. In fed-batch cultivations with slow glycerol feeding, CalB gene expression under p*DH* was increased 2.3-fold compared to control cultivations using the constitutive p*GAP* promoter (Bernat-Camps et al., 2023).

Metabolite-responsive systems that detect the accumulation of specific intracellular signals have been investigated. Recently, a hypoxia-responsive expression system has been constructed (Zhou et al., 2023), which triggers induction under oxygen-limited conditions, commonly encountered in high-cell-density bioreactors.

Further strategies involve responsive systems to stress signals, oxygen availability, or metabolite accumulation (Figure 2-4), creating robust, self-regulating expression platforms capable of adjusting to bioprocess conditions (Vogl et al., 2016). Collectively, these advances underscore the diversity of metabolic and regulatory contexts being harnessed to create robust, self-regulating expression platforms in *K. phaffii,* relevant for regulatory standards (e.g., European Medicines Agency (EMA),

US Food and Drug Administration (FDA), approving the development of industrial microbial bioprocesses to mitigate use of volatile organic solvents (P. Kumar & Singh, 2024). In this context, autoinducible systems represent a key direction for developing the next generation of safe, scalable, and efficient bioprocesses.

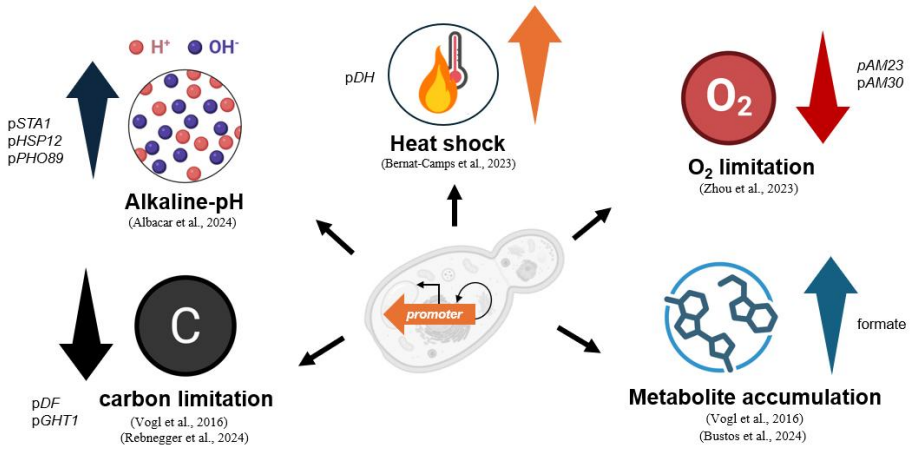

Figure 2-4. Main approaches in advances in autoinduced methanol-free expression systems in *K. phaffi.*

4.1 Formate as an emerging inducer of p*AOX1.*

Formate is a particularly interesting inducer. Early studies showed that co-fed with methanol significantly induced p*AOX1*, even in wild-type strains, suggesting a previously underexplored pathway of induction.(Jayachandran et al., 2017b). Years after it was demonstrated that this metabolite may also induce p*AOX1* (Singh & Narang, 2020).

The effect of ammonium formate concentration in glycerol media on p*AOX1* induction was investigated. The optimal concentration was found to be 0.7%, which produced 17.5% of the induction level observed with methanol. Under these conditions, reduced energy availability has been reported, and ATP supplementation in the culture media was shown to improve recombinant protein expression by enhancing cellular energy status (Feng et al., 2022).

In other studies, different ammonium formate concentrations were tested using formate as an inducer through Mit1 overexpression to enhance p*AOX1* induction. Xylanase was used as a model protein. The highest induction was achieved with 0.2% ammonium formate, resulting in a 1.43-fold increase of xylanase activity compared with only ammonium formate induction. Under these conditions, xylanase yield increased by 42% when 0.05% sorbitol was added as a supplemental carbon source (B. Liu, Li, et al., 2022a). Lately, this strategy was further improved by incorporating additional genes: acetaldehyde dehydrogenase (ACDH) from the non-pathogenic

Listeria innocua and acetyl-CoA synthase (ACS) from *Escherichia coli,* achieving 73% higher than the control strain in these conditions (B. Liu, Zhao, et al., 2022a).

The previously described formate-based systems rely on external supplementation, as formate must be added to the culture medium to act as an inducer of p*AOX1*. In contrast, autoinduction systems have been developed to overcome the need for exogenous inducers. In these systems, intracellular metabolic states or environmental cues are exploited to regulate gene expression, thereby eliminating the requirement for external inducer addition and enabling the use of metabolites naturally present in the medium or generated by the cells.

In this context, a methanol-regulated *AOX1* expression system was re-engineered in *K. phaffii* FDH-deficient strains to enable endogenous formate-driven induction (Bustos et al., 2024). In this system, a metabolic engineering approach was implemented to exploit p*AOX1* induction in FDH-deficient strains.

To establish the metabolic conditions supporting promoter induction, an initial carbon source screening (sorbitol/formate, methanol, and sorbitol media) was performed using enhanced green fluorescent protein (eGFP) as a reporter system for p*AOX1* induction. In this experiment, FDH wild-type and FDH-deficient strains were compared to evaluate the eGFP expression level. Based on these results, sorbitol was identified as a suitable non-repressive carbon source for subsequent experiments, and all further analyses were therefore focused on sorbitol-based cultivation systems (Figure 2-5).

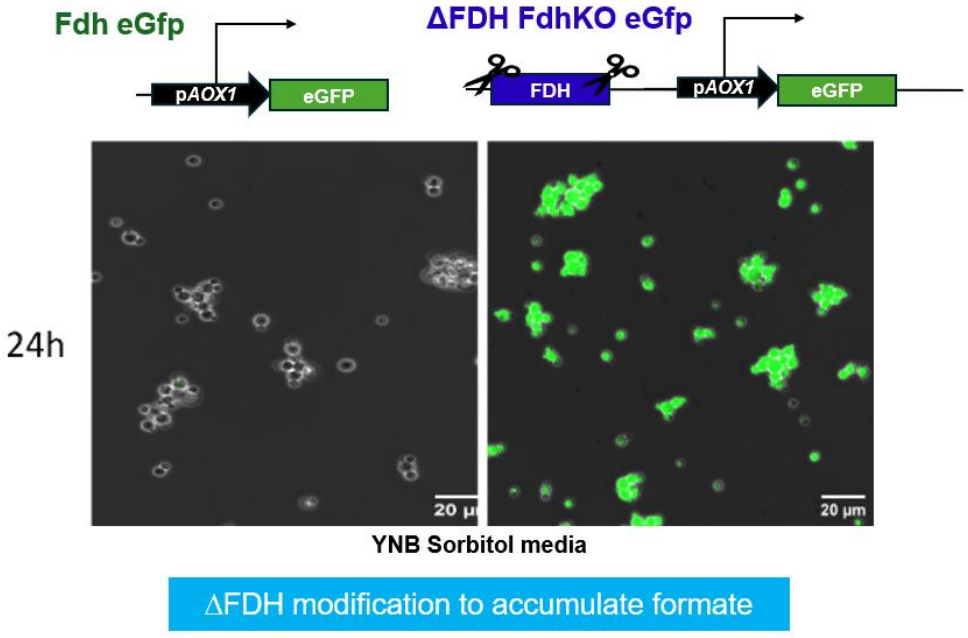

Figure 2-5. Observation of *Komagataella phaffii*, Fdh eGfp strain, and FdhKO eGfp strain (FDH-deficient strain) after 24h of growth in YNB-sorbitol by fluorescent microscopy (Adapted from Bustos, 2024)

To elucidate the underlying mechanism, stepwise gene deletions were performed to modify formate metabolism. Enzymes involved in THF-C1 pathway were selectively disrupted, including mitochondrial serine hydroxymethyltransferase (*SHM1*) and cytosolic serine hydroxymethyltransferase (*SHM2*), both individually and in combination. These results substantiate the hypothesis that intracellular formate is higher in the FDH-deficient eGFP strain, accounting for p*AOX1* induction under non-repressive cultivation conditions.

Within this framework, serine metabolism was experimentally validated as a functional contributor to one-carbon flux. A significant increase in *AOX1*-driven specific fluorescence was observed compared to non-supplemented controls. The specific fluorescence values for the FDH-deficient strain were 4.0- and 6.1-fold increased on sorbitol and sorbitol-serine media, respectively, compared to the control strain. This response confirmed enhanced availability of C1 units through the tetrahydrofolate-linked network. Serine-derived carbon was therefore directly linked to promoter induction output (Figure 2-6).

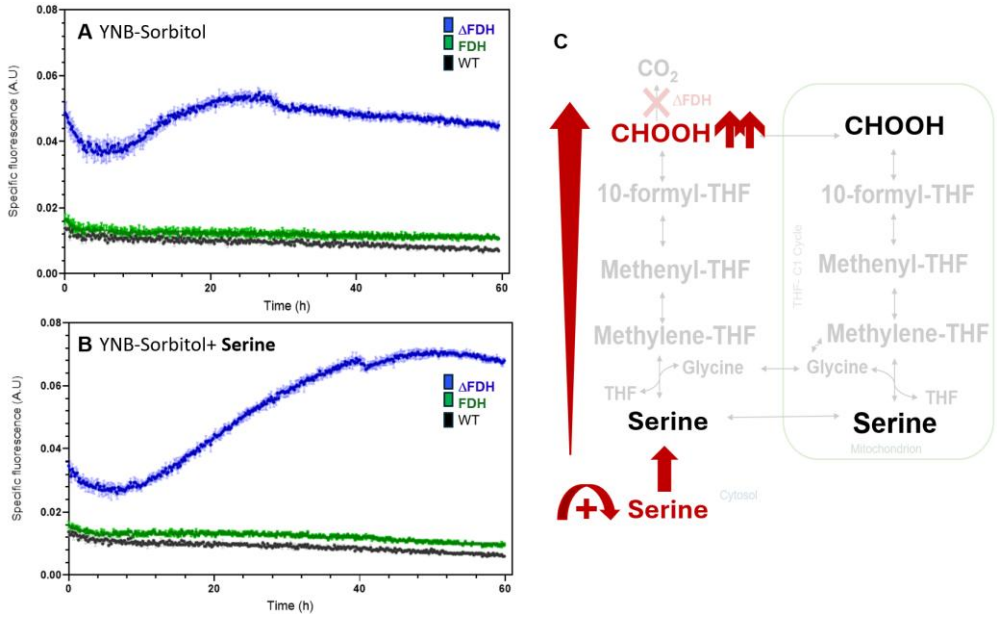

Figure 2-6. Specific eGFP fluorescence of Fdh strain (black); Fdh eGfp strain (green); FdhKO eGfp strain (blue); during growth in YNB minimal medium containing sorbitol, panel A, YNB minimal medium containing sorbitol and serine, panel B, THF-C1 metabolism scheme with adding serine, red effect indicated in panel C. Cells were grown in BioLector, and specific fluorescence values are means and standard deviation on four culture replicates. sFU: Specific fluorescence unit. (Adapted from Bustos, 2024)

The system was further evaluated using eGFP as a quantitative reporter to characterize p*AOX1* induction under FDH-deficient conditions. A 1.9-fold increase was measured in the FDH-deficient eGFP strain compared to the control strain, with absolute fluorescence values of 100,359 TFU and 51,724 TFU, respectively, in sorbitol media. These results confirmed that promoter induction was strongly dependent on intracellular metabolic rewiring under the selected carbon source.

Subsequently, recombinant protein production was assessed using *Candida antarctica lipase* B (CalB) as a functional secretion model. The specific lipase activity was significantly increased in the FDH-deficient CalB strain, reaching a 130-fold higher activity compared to the control strain under sorbitol cultivation. This transition from reporter-based analysis to secreted protein production validated the scalability of the metabolic effect.

The observed phenotype was attributed to intracellular formate accumulation driven by both reduced sorbitol consumption capacity and increased upstream C1 flux. Formate was proposed as an indirect endogenous effector of p*AOX1* induction, establishing a metabolically driven self-induction mechanism.

This finding demonstrates the expanded utility of endogenous C1 metabolism in regulatory control on this system (Figure 2-7). Formate is positioned as a potential indirect regulation, enabling an autonomous induction system without methanol or formate supplementation.

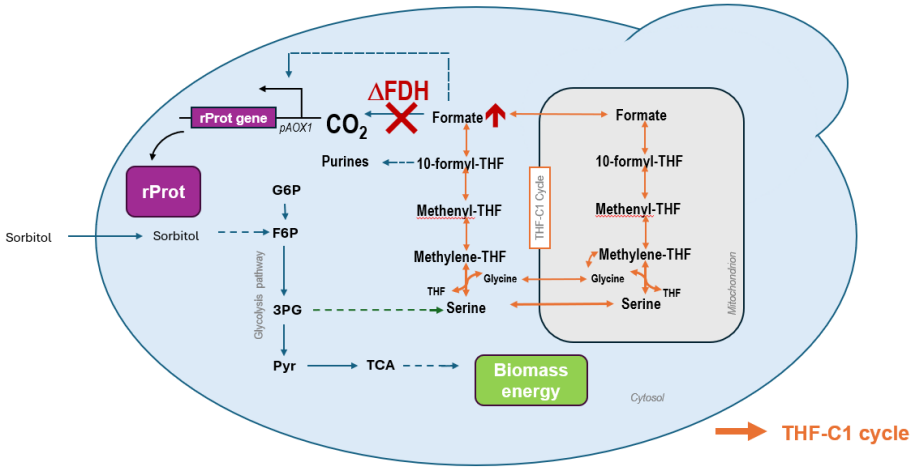

Figure 2-7. Overview of the connection between sorbitol metabolism, serine pathway, and Tetrahydrofolate (THF) mediated one-carbon (THF-C1) metabolism in FDH-deficient K. phaffii. Arrows in orange are related exclusively to THF-C1 metabolism. ΔFDH: formate dehydrogenase gene deleted; THF, tetrahydrofolate; rProt: recombinant protein. G6P, glucose-6-phosphate; F6P: fructose-6-phosphate; G3P, 3-phosphoglycerate; Pyr, pyruvate; TCA: tricarboxylic acid cycle.

Despite these advances, reduced growth performance was still observed in FDH-deficient strains cultivated on sorbitol compared to glycerol, with specific growth rates of 0.02 $g \cdot gDCW^{-1} \cdot h^{-1}$ and 0.9 $g \cdot gDCW^{-1} \cdot h^{-1}$, respectively. This limitation

indicated an underlying constraint in carbon assimilation and metabolic efficiency under sorbitol-based conditions.

Serine supplementation was shown to increase intracellular formate accumulation in the FDH-deficient mutant strain when grown on sorbitol media, confirming the functional contribution of serine-derived carbon units to the THF-C1 pathway and formate pool formation. However, despite its positive effect on formate accumulation, serine addition was considered poorly scalable and economically impractical for large-scale bioprocess applications.

Therefore, these observations highlighted a key metabolic bottleneck in endogenous formate generation under sorbitol-based cultivation. In this framework, both carbon assimilation capacity and C1 precursor availability were identified as limiting factors for optimal formate accumulation and *AOX1* promoter induction. Consequently, these constraints directly support the rationale of this doctoral project. The following chapters build progressively on this foundation through strategies aimed at increasing endogenous formate availability in the FDH-deficient platform: Chapter 3 focuses on improving sorbitol utilization, based on the hypothesis that enhancing sorbitol uptake and metabolism would increase carbon flux towards formate formation, a key metabolite known to accumulate in the FDH-deficient strain and to act as an auto-inducer of the p*AOX1* promoter. Chapter 4 focuses on metabolic flux redirection through the serine pathway, building on prior observations that serine supplementation in sorbitol-based cultures enhances p*AOX1* induction in the FDH-deficient strain, though to enhance endogenous formate accumulation. Finally, chapter 5 addresses secretion as a downstream bottleneck, identifying improved signal peptides using *Y. lipolytica* as a discovery platform to support future optimization of methanol-free protein production in *K. phaffii.*

Chapter 3

Sorbitol uptake and oxygen transfer shape AOX1 promoter induction under methanol-free condition in Komagataella phaffi lacking formate deshydrogenase

Description of Chapter 3

In the previous chapter, recent advances in Komagataella phaffii as a yeast cell factory were discussed, with particular emphasis on the p*AOX1* promoter and methanol-free expression systems, especially those based on formate as an autoinducer.

Building on this context, the present chapter investigates the impact of carbon source metabolism on the FdhKO strain through metabolic engineering approaches, with a specific focus on sorbitol utilization and its influence on p*AOX1* promoter induction.

The work presented in this chapter constitutes an integral part of my doctoral research and is based on a co-authored publication. The study was carried out in close collaboration with PhD C. Bustos, with joint involvement throughout all stages of the work.

The chapter reflects my direct scientific contribution to the conception and development of the study within the framework of my doctoral project.

Within this framework, my contribution encompassed the experimental design, execution of culture and molecular biology experiments, data analysis, interpretation of results, and manuscript preparation. The study reflects a shared intellectual and experimental contribution between both authors.

This work is an original contribution adapted from:

- Bustos, C., Cozmar, R., Berrios, J., & Fickers, P. (2025). “Sorbitol Uptake and Oxygen Transfer Shape *AOX1* Promoter Induction in Formate Dehydrogenase-Deficient. *Komagataella phaffii*”. *Microbial Biotechnology*, *18*(11), e70263. https://doi.org/10.1111/1751-7915.70263

Chapter 3: Sorbitol uptake and oxygen transfer shape *AOX1* promoter induction under methanol-free conditions in *Komagataella phaffi* lacking formate dehydrogenase.

1. Introduction.

Recently, we demonstrated that formate from THF-C1 metabolism is accumulated in FDH-deficient *K. phaffii* strain (FdhKO) when grown in a sorbitol-based methanol-free medium. This endogenous formate was shown to be sufficient to trigger p*AOX1* induction without the need for external inducer supplementation, indirectly influencing p*AOX1* induction. This finding is particularly significant because any p*AOX1*-based expression system can be converted into a self-induced system in ~~an~~ FdhKO strain. When cells are cultivated in a mixture of glycerol and sorbitol, recombinant protein (rProt) synthesis is initiated at the end of the exponential growth phase, upon glycerol depletion from the culture medium. Using the secreted lipase CalB from *Candida antarctica* as a model protein, comparable productivities were obtained with an FdhKO CalB strain grown on sorbitol and an Fdh-expressing CalB strain grown on methanol (Bustos et al., 2024).

Within this context, the choice of carbon source becomes particularly relevant. Unlike glucose or methanol, which strongly influence repression or induction dynamics, alternative substrates such as sorbitol can offer a more balanced metabolic input. Sorbitol is considered a non-repressing carbon source in *K. phaffii.* Sorbitol is a six-carbon polyol that does not repress p*AOX1* induction and can, therefore, be used as a co-substrate during methanol induction (Ergün et al., 2022; Niu et al., 2013). After being transported across the plasma membrane by a hexose transporter (Jordan et al., 2016), sorbitol is converted into fructose by sorbitol dehydrogenase. Fructose is subsequently phosphorylated by hexokinase before entering the glycolysis pathway (Figure 3-4). The *K. phaffii* growth rate on sorbitol is low, 0.03 h^{-1} (Niu et al., 2013; Singh & Narang, 2023) with a substrate to biomass conversion yield ($Y_{x/s}$) of 0.56 $g \cdot g^{-1}$ (Singh & Narang, 2023). Recently, formate has emerged as a promising alternative inducer of p*AOX1*-driven rProt production (Jayachandran et al., 2017b; Singh & Narang, 2020; Tyurin & Kozlov, 2015). In the methanol dissimilation pathway (Berrios et al., 2022), formate is generated from formaldehyde by formaldehyde dehydrogenase (Fld) and further converted into carbon dioxide by formate dehydrogenase (Fdh) (Hartner & Glieder, 2006; Figure 3-4). Additionally, formate is an intermediate in the tetrahydrofolate-mediated one-carbon (THF-C1) metabolism, which plays a role in several anabolic pathways, including de novo purine synthesis (Christensen & MacKenzie, 2006; Figure A3-4).

However, in *K. phaffii* energy generation is a known bottleneck for rProt synthesis in methanol-free p*AOX1*-based processes (Feng et al., 2022). Since the low sorbitol consumption rate by *K. phaffii* could potentially limit rProt productivity in an FdhKO strain, we aimed to enhance sorbitol metabolism in an FdhKO strain and assess the

impact on rProt productivity. Limitations in uptake sorbitol and downstream metabolic assimilation can restrict its effectiveness as a carbon backbone supporting growth and rProt production. As oxygen availability to cells can also be a limiting factor for rProt synthesis, this parameter was also considered for strains optimized for sorbitol metabolism. Our results highlight that the combination of poor sorbitol utilization and low oxygen transfer conditions (OTC) enhances formate accumulation in *K. phaffii* FdhKO cells, thereby promoting higher rProt productivity.

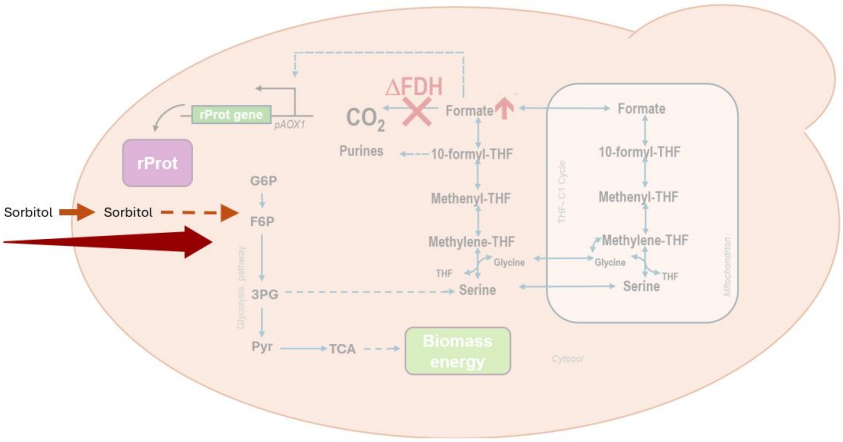

Figure 3-1. Strategy proposal overview focused on enhancing sorbitol metabolism in FDH-deficient strain.

Therefore, this chapter has been focused on the metabolic engineering of sorbitol uptake and in FDH-deficient *K. phaffii* (Figure 3-1) by enhancing sorbitol entry and assimilation at the level of transport and primary metabolism and test of OTC conditions, we aim to establish a metabolic state that supports improved cellular performance and indirectly enhances conditions favorable for *AOX1*-driven expression systems.

2. Experimental procedures.

2.1 Strains, media and culture conditions.

The *Escherichia coli* and *K. phaffii* strains used in this study are listed in Table 3-1 and A3-1. *E. coli* was grown at 37°C in Luria-Bertani medium (LB), supplemented with antibiotics as follows: 100 $\mu g \cdot mL^{-1}$ ampicillin, 50 $\mu g \cdot mL^{-1}$ kanamycin, or 25 $\mu g \cdot mL^{-1}$ zeocin. *K. phaffii* was grown at 30 °C either on YPD medium (20 $g \cdot L^{-1}$ glucose, 10 $g \cdot L^{-1}$ Difco yeast extract, and 10$g \cdot L^{-1}$ Difco bacto peptone) or in YNB medium (1.7 $g \cdot L^{-1}$ Difco YNB w/o ammonium chloride and amino acids, 5 $g \cdot L^{-1}$ NH_4Cl and, 0.4 $mg \cdot L^{-1}$ biotin, 100 mM potassium phosphate buffer, pH 6.0) supplemented with 10 $g \cdot L^{-1}$ sorbitol (YNBS), 1.75 $g \cdot L^{-1}$ glycerol (YNBG0), 1.75 $g \cdot L^{-1}$ glycerol and 1.75 $g \cdot L^{-1}$ sorbitol (YNBGS2), 1.75 $g \cdot L^{-1}$ glycerol and 3.5 $g \cdot L^{-1}$ sorbitol

(YNBGS4) or 20 $g \cdot L^{-1}$ sorbitol (YNBS2). *K. Phaffii* transformants were selected on YPD agar plates, supplemented with 25 $\mu g \cdot mL^{-1}$ zeocin (YPD-Zeo). Precultures were operated as previously described (Bustos et al., 2024). Cultures were performed in Erlenmeyer shake flasks (50 mL or 250 mL) or in microbioreactors (BioLector 2, m2p-labs, Baesweiler, Germany) as previously described (Bustos et al., 2024). Cultures under different oxygen transfer conditions (OTC) were carried out as previously described in 250 mL Erlenmeyer flasks containing varying medium volumes to benchmark oxygen transfer coefficients (K_La) of 10, 50, and 100 h^{-1} (Gorczyca et al., 2020).

2.2 Construction of plasmid and K. phaffii strains.

The general genetic techniques were as described elsewhere (Bustos et al., 2024). The plasmids and primers used are listed in Tables A3-1 and A3-2. The SdOE and StOE expression vectors were constructed using the GoldenPiCS (Prielhofer et al., 2017).

Design and preparation of gene inserts.

The gene PAS_chr1-1_0490 (*SOR1*) was PCR-amplified using *K. Phaffii* GS115pro genomic DNA as a template, and an internal *Bpi*I recognition sequence in gene PAS_chr1-1_0490 (*SOR1*) was removed by overlapping PCR with primers SOR1-Fw/ SOR1-Rv.

In the gene PAS_chr1-4_0570 (Pp*HXT1*), internal *Bpi*I and *Bsa*I recognition sequences were removed through in silico design by selecting alternative commonly used synonymous codons, and the synthetic gene was designed with the addition of external *Bsa*I recognition sequences.

The corresponding synthetic DNA fragment was obtained from Eurofin Genomic (Ebersberg, Germany).

Plasmid construction.

Both *SOR1* and Pp*HXT1* inserts were cloned into plasmid A2 (BB1_23) at the BsaI site, generating:

Table 3-1. Plasmids with *SOR1* and Pp*HXT1* genes cloned.

Plasmid	Construct
RIE341 (RIP341)	A2_BB1_23_*SOR1*
RIE343 (RIP343)	A2_BB1_23_Pp*HXT1*

Supporting information of plasmids in Table A3-1

Positive constructs were verified by colony and plasmid PCR with M13-Fw/M13-Rv.

Construction of single expression cassettes.

Expression cassettes were assembled using GoldenGate with *Bpi*I as restriction enzyme from:

- A4 (p*GAP* promoter)
- C1 (*ScCYC1* terminator)
- D12 (BB3aZ backbone)
- RIP341 or RIP343 inserts

This yielded the plasmid described in Table 3-2:

Table 3-2. Plasmids with *SOR1* and Pp*HXT1* expression vectors.

Plasmid	Description
RIE354 (RIP354)	p*GAP*-S*OR1*-*ScCYC1*tt
RIE355 (RIP355)	p*GAP*-Pp*HXT1*-*ScCYC1tt*

Supporting information of plasmids in Table A3-1

The correctness of the assembly constructs was verified by colony and plasmid PCR with primers pair pGAPInt-Fw/ScCYC1tt.Int-Rv. This procedure is illustrated in Figure 3-2.

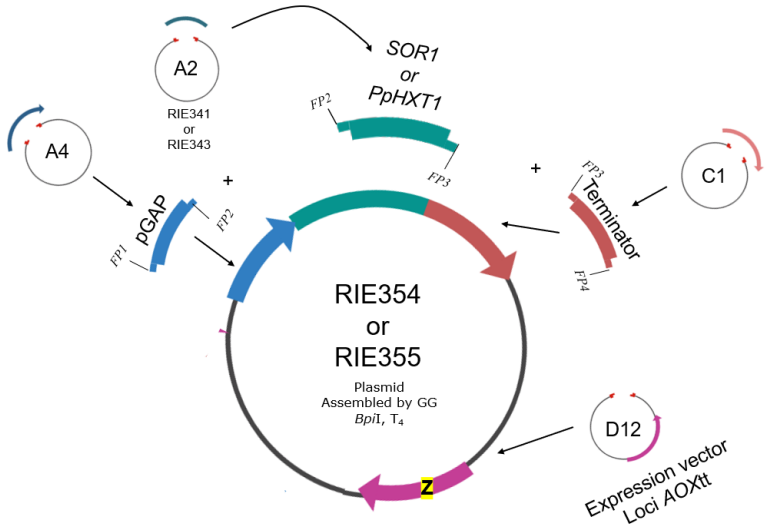

Figure 3-2. Scheme of plasmid construction to obtain RIE354 and RIE355 by GoldenPiCS assembly of different gene fragments. GG: GoldenPiCS assembly method; T_4: Ligase T_4; Z: Zeocin selection marker.

Construction of multi-gene assembly platform.

The Loxp-Zeo-Loxp was released from plasmid D12 (BB3aZ_14) by *Hind*III and *Pst*I restriction and cloned at the corresponding site of C12(BB3aK_AC) to yield plasmid RIE370 (BB3-AC-LoxP-Zeo-loxP, hereafter RIE370).

A three-step GoldenPiCS assembly strategy was used:

Step 1 – *SOR1* cassette
- Plasmid: RIE372 (RIP372)
- Construct: p*GAP*-*SOR1*-*ScCYC1*tt
- Assembly from: RIE341, A4, C1, D4 (*Bsa*I)

Step 2 – Pp*HXT1* cassette
- Plasmid: RIE374
- Construct: p*GAP*-Pp*HXT1*-*RPS3*tt
- Assembly from: RIE343, A4, C9, D5 (*Bsa*I)

Step 3 – Final dual construct
- Plasmid: RIE378 (RIP378)
- Construct: dual cassette *SOR1* + P*pHXT1*

Assembly from: RIE372 + RIE374 + RIE370 (*Bpi*I)

Plasmid construct confirmation was performed with colony and plasmid PCR with the couple of primers pGAP.Int-Fw/ScCYC1tt.Int-Rv, and pGAP.Int-Fw/ Rps3tt.Int-Rv respectively. This procedure is illustrated in Figure 3-3.

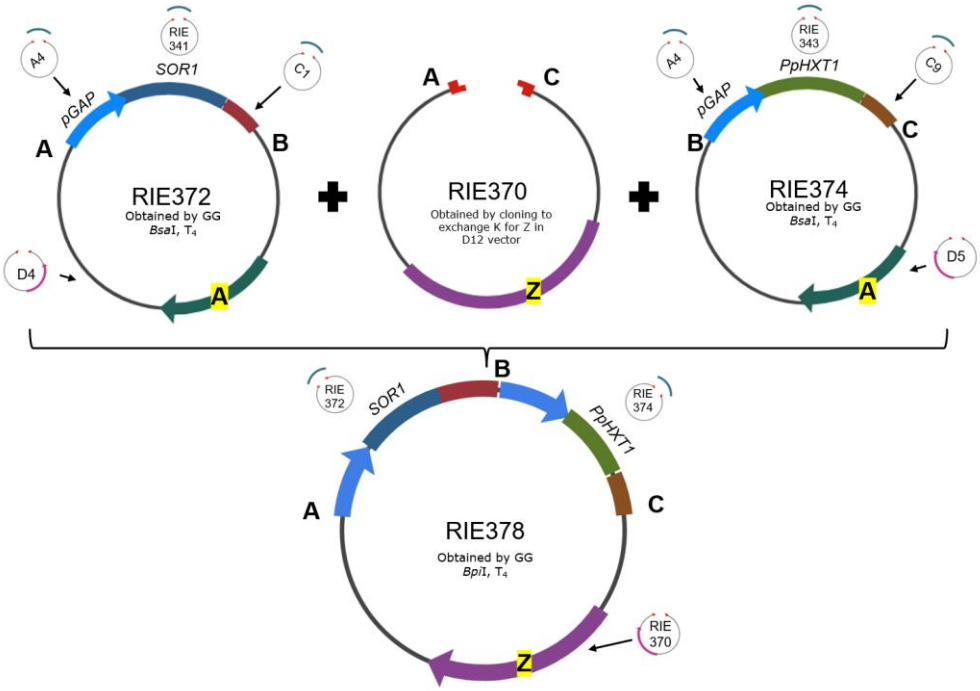

Figure 3-3. Scheme of plasmid construction to obtain RIE370, RIE372, RIE374, and RIE378 by GoldenPiCS assembly of different gene fragments. GG: GoldenPiCS assembly method; T_4: Ligase T_4; Z: Zeocin selection marker.

Yeast strain construction.

The construction of yeast strains RIY230 (Fdh eGfp), RIY308 (Fdh CalB), RIY536 (FdhKO eGfp Z^+), RIY537 (FdhKO CalB Z^+), RIY540 (FdhKO eGfp), and RIY561 (FdhKO CalB) is described elsewhere (Bustos et al., 2024; Velastegui et al., 2019). Strains of this study were obtained by transformation of RIY232, RIY540, and RIY561 with *Asc*I-linearized plasmids described in Table 3-3:

Table 3-3. Yeast strains generated by transformation using plasmids constructed for this study.

Strain	Simplified genotype	Plasmid	Host strain
RIY529 (SdOE)	p*GAP-SOR1*	RIP354	RIY232
RIY530 (StOE)	p*GAP*-Pp*HXT1*	RIP355	RIY232
RIY532 (St&SdOE)	p*GAP-SOR1* + p*GAP*-Pp*HXT1*	RIP378	RIY232
RIY643 (FdhKO-SdOE eGFP)	fdh1Δ, p*GAP-SOR1*, p*AOX1-eGFP*	RIP355	RIY540
RIY562 (FdhKO-SdOE CalB)	fdh1Δ, p*GAP-SOR1*, p*AOX1-CalB*	RIP355	RIY561

Table 3-4. *Komagataella phaffii* strains used in the 3rd chapter.

Number	Names	Parental strain, genotype	Reference
RIY232	GS115pro	GS115, *HIS4*	(Theron et al., 2019)
RIY230	Fdh eGfp	GS115, p*AOX1-eGFP*	(Velastegui et al., 2019)
RIY308	Fdh CalB	GS115, p*AOX1-αMF-CalB*	(Velastegui et al., 2019)
RIY536	FdhKO eGfp Z+	*RIY230, fdh1*Δ, p*AOX1-eGFP* Zeo+	(Bustos et al., 2024)
RIY537	FdhKO CalB Z^+	*RIY308, fdh1*Δ, p*AOX1*-αMF-*CalB* Zeo^+	(Bustos et al., 2024)
RIY540	FdhKO eGfp	RIY536, *fdh1*Δ, p*AOX1-eGFP* Zeo^-	(Bustos et al., 2024)
RIY561	FdhKO CalB	RIY537, *fdh1*Δ, p*AOX1*-αMF-*CalB* Zeo^-	(Bustos et al., 2024)
RIY529	SdOE	RIY232, p*GAP-SOR1*	This work
RIY530	StOE	RIY232, p*GAP*-Pp*HXT1*	This work
RIY532	St&SdOE	RIY232, p*GAP-SOR1,* p*GAP*-Pp*HXT1*	This work
RIY643	FdhKO-SdOE eGfp	RIY540, *fdh1*Δ, p*AOX1-eGFP,* p*GAP-SOR1*	This work
RIY562	FdhKO-SdOE CalB	RIY561, *fdh1*Δ, p*AOX1-αMF-CalB*, p*GAP-SOR1*	This work
RIY655	FdhKO GOx	*fdh1*Δ, p*AOX1-αMF-GOX*	Lab stock (unpublished)
RIY656	FdhKO SdOE GOx	*fdh1*Δ, p*AOX1-αMF-GOX, pGAP-SOR1*	Lab stock (unpublished)

The genotype of RIY529, RIY530, RIY532, RIY643, and RIY564 strains was verified by PCR using the primers pGAP.Int-Fw/ScCYC1tt.Int-Rv, pGAP.Int-Fw/ Rps3tt.Int-Rv, which annealed to the p*GAP*, *ScCYC1*tt, and *RPS3*tt regions, respectively. A schematic representation of the strain genotype is presented in Figure A3-7, and the detailed strain genotype is in Table 3-1.

For clarity and readability, plasmids, primers used, and strains are listed in Tables A3-1, A3-2, and Table 3-4, respectively, while only strain codes are used throughout this chapter.

2.3 Analytical methods.

Cell growth was monitored either by optical density at 600nm (OD_{600}) or dry cell weight (DCW). An OD_{600} value of 1 was found to correspond to 0.65 $gDCW \cdot L^{-1}$. Sorbitol and glycerol concentrations were determined using high-performance liquid chromatography as described elsewhere (Bustos et al., 2024).

Intracellular eGFP fluorescence was quantified using a BD Accuri C6 Flow Cytometer (BD Biosciences, San Jose, CA, USA), as described elsewhere (Bustos et al., 2024; Sassi et al., 2016). To calculate the total value of fluorescence in the cell population, the FL1-A median value (i.e., the eGFP fluorescence) was multiplied by the fraction of cells with eGFP fluorescence (i.e., induced cells). It was expressed in total fluorescence unit (TFU). During cultures in microbioreactor, the eGFP fluorescence was quantified at 620 nm (excitation at 488) and expressed as specific fluorescence (sFU). For that purpose, fluorescence values were divided by the biomass values. The specific fluorescence value of the parental strain GS115pro was subtracted from the specific fluorescence of eGFP-producing strains to normalize the data.

Formate concentration in the culture supernatant were measured using the formic acid assay kit (Megazyme Inc., Bray, Ireland) according to the manufacturer's instructions. Lipase activity in the culture supernatant was determined by monitoring the hydrolysis of p-nitrophenylbutyrate (p-NPB), following the protocols detailed elsewhere(Fickers et al., 2003). Glucose oxidase activity was monitored using a glucose oxidase assay kit (Megazyme Inc., Bray, Ireland) according to the manufacturer's instructions. For formate and enzymatic assay absorbance at a specific wavelength were monitored over time using a SpectraMax M2 (Molecular Devices, San Jose, CA, USA). All assays were conducted in triplicate.

2.4 Calculations of Cultivation Kinetic Parameters.

The specific growth rate was calculated as:

$$\mu = \frac{1}{X}\frac{dX}{dt}$$

Where X is the biomass ($gDCW \cdot L^{-1}$) and t is the time (h)

The specific sorbitol up-take rate (qSor) was calculated as:

$$qSor = \frac{d[sorbitol]}{dX.t}$$

Where [sorbitol] is the sorbitol concentration, X is the biomass ($gDCW \cdot L^{-1}$) and t is the time (h).

3. Results and Discussion.

3.1 Overexpression of the sorbitol dehydrogenase encoding gene increases the sorbitol uptake rate.

In *K. phaffii*, low energy generation is known as a limitation for rProt production in methanol-free processes based on the p*AOX1* (Feng et al., 2022). During the rProt production phase, sorbitol is one of the most widely used co-substrates (Carly et al., 2016; Çelik et al., 2009; Niu et al., 2013. Unfortunately, the ability of *K. phaffii* to catabolize sorbitol is low, potentially limiting the energy and carbon provision required for rProt synthesis. Sorbitol transport across the plasma membrane and its conversion to fructose by sorbitol dehydrogenase (Figure 3-4) have been identified as potential bottlenecks in sorbitol assimilation (Akentyev et al., 2023).

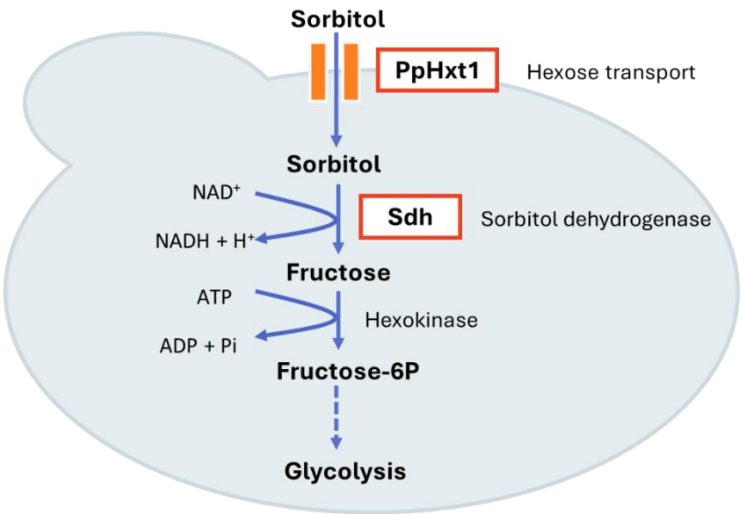

Figure 3-4. Sorbitol metabolism in *K. phaffii*: PpHxt1, a hexose transporter, is evaluated in this investigation as a putative sorbitol transporter; Sdh refers to sorbitol dehydrogenase.

The genes encoding these proteins have not yet been reported in *K. phaffii*. In *Saccharomyces cerevisiae*, the hexose transporter Hxt15 has been identified as a versatile polyol transporter, including for sorbitol (Jordan et al., 2016). Additionally,

the gene encoding sorbitol dehydrogenase (Sdh, *SOR1*) has been characterized in both *S. cerevisiae* and *Komagataella kurtzmanii* (Akentyev et al., 2023; Toivari et al., 2004). A protein BLAST search using the translated *SOR1* and *HXT15* sequences from *S. cerevisiae* as queries highlighted the genes PAS_chr1-1_0490 (*SOR1*, 55.6% identity) and PAS_chr1-4_0570 (Pp*HXT1*, 51% identity) as putative Sdh and Hxt candidates, respectively (Figure A3-5 and A3-6).

To increase the sorbitol uptake rate, these two genes were expressed under the control of the constitutive p*GAP* promoter, either individually or in combination, in the GS115pro strain, a prototrophic derivative of strain GS115 (Table 3-4). In the resulting StOE strain, the sorbitol uptake rate and cell growth rate increased by 1.7 and 1.2-fold, respectively, compared to the parental GS115pro strain (Table 3-5). For the SdOE strain, these rates were enhanced by 5.0 and 3.3-fold, respectively. However, for the St&SdOE strain, which co-expressed both, the sorbitol uptake rate and cell growth rate were not further enhanced compared to the SdOE strain (1.06 and 1.03-fold, respectively). These findings demonstrate that the expression of the *SOR1* gene alone can overcome the limiting step of sorbitol assimilation in *K. phaffii*.

Table 3-5. Effects of *SOR1* and Pp*HXT1* genes overexpression on specific growth rate and the specific consumption rate of sorbitol.

Strains (genotypes)	μ (h^{-1})	qSor ($g \cdot gDCW^{-1} \cdot h^{-1}$)
GS115pro (GS115 prototroph)	0.036	0.03
StOE (p*GAP*-Pp*HXT1*)	0.042	0.05
SdOE (p*GAP-SOR1*)	0.119	0.15
St&SdOE (p*GAP-SOR1*, p*GAP*-Pp*HXT1*)	0.122	0.16

Abbreviations: μ, specific growth rate; DCW, dry cell weight; qSor, specific sorbitol uptake rate. These cultures were performed in triplicate 250 mL flasks containing 25 mL of medium. Standard deviations were less than 10% of the presented mean values.

3.2 Enhancing sorbitol metabolism decreases pAOX1 induction in FdhKO strains on methanol-free medium

In many rProt production processes, glycerol is commonly used as a carbon source for biomass formation, while a p*AOX1* non-repressive carbon source, such as sorbitol, is preferred during the rProt synthesis phase (Ergün et al., 2022). Therefore, biomass and eGFP fluorescence were monitored for strains FdhKO eGfp and FdhKO SdOE eGfp grown in microbioreactors in media containing glycerol and sorbitol in different ratios (1:0, 1:1, 1:2; YNBG0, YNBGS2, and YNBGS4 medium, respectively (Figure 3-5). Both strains exhibited diauxic growth, consuming glycerol within the first 8 hours of culture, followed by a sorbitol consumption phase (Figure A3-8). While both strains grew similarly on glycerol, marked differences were observed during the sorbitol consumption phase for the FdhKO eGfp and FdhKO SdOE eGfp strains (e.g., 0.035 ± 0.001 and 0.129 ± 0.001 h^{-1} on YNBGS4 medium, respectively). This

confirms that the overexpression of *SOR1* increases the carbon assimilation and energy generation in *K. phaffii* grown on sorbitol.

Upon glycerol depletion in YNBG0 medium (in the absence of sorbitol), the specific fluorescence signals increased slightly within the same range for both the FdhKO eGfp and FdhKO SdOE eGfp strains (i.e., between 0.015 and 0.014 sFU), likely due to the derepression of p*AOX1* following glycerol depletion. Conversely, in sorbitol-containing media (YNBGS2 and YNBGS4), eGFP-specific fluorescence markedly increased for the FdhKO eGFP strain, reaching maximal values of 0.060 and 0.065 sFU, respectively. In contrast, the increase was less pronounced in the FdhKO SdOE eGfp strain, with maximal values of 0.032 and 0.028 sFU, respectively. These findings highlight that p*AOX1* induction is lower at higher sorbitol uptake rates (i.e., upon *SOR1* expression) and that sorbitol concentration does not significantly impact the strength of p*AOX1* induction.

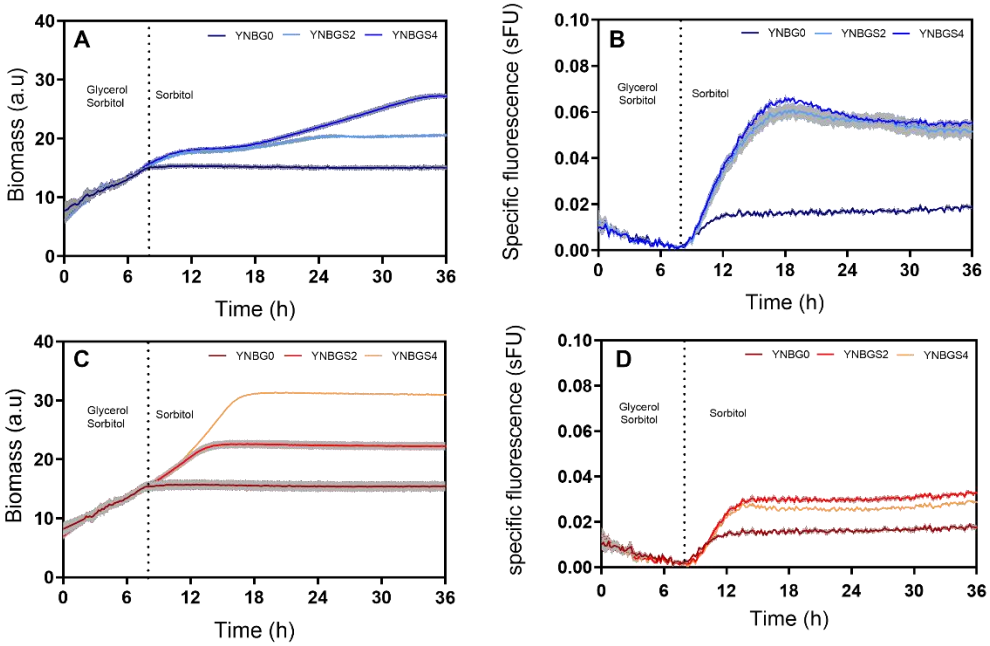

Figure 3-5. Biomass (panels A and C) and specific fluorescence (panels B and D) during the growth of FdhKO eGfp strain (blue colors) and FdhKO SdOE eGfp strain (orange colors) in YNB minimal medium containing different mixtures of glycerol and sorbitol (1:0, 1:1, 1:2; medium YNBG0, YNBGS2, and YNBGS4, respectively). Cells were grown in a BioLector system, and data represent the mean and standard deviation of triplicate cultures. sFU: specific fluorescence unit; a.u: arbitrary units.

Similar experiments were conducted using two secreted enzymes, lipase B (CalB) from *Candida antarctica* and glucose oxidase (Gox) from *Aspergillus niger*, as model proteins. Cell growth and respective enzyme activities, namely lipase or glucose oxidase, were quantified for strains FdhKO CalB, FdhKO SdOE CalB, FdhKO GOx and FdhKO SdOE GOx grown on sorbitol in shake flasks (Figure 3-6). After 36 hours

of culture, both FdhKO SdOE strains showed higher biomass compared to their non-*SOR1*-expressing counterparts, with increases of 4.8 and 6.7-fold observed for the CalB and GOx expressing strains, respectively (Figure 3-6A, C). In contrast, these strains exhibited a 3.5 and 3.6-fold decrease in specific lipase and glucose oxidase activities, respectively, compared to their FdhKO counterparts (Figure 3-6B, D). These results for the secreted proteins align with the trend observed in the eGFP strains (i.e., FdhKO eGfp and FdhKO SdOE eGfp strains, Figure 3-5).

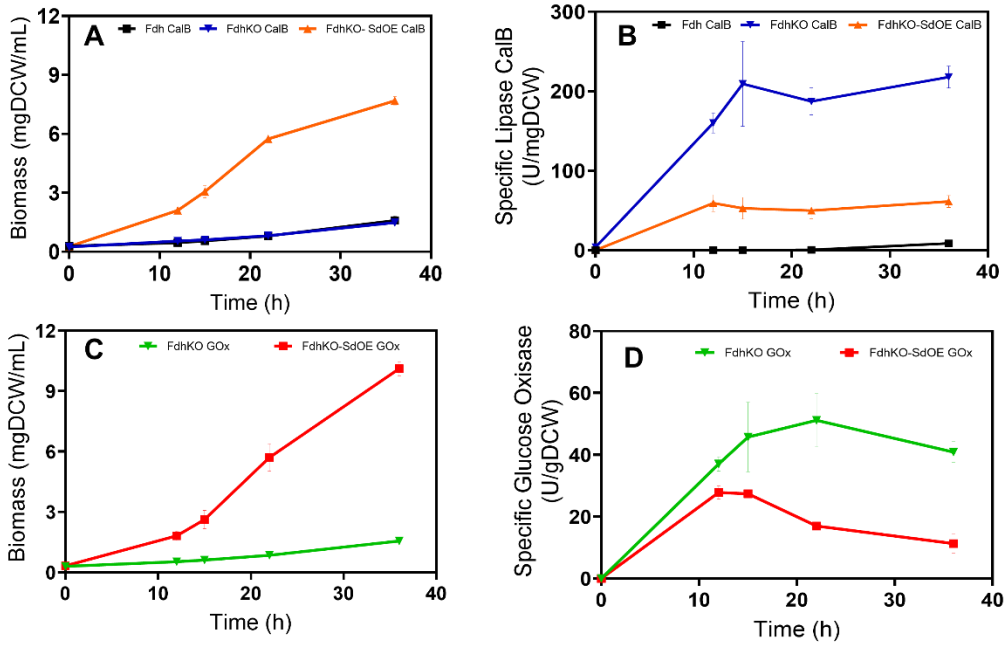

Figure 3-6. Biomass (panel A and C) and specific enzyme activity (panel B and D) during growth of FdhKO CalB (blue), FdhKO GOx (green), FdKO SdOE CalB (orange) and FdKO SdOE GOx (red) strains on YNB minimal medium containing sorbitol (YNBS). Data are the mean and standard deviation of triplicate cultures conducted in shake flasks. Lipase and glucose oxidase assays were performed in triplicates.

3.3 Low oxygen transfer conditions favor the induction of pAOX1 of FdhKO strains grown on sorbitol-based methanol-free medium

Low oxygen availability has been reported to positively influence p*AOX1* induction for cells grown on methanol (Velastegui et al., 2023). This has also been reported for Fab-producing strains grown under carbon-limited conditions at different oxygen supplies (Carnicer et al., 2009). To examine a similar effect on sorbitol media, FdhKO eGfp and FdhKO SdOE eGfp strains were cultivated under different oxygen transfer conditions (OTC). This was achieved by varying the ratio between volumes of the culture medium and the culture flask, yielding culture systems characterized by

different volumetric oxygen transfer coefficients K_La (Gorczyca et al., 2020) K_La values of 10, 50, and 100 h^{-1} were used as benchmarks for low, medium, and high OTC levels, respectively.

The biomass values were measured at mid-exponential growth phase (i.e., after 22 h), and the average growth rate were calculated (Figure 3-7A). For the FdhKO eGfp strain, the growth rate was within the same range for all culture conditions tested with an average value of 0.028 $mgDCW \cdot mL^{-1} \cdot h^{-1}$ on average (Figure 3-7A). Conversely, significant differences were observed for the FdhKO SdOE eGfp strain, with growth rate values of 0.109, 0.285, and 0.337$mgDCW \cdot mL^{-1} \cdot h^{-1}$ on average under low, medium, and high OTC. Therefore, oxygen transfer was most likely a limiting factor for the growth of the FdhKO SdOE eGfp strain compared to the FdhKO eGfp strain. Under all tested culture conditions, the higher growth rate observed in the FdhKO SdOE eGfp strain compared to the FdhKO eGfp strain is due to the overexpression of *SOR1*, which allows the FdhKO SdOE eGfp strain to metabolize sorbitol at a higher rate. At the sampling time, cell growth was not limited by sorbitol availability, as it remained in excess in the culture medium (i.e., at 22h, Figure A3-9).

Cells were also analyzed by flow cytometry to assess both the median eGFP fluorescence and the distribution of the cell population according to eGFP fluorescence signal, distinguishing between non-induced and induced cells (*i.e.*, with eGFP signal above a defined threshold (Theron et al., 2019). The eGFP signal decreased as the oxygen transfer increased (i.e., 36% for FdhKO eGfp and 23% for FdhKO SdOE eGfp strains, on average), although the values did not markedly different between the two strains for a given OTC (with a maximum of 12%) (Figure 3-7B). The comparable reduction in specific eGFP fluorescence observed in the FdhKO eGfp strain, despite its constant growth rate across all OTC conditions ($0.028 \pm 0.002\ h^{-1}$), rules out protein dilution as the cause of the decreased eGFP fluorescence signal in the FdhKO SdOE eGfp strain, where the growth rate increased threefold between low and high OTC. Therefore, the observed reduction in eGFP fluorescence reflects a decrease in p*AOX1* induction.

A significant difference was observed in the fraction of the cell population in an induced state between the two strains and the culture conditions. The FdhKO SdOE eGfp strain exhibited a significantly lower fraction of the population in an induced state compared to the FdhKO eGfp strain, especially at low OTC, with a 7.8-fold difference (i.e., 5.1% vs. 39.2%, respectively; Figure 3-7C). The fraction of the population in an induced state also decreased significantly as oxygen transfer increased, with a 7.6-fold decrease for the FdhKO eGfp strain (i.e., 39.2% vs. 5.2%, respectively). Therefore, at low oxygen transfer, a greater portion of cells are in an induced state. This observation aligns with our previous findings of elevated *AOX1* expression levels under transient hypoxic conditions (Velastegui et al., 2023). In experiments using a p*AOX1-eGFP* strain grown on methanol, phenotypic diversification toward a highly fluorescent phenotype was observed under transient

anoxic stress, with the fraction of the population in the highly fluorescent state increasing as hypoxic stress intensified.

By combining the eGFP fluorescence and the percentage of induced cells, the total fluorescence was calculated. It increased 12-fold for the FdhKO eGfp strain at low OTC compared to high one (i.e., 105,267 and 8,939 TFU, respectively). A similar trend was observed for the FdhKO SdOE eGfp strain, but to a lesser extent, with a 5-fold decrease (i.e., 12,184 and 2,709 TFU, respectively). The total eGFP fluorescence signal, and thus p*AOX1* induction, was 39-fold higher for the FdhKO eGfp strain at low OTC compared to the FdhKO SdOE eGfp strain at high OTC (i.e., 105,267 and 2,709 TFU, respectively) (Figure 3-7D). At low OTC, the e*GFP* gene expression level for the FdhKO eGfp strain was 5.4-fold higher than for the FdhKO SdOE eGfp strain (Figure A3-10). According to these results, the fraction of the cell population in an induced state is greatly affected by the level of oxygen transfer as compared to the strength of induction. Strain behavior is also influenced by the cells ability to metabolize sorbitol (i.e., *SOR1* expression).

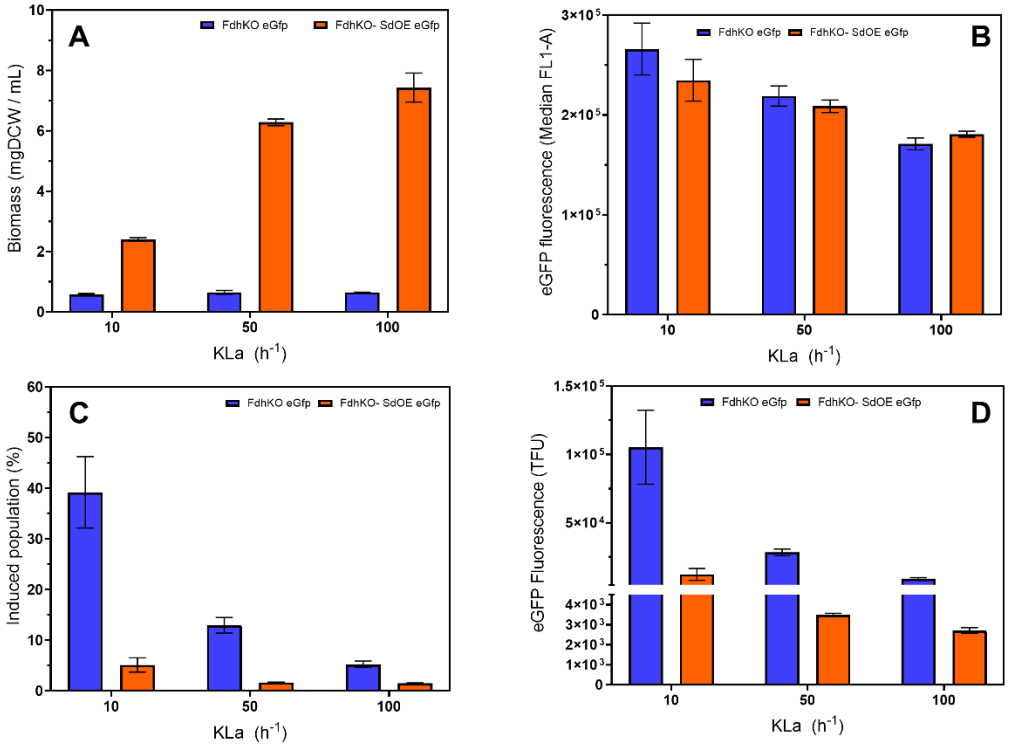

Figure 3-7. Biomass (panel A), Median FL1-A (panel B), induced population (panel C) and total eGFP fluorescence (panel D) for FdhKO eGfp and FdhKO-SdOE eGfp strains cultured strains grown in YNBS2 under different OTC (low, K_La 10 h^{-1}; medium, K_La 50 h^{-1}; high, K_La 100 h^{-1}), in shake-flask cultures. Culture samples were taken at the mid-exponential growth phase (i.e., after 22 h). eGFP fluorescence was quantified by flow cytometry on 20,000 cells

and expressed as TFU (total fluorescence, see materials and method for calculation details). Data are means and standard deviations of triplicate cultures.

3.4 Understanding the differences in pAOX1 induction levels between FdhKO and FdhKO-SdOE strains grown on sorbitol-based methanol-free medium.

In yeast, cytoplasmic formate serves as an intermediate in the THF-C1 pathway, the primary source of C1 units for *de novo* purine synthesis and energy storage molecules (e.g., adenosine triphosphate, ATP; (Christensen & MacKenzie, 2006; Figure A3-4). Disruption of the Fdh encoding gene has been identified as a key factor in intracellular formate accumulation in cells grown on sorbitol, thereby enhancing p*AOX1* induction in a sorbitol-based methanol-free medium (Bustos et al., 2024). However, the reduced eGFP-specific fluorescence, lipase CalB and Gox activities observed in FdhKO-SdOE strains compared to their FdhKO counterparts (Figures 3-5 and 3-6) suggest that additional factors may influence p*AOX1* induction.

Overexpression of *SOR1* in FdhKO strains led to an increased sorbitol uptake rate, resulting in a higher growth rate (Table 3-2). This increased demand for anabolic precursors, including C1 units, likely reduces formate accumulation. To test this hypothesis, formate levels were quantified in the culture supernatants of FdhKO eGfp and FdhKO SdOE eGfp strains grown on sorbitol at different OTC. For the FdhKO SdOE eGfp strain, formate concentrations were markedly lower than for the FdhKO-eGfp strain across all tested OTC (Figure 3-8A). Additionally, formate content decreased for both strains as the oxygen transfer increased. For FdhKO eGfp strain, formate concentration was 32.3 µmol·mgDCW^{-1} at low OTC, whereas it was nearly undetectable for the FdhKO SdOE eGfp strain at high OTC (0.33 µmol·mgDCW^{-1}). Sorbitol metabolism differs between FdhKO-eGfp and FdhKO-SdOE-eGfp strains due to *SOR1* overexpression. The FdhKO eGfp strain exhibited a low conversion efficiency of sorbitol into biomass, with a substrate-to-biomass yield coefficient ($Y_{x/s}$) ranging from 0.18 to 0.22 g·g^{-1} across all tested OTC. At low OTC, the $Y_{x/s}$ of FdhKO SdOE eGfp strain was 1.9-fold higher than FdhKO eGfp (0.36 g·g^{-1}), increasing further to 0.7 g·g^{-1} at medium and high OTC (Figure 3-8B). Conversely, when considering eGFP as a product, the substrate-to-product yield coefficient ($Y_{p/s}$) for the FdhKO SdOE eGfp strain was 18-fold lower than that of the FdhKO eGfp strain at low OTC (38,586 vs. 2,110 TFU·g^{-1}, respectively, Figure 4-8C). For both strains, $Y_{p/s}$ decreased as oxygen transfer increased, with a 10.9-fold reduction between low and high OTC for the FdhKO eGfp strain (38,586 vs. 3,521 TFU·g^{-1}, respectively).

Elevated formate concentrations were associated with low OTC, low $Y_{x/s}$, and high $Y_{p/s}$. Under these conditions, e*GFP* gene expression for the FdhKO eGfp strain was 5.4-fold higher than under conditions of high $Y_{x/s}$ and low $Y_{p/s}$ (i.e., high OTC, Figure A3- 10). This suggests that when less substrate energy is directed toward biomass formation and instead allocated to secondary metabolism (e.g., eGFP synthesis), fewer C1 units are used in anabolic pathways, resulting in greater formate

accumulation. This observation highlights the role of low $Y_{x/s}$, favored under low OTC, in enhancing p*AOX1* induction.

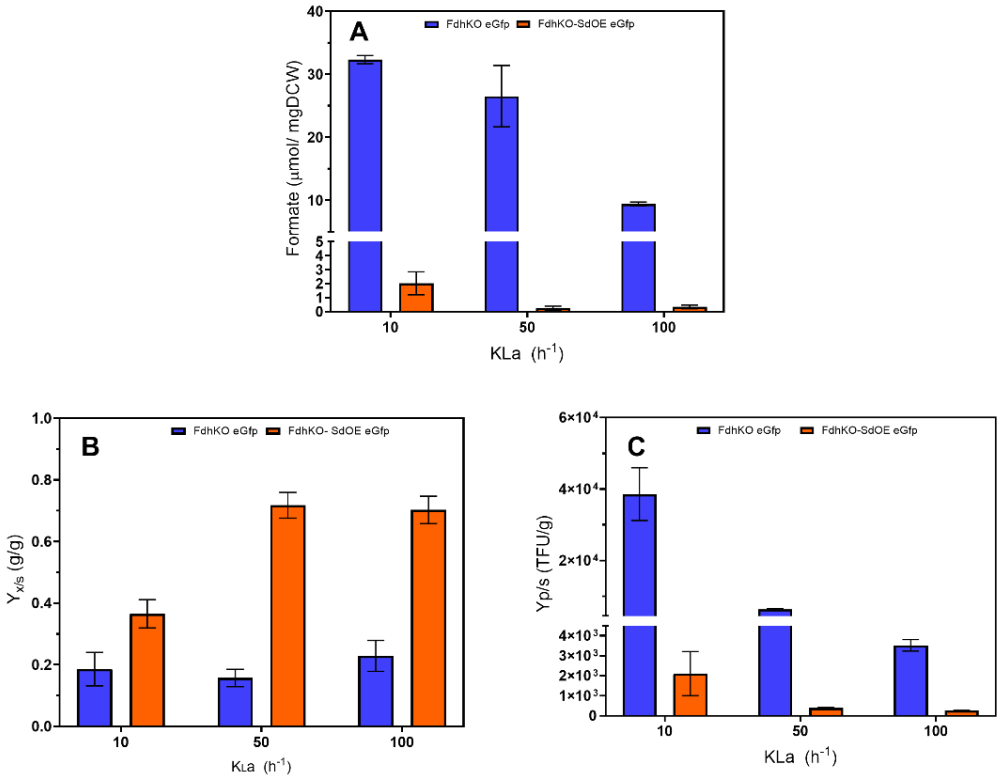

Figure 3-8: Specific formate concentration (panel A), biomass-substrate yield coefficient ($Y_{x/s}$, panel B) and product-to-substrate yield coefficient ($Y_{p/s}$, panel C) for FdhKO eGfp (blue bars) and FdhKO-SdOE eGfp (orange bars) strains grown under different OTC, benchmarked by K_La, in shake-flask cultures. Culture samples were taken at the mid-exponential growth phase (*i.e.*, after 22 h). Data are means and standard deviations of biological triplicate.

4. Conclusion

We recently demonstrated that *Komagataella phaffii* FdhKO strains exhibit self-induction of the p*AOX1*-based expression system when grown on sorbitol. In this study, we further show that these strains undergo diauxic growth in methanol-free glycerol-sorbitol media, effectively decoupling cell growth from recombinant protein production. Under these conditions, accumulated formate from the THF-C1 metabolism triggers p*AOX1* induction. To increase energy generation in FdhKO strain, sorbitol catabolism was optimized by overexpression of *SOR1*. Although increased sorbitol metabolism enhances biomass formation, it simultaneously reduced p*AOX1* induction, as evidenced by lower formate accumulation, decreased eGFP fluorescence, and reduced secreted CalB and Gox activities in *SOR1*-overexpressing strains. Oxygen transfer also modulates these dynamics, with lower oxygen availability favoring higher p*AOX1* induction due to increased formate accumulation. Notably, the observed increase in p*AOX1* expression appears to result from phenotypic diversification within the cell population, leading to a higher fraction of induced cells rather than an overall increase in p*AOX1* induction per cell. These findings underscore the metabolic trade-offs in sorbitol-based processes and highlight the potential for optimizing carbon flux to balance recombinant protein production and cell growth. Future studies should focus on fine-tuning metabolic pathways to enhance energy efficiency while sustaining robust p*AOX1* induction in methanol-free, sorbitol-based media.

Chapter 4

Engineering serine metabolism to enhance AOX1 promoter self-induction in a formate dehydrogenase-deficient Komagataella phaffii

Description of Chapter 4

In the previous chapter, it was demonstrated that overexpression of the *SOR1* gene in the FdhKO strain alleviates the bottleneck in sorbitol uptake, improving growth rate at the expense of increased formate accumulation and enhanced p*AOX1* induction under non-repressive conditions. In addition, it was shown that low oxygen transfer conditions (OTC) positively influence p*AOX1* induction, leading to improved recombinant protein production in a methanol-free system.

Building on these findings, the present chapter investigates the enhancement of the serine biosynthesis pathway in the FdhKO strain through metabolic engineering approaches. For this purpose, key enzymes involved in serine biosynthesis were overexpressed under both strong and weak promoters. Among these targets, the *SER3* gene was selected for further analysis due to its central role in serine metabolism and its potential impact on p*AOX1* induction. The following sections provide a detailed examination of these results.

This chapter is based on a first-author publication:

-llCozmar, R., Berrios, J. & Fickers, P. Engineering serine metabolism to enhance *AOX1* promoter self-induction in formate dehydrogenase-deficient *Komagataella phaffii*. *Microb Cell Fact* 25, 96 (2026). https://doi.org/10.1186/s12934-026-02968-1

Chapter 4: Engineering serine metabolism to enhance *AOX1* promoter self-induction in a formate dehydrogenase-deficient *Komagataella phaffii.*

1.Introduction.

Building upon the metabolic framework established in the previous chapter, where carbon source utilization in FDH-deficient *K. phaffii* was enhanced through engineering of sorbitol uptake and metabolism. As consequence of this modification p*AOX1* induction, formate accumulation and recombinant protein (rProt) production have been decreased. The next layer of metabolic limitation arises downstream in central one-carbon metabolism.

In methylotrophic yeasts such as *K. phaffii*, one-carbon (C1) metabolism plays a central role in integrating carbon flux with biosynthetic demand. The tetrahydrofolate (THF)-dependent C1 network serves as a metabolic hub connecting carbon metabolism with the synthesis of nucleotides, amino acids, and other essential biomass precursors. Within this system, formate-derived units represent a key entry point into cellular C1 metabolism. Recently, we demonstrated that FDH-deficient K. *phaffii* (FdhKO) specifically generate formate through the THF–C1 pathway and that this endogenous formate is capable of inducing p*AOX1* (Bustos et al., 2024). When cultivated in sorbitol-based medium, the FdhKO mutant partially exported formate into the culture supernatant, likely via carboxylate transporters (Casal et al., 2008), leading to extracellular concentrations of up to 15 µM (0.7 $mg \cdot L^{-1}$). By contrast, formate was not detected for the non-disrupted strain. The FdhKO mutant and the non-disrupted strain exhibited comparable growth kinetics on sorbitol, indicating that formate accumulation was not toxic under these conditions. Notably, the endogenous formate produced by the FdhKO strain induced p*AOX1* to levels comparable to those obtained with methanol induction (Bustos et al., 2024). This was demonstrated using the secreted model protein lipase CalB, for which the maximal specific activities were similar on sorbitol and sorbitol–methanol media [136 and 113 $U \cdot mgDCW^{-1}$, respectively, (Bustos et al., 2024)]. Formate accumulation and p*AOX1* induction were further modulated by strain genotype and culture conditions. Enhancing sorbitol uptake in the FdhKO eGFP strain through constitutive expression of sorbitol dehydrogenase increased the specific growth rate from 0.036 h^{-1} to 0.119 h^{-1}, while markedly reducing eGFP fluorescence and consequently p*AOX1* induction. Likewise, cultivation of the FdhKO eGFP strain under different oxygen transfer conditions (For reference see section 3, 3rd chapter) resulted in significantly higher formate accumulation and eGFP expression at K_La values of 10 and 50 h^{-1} (Figure 3-7A). In contrast, the growth rate remained unchanged across all OTCs (average value of 0.039 h^{-1}), indicating that oxygen availability did not limit cell growth under these conditions (Bustos et al., 2025). Furthermore, when the FdhKO mutant was cultivated on a glycerol–sorbitol mixture, p*AOX1* induction occurred only after glycerol depletion and reached levels significantly higher than those observed during simple de-repression on glycerol medium (Figure 3-5A) (Bustos et al., 2025). Collectively,

these findings demonstrate that disruption of the Fdh-encoding gene enables *K. phaffii* to autonomously generate formate, resulting in p*AOX1* self-induction. This provides a novel strategy for converting any p*AOX1*-based expression system into a fully self-inducing platform in an FdhKO background. This modification reshapes the availability and routing of C1 units within the THF cycle. Consequently, the balance of C1 donor and acceptor reactions becomes a limiting factor for optimal metabolic performance.

In FdhKO strains, the formate is accumulated due to the disruption of formaldehyde dehydrogenase. Formate, an intermediate of the methanol catabolism, has been identified previously as a putative p*AOX1* inducer in strains exhibiting different methanol utilization phenotypes (Mut^{+}, Mut^{s}, and Mut$^{–}$) (Jayachandran et al., 2017b; B. Liu, Li, et al., 2022a; Singh & Narang, 2020; Tyurin & Kozlov, 2015). As a C1 molecule with a low energy content, formate must be supplemented with a non-repressive carbon source during the rProt production phase. Sorbitol has proven to be an effective co-substrate in this context (Berrios et al., 2017; Niu et al., 2013; Singh & Narang, 2023). Metabolically, formate is an intermediate in the methanol dissimilative pathway, where it is oxidized to carbon dioxide by formate dehydrogenase (FDH) (Bustos et al., 2022). Additionally, formate is a key intermediate in the tetrahydrofolate-mediated one-carbon (THF-C1) metabolism, which contributes to several anabolic processes, including de novo purine synthesis (Christensen & MacKenzie, 2006; Figure 4-1). The THF-C1 pathway operates in both the mitochondria and cytoplasm, with formate serving as a C1 shuttle between the two compartments.

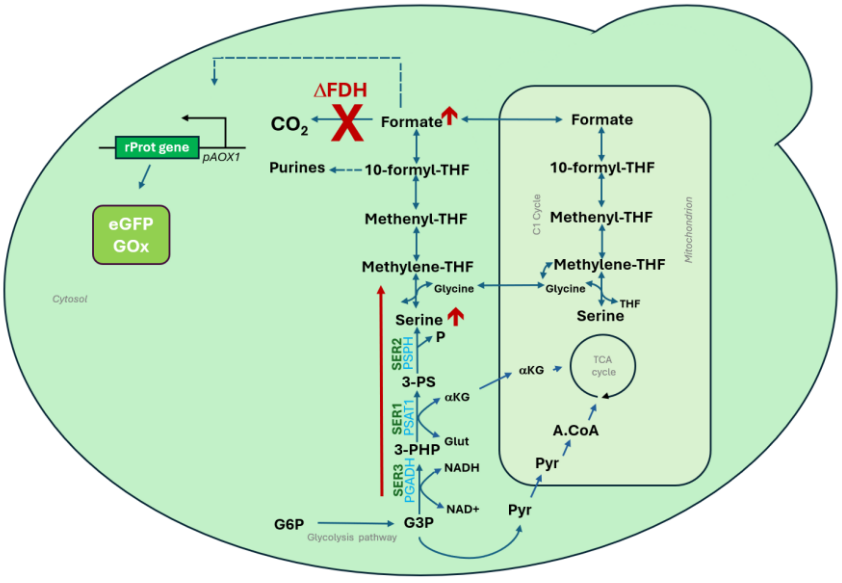

Figure 4-1. Schematic diagram illustrating the targeting serine biosynthesis pathway in a formate dehydrogenase-deficient *Komagataella phaffii.* Formate from THF-C1 metabolism induces the p*AOX1* promoter.

In THF-C1 metabolism, formate is derived from serine metabolism, a central node within this network. Serine biosynthesis, particularly via the glycolytic intermediate 3-phosphoglycerate, is tightly coupled to THF-dependent reactions through serine hydroxymethyltransferase. This reaction represents a major entry point for the generation of 5,10-methylene-THF, directly linking purines pathway and amino acid metabolism with the cellular C1 pool.

We previously showed that serine supplementation markedly increases p*AOX1* induction and rProt productivity (Bustos et al., 2024). Serine is synthesized from the glycolytic intermediate 3-phosphoglycerate through three enzymatic steps involving 3-phosphoglycerate dehydrogenase (Pgdh), phosphoserine aminotransferase (Psat1), and phosphoserine phosphatase (Psph), encoded by *SER3*, *SER1*, and *SER2*, respectively (Kobayashi et al., 2022; Pruneski et al., 2011; Figure 4-2). In *Saccharomyces cerevisiae*, this pathway is tightly regulated as serine represses *SER1* transcription (Delic et al., 2013), whereas *SER3* expression is modulated by the non-coding RNAi *SRG1* (Martens et al., 2005; Pruneski et al., 2011). In addition, serine can be reversibly converted from glycine by serine hydroxymethyltransferases Shm1 and Shm2, which also participate in THF-C1 metabolism (Esch et al., 2020; Figure 4-1).

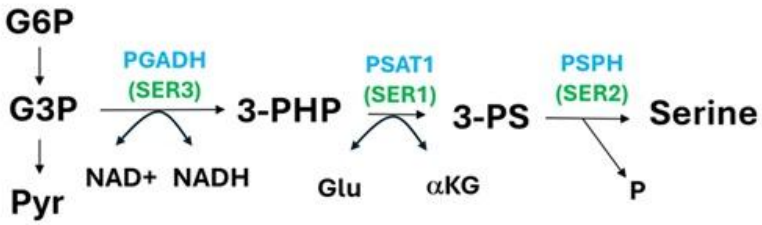

Figure 4-2. Serine biosynthesis pathway in *Komagataella phaffii.* Abbreviations are as follows: PGADH, 3-phophoglicerate dehydrogenase; PSAT1, phosphoserine aminotransferase encoded; PSPH, phosphoserine phosphatase; G6P, glucose-6-phosphate; G3P, 3-phosphoglycerate; NAD^+, nicotinamide adenine dinucleotide oxidized; NADH, nicotinamide adenine dinucleotide reduced; Glu, glutamate; αKG, alfa-ketoglutarate; Pyr, pyruvate; P, phosphate.

Given that supplementation is not economically viable at an industrial scale, we further engineered the FdhKO strain by overexpressing the SER genes individually or in combination (Figure 4-3).

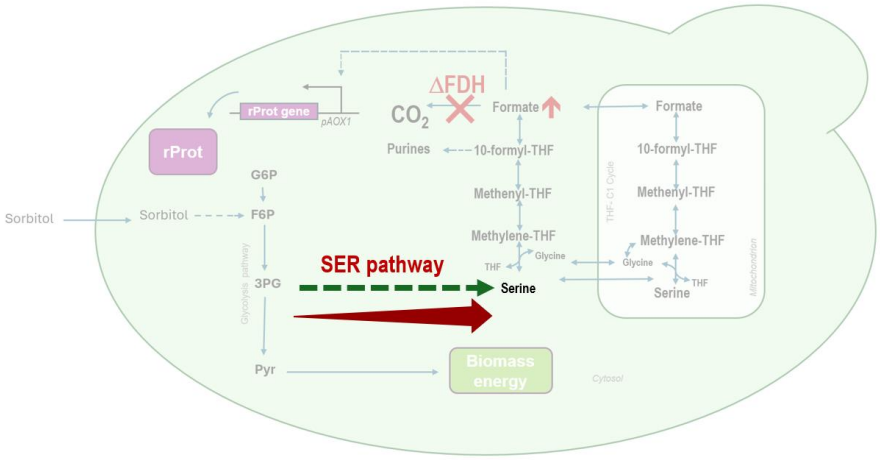

Figure 4-3. Strategy proposal overview focused on enhancing serine pathway in FDH-deficient strain.

Based on this framework, the strategy presented was designed to enhance intracellular formate accumulation and thereby strengthen *AOX1*-driven gene expression under methanol-free conditions.

2. Materials and methods.

2.1 Strain construction.

The *Escherichia coli* and *Komagataella phaffii* strains used in this study are listed in Table A4-1 and supporting information Table 4-1. The general genetic techniques were as described elsewhere (Bustos et al., 2024). The plasmids, GoldenPiCS genetic parts and primers used are listed in Supporting Information Table A4-1 and A4-2.

Codon optimization and gene synthesis of *αMF* and *GOX*.

The following sequences were codon-optimized for *K. phaffii* using SnapGene (GSL Biotech LLC):

- Signal peptide of the Saccharomyces cerevisiae α-mating factor (*αMF*; NM_001184001.1)
- Intron-less coding sequence of Aspergillus niger glucose oxidase (*GOX*; X60601.1)

Codons with a frequency below 10% were replaced with the most abundant one coding for the same amino acid.

Recognition sequence for *Bsa*I or *Bpi*I were added as shown in Supporting information Figures A4-5 and A4-6.

The *αMF* and *GOX* synthetic DNA fragments obtained from IDT technologies (Leuven, Belgium) were cloned into pUC57 and pGEM®-T Easy vector, respectively, to yield plasmids RIE457 and RIE585, hereafter RIP457 and RIP485:

Table 4-1. Cloned vectors containing αMF and GOX synthetic genes.

Fragment	Cloning vector	Resulting plasmid
αMF	pUC57	RIE457
GOX	pGEM®-T Easy	RIE585

Supporting information of plasmids in Table A4-1

Construction of the *αMFGOX* plasmid gene: The αMF fragment from RIP457 was:

1. Digested with *Bsa*I
2. Ligated into plasmid A2 (BB1_23)

yielding plasmid: RIE504 (A2_BB1_23_*αMFGOX*, hereafter RIP504)

Golden Gate assembly of the expression plasmid for *αMFGOX*: The final expression plasmid for *αMFGOX* was assembled using the GoldenPiCS system (Prielhofer et al., 2017). Golden Gate assembly (*Bpi*I) was performed using:

Table 4-2. Components of GoldenGate assembly to obtain RIP507.

Component	Plasmid
Promoter	B8 (BB1_12_p*AOX1*)
Terminator	C1 (BB1_34_*ScCYC1*tt)
Backbone	D12 (BB3aZ_14)
Insert	RIP504

Supporting information of plasmids in Table A4-1

yielding plasmid RIE507 (BB3aZ_14-p*AOX1*-*αMFGOX*-*ScCYC1*tt; hereafter RIP507)

The correctness of the assembly was verified by DNA sequencing using primers pair CkBB3aZ14-Fw/CkBB3aZ1-Rv.

Construction of SER expression vectors.

Amplification and cloning of SER genes: The genes PAS_chr3_0566 (*SER1*), PAS_chr4_0285 (*SER2*), and PAS_chr2-1_0657 (*SER3*) were PCR-amplified from *K. Phaffii* GS115pro genomic DNA used as a template using primer pairs SER1-Fw/SER1-Rv; SER2-Fw/SER2-Rv and SER3-Fw/SER3-Rv, respectively.

PCR products were cloned into the Zero Blunt TOPO vector, generating plasmids:

- RIE508 (TOPO_*SER1*, hereafter RIP508)

- RIE509 (TOPO_*SER2*, hereafter RIP509)
- RIE510 (TOPO_*SER3*, hereafter RIP510)

Positive constructs were verified by DNA sequencing with M13-Fw/M13-Rv primers

Strategy for expression cassette assembly.

To construct the SER gene expression vectors, promoter, gene and terminator parts were first PCR amplified using specific primer pairs designed to generate specific overlaps for subsequent Gibson assembly using the NEBuilder HiFi DNA assembly kit (NewEngland Biolabs).

To improve readability, the fragments are referred to as Parts 1–18 (primer details for each fragment amplified in Table 4-3). PCR amplification of individual parts was obtained as follows:

Promoter fragments.

p*GAP* promoter fragments (Parts 1–3). Amplified from plasmid A4 (BB1_12_p*GAP*):

- Part 1: primers 1.pGAP.SER1-Rv / 2.pGAP-Fw
- Part 2: primers 1.pGAP.SER2-Rv / 2.pGAP-Fw
- Part 3: primers 1.pGAP.SER3-Rv / 2.pGAP-Fw

p*MDH3* promoter fragments (Parts 4–7): Amplified from plasmid A9 (BB1_12_p*MDH3*):

- Part 4: 1.pMDH3.SER1-Rv / 2.pMDH3-Fw
- Part 5: 1.pMDH3.SER2-Rv / 2.pMDH3-Fw
- Part 6: 1.pMDH3.SER3-Rv / 2.pMDH3-Fw
- Part 7: 1.pMDH3.SER3-Rv / 1.BB3rN14pMDH3-Fw

SER gene fragments.

Amplified from TOPO plasmids:

SER1 (RIP508)

- Part 8: 3.SER1Rv / 2.pGAP.SER1Fw
- Part 9: 3.SER1Rv / 2.pMDH3.SER1Fw

SER2 (RIP509)

- Part 10: 3.SER2Rv / 2.pGAP.SER2Fw
- Part 11: 3.SER2Rv / 2.pMDH3.SER2Fw

SER3 (RIP510)

- Part 12: 3.SER3Rv / 2.pGAP.SER3Fw

- Part 13: 3.SER3Rv / 2.pMDH3.SER3Fw

Terminator fragments

*ScCYC1*tt terminator (Parts 14–18). Amplified from plasmid C1 (BB1_34_*ScCYC1*tt):

- Part 14: 4.CYC1-Rv / 4.SER1.C1-Fw
- Part 15: 4.BB3eH14.C1-Rv / 4.SER1.C1-Fw
- Part 16: 4.CYC1-Rv / 4.SER2.C1-Fw
- Part 17: 4.CYC1-Rv / 4.SER3.C1-Fw
- Part 18: 4.BB3rN14.C1-Rv / 4.SER3.C1-Fw

All the obtained PCR fragments were gel purified and quantified with a nanodrop (Thermo Fisher Scientific)

Table 4-3. Fragments described as parts to construct plasmid required using Gibson assembly.

Part	Fragment	Template plasmid	Gene/element	Primer pair
1	Promoter	A4 (BB1_12_p*GAP*)	p*GAP –SER1* overlap	1.pGAP.SER1-Rv/2.pGAP-Fw
2	Promoter	A4 (BB1_12_p*GAP*)	p*GAP – SER2* overlap	1.pGAP.SER2-Rv/2.pGAP-Fw
3	Promoter	A4 (BB1_12_p*GAP*)	p*GAP – SER3* overlap	1.pGAP.SER3-Rv/2.pGAP-Fw
4	Promoter	A9 (BB1_12_p*MDH3*)	p*MDH3 – SER1* overlap	1.pMDH3.SER1-Rv/2.pMDH3-Fw
5	Promoter	A9 (BB1_12_p*MDH3*)	p*MDH3 – SER2* overlap	1.pMDH3.SER2-Rv/2.pMDH3-Fw
6	Promoter	A9 (BB1_12_p*MDH3*)	p*MDH3 – SER3* overlap	1.pMDH3.SER3-Rv/2.pMDH3-Fw
7	Promoter	A9 (BB1_12_p*MDH3*)	p*MDH3* – BB3rN overlap	1.pMDH3.SER3-Rv/1.BB3rN14pMDH3-Fw
8	CDS	RIP508(TOPO_*SER1*)	*SER1*(p*GAP* overlap)	3.SER1Rv / 2.pGAP.SER1Fw
9	CDS	RIP508 (TOPO_*SER1*)	*SER1*(p*MDH3* overlap)	3.SER1Rv / 2.pMDH3.SER1Fw
10	CDS	RIP509 (TOPO_*SER2*)	*SER2*(p*GAP* overlap)	3.SER2Rv / 2.pGAP.SER2Fw
11	CDS	RIP509 (TOPO_*SER2*)	*SER2*(pMDH3 overlap)	3.SER2Rv / 2.pMDH3.SER2Fw
12	CDS	RIP510 (TOPO_*SER3*)	*SER3*(p*GAP* overlap)	3.SER3Rv/2.pGAP.SER3Fw
13	CDS	RIP510 (TOPO_*SER3*)	*SER3*(p*MDH3* overlap)	3.SER3Rv/2.pMDH3.SER3Fw
14	Terminator	C1 (BB1_34_*ScCYC1*tt)	*ScCYC1*tt – *SER1*	4.CYC1-Rv/4.SER1.C1-Fw

Part	Fragment	Template plasmid	Gene/element	Primer pair
15	Terminator	C1 (BB1_34_*ScCYC1*tt)	*ScCYC1*tt–BB3eH	4.BB3eH14.C1-Rv/4.SER1.C1-Fw
16	Terminator	C1 (BB1_34_*ScCYC1*tt)	*ScCYC1*tt – *SER2*	4.CYC1-Rv/4.SER2.C1-Fw
17	Terminator	C1 (BB1_34_*ScCYC1*tt)	*ScCYC1*tt – *SER3*	4.CYC1-Rv/4.SER3.C1-Fw
18	Terminator	C1 (BB1_34_*ScCYC1*tt)	*ScCYC1*tt–BB3rN	4.BB3rN14.C1-Rv/4.SER3.C1-Fw

Supporting information of parts in Table A4-1 and primers in Table A4-2

Gibson assembly of expression plasmids

Final plasmids were assembled by Gibson assembly using the parts listed below and *Bpi*I-digested destination vectors.

BB3aZ backbone
- RIE511 (RIP511): Parts 1 + 8 + 14 + D12 → p*GAP-SER1-ScCYC1*tt
- RIE512 (RIP512): Parts 4 + 9 + 14 + D12 → p*MDH3-SER1-ScCYC1*tt
- RIE513 (RIP513): Parts 2 + 10 + 16 + D12 → p*GAP-SER2-ScCYC1*tt
- RIE514 (RIP514): Parts 5 + 11 + 16 + D12 → p*MDH3-SER2-ScCYC1*tt
- RIE515 (RIP515): Parts 1 + 12 + 17 + D12 → p*GAP-SER3-ScCYC1*tt
- RIE516 (RIP516): Parts 6 + 13 + 17 + D12 → p*MDH3-SER3-ScCYC1*tt

BB3eH backbone
- RIE517 (RIP517): Parts 1 + 8 + 15 + E1 → p*GAP-SER1-ScCYC1*tt
- RIE518 (RIP518): Parts 4 + 9 + 15 + E1 → p*MDH3-SER1-ScCYC1*tt

BB3rN backbone
- RIE519 (RIP519): Parts 7 + 4 + 18 + E8 → p*MDH3-SER3-ScCYC1*tt

Assembly correctness was verified by diagnostic PCR:
- RIP511–RIP516 → primers CkBB3aZ14-Fw / CkBB3aZ1-Rv
- RIP517–RIP518 → primers 1BB3aZ14-Rv / 4.BB3eH14-Fw
- RIP519 → primers 1.BB3rN14-Rv / 4.BB3rN14-Fw

Final plasmid sequences were confirmed by DNA sequencing. This Strategy for expression cassette assembly is illustrated in Figure 4-4.

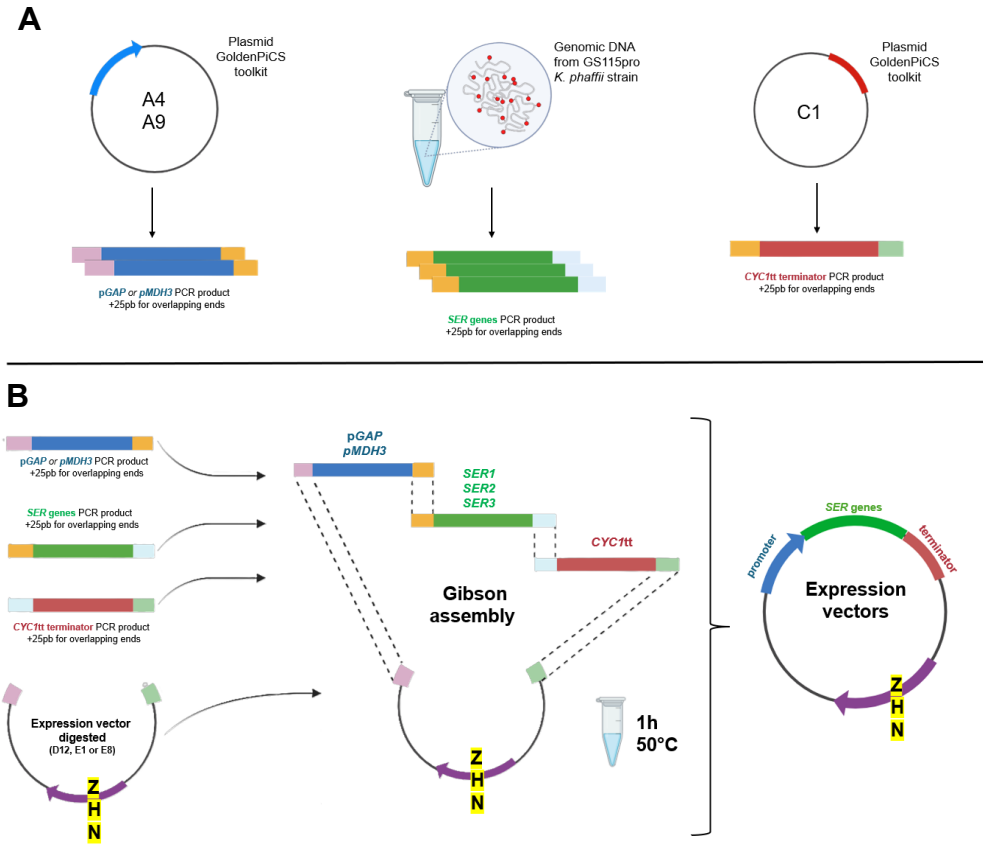

Figure 4-4. General overview of plasmids construction by NEBuilder HiFi DNA assembly kit of different gene fragments. Z: Zeocin selection marker; H: hygromycin selection marker; N: Nourseothricin selection marker

Construction of SER-expressing strains

The construction of yeast strains RIY230 (Fdh eGfp), RIY536 (FdhKO eGfp Z^{+}), RIY540 (eGfp) is described elsewhere (Bustos et al., 2024).

A series of strains expressing *SER1–SER3* under p*GAP* or p*MDH3* promoters were generated by transformation of strain RIY540 with *Asc*I-linearized plasmids (Table 4-4). All integrations were targeted to the *AOX1*tt locus.

Table 4-4. *K. phaffi* strains generated by transformation of RIY540.

Strain	Genotype (simplified)	Plasmid
RIY657(*g*SER1-eGfp)	*fdh1*Δ, p*GAP-SER1*, p*AOX1-eGFP*	RIP511
RIY658(*m*SER1-eGfp)	*fdh1*Δ, p*MDH3-SER1*, p*AOX1-eGFP*	RIP512
RIY659(*g*SER2-eGfp)	*fdh1*Δ, p*GAP-SER2*, p*AOX1-eGFP*	RIP513
RIY660(*m*SER2-eGfp)	*fdh1*Δ, p*MDH3-SER2*, p*AOX1-eGFP*	RIP514
RIY661(*g*SER3-eGfp)	*fdh1*Δ, p*GAP-SER3*, p*AOX1-eGFP*	RIP515
RIY662(*m*SER3-eGfp)	*fdh1*Δ, p*MDH3-SER3*, p*AOX1-eGFP*	RIP516

Additional strains expressing multiple SER cassettes were obtained by transformation of RIY662 with *Pme*I-linearized plasmids (Table 4-5) for integration targeted to the *ENO1* locus.

Table 4-5. *K. phaffi* strains generated by transformation of RI662.

Strain	Genotype (simplified)	Plasmid
RIY663 (*m*SER3-*g*SER1-eGfp)	*fdh1*Δ, p*MDH3-SER3* + p*GAP-SER1*, p*AOX1-eGFP*	RIP517
RIY664 (*m*SER3-*m*SER1-eGfp)	*fdh1*Δ, p*MDH3-SER3* + p*MDH3-SER1*, p*AOX1-eGFP*	RIP518

For GOX strain and SER-GOX strain construction the strategy is presented as follows:

For marker rescue, RIY538 (FdhKO Z^+) strain was transformed with the replicative vector RIP396 (pKTAC-Cre) and transformants were selected on YPD-Genet. The resulting strain was RIY539 (FdhKO).

RIY655 (*fdh1*Δ, p*AOX1-αMF-GOX*, hereafter GOX) strain was obtained by transformation of strain RIY539 with *Asc*I linearized plasmid RIP507 for the integration of the expression cassette at the *AOX1*tt locus (Table 4-6).

RIY665 strain (*fdh1*Δ, p*AOX1-αMF-GOX,* p*MDH3-SER3*, hereafter SER3-GOX strain) was obtained by transformation of strain RIY655 with *Asc*I linearized plasmids RIP519 for the integration of the expression cassette at the *RIG2* locus (Table 4-6).

Table 4-6. *K. phaffi* strains with GOX as recombinant protein.

Strain	Genotype (simplified)	Plasmid
RIY539(GOX)	f*dh1*Δ, p*AOX1-αMF-GOX*,	RIP507
RIY655(GOX-SER3)	*fdh1*Δ, p*AOX1-αMF-GOX*, p*MDH3-SER3*	RIP519

Correct integration of constructs was verified by PCR using locus-specific primers:

- RIY655, RIY657–RIY662: CkBB3aZ14-Fw / CkBB3aZ1-Rv
- RIY663, RIY664: 1BB3aZ14-Rv / 4.BB3eH14-Fw
- RIY665: 1.BB3rN14-Rv / 4.BB3rN14-Fw

Table 4-7. *Komagataella phaffii* strains used in the 4th chapter.

Number	Names	Parental strain, relevant genotype	Reference
RIY232	GS115pro	GS115, HIS4	(Theron et al., 2019)
RIY230	Fdh eGfp	RIY232, p*AOX1-eGFP*, Zeo$^+$	(Bustos et al., 2024)
RIY536	FdhKO eGfp Z$^+$	RIY230, *fdh1*Δ, p*AOX1-eGFP*, Zeo$^+$	(Bustos et al., 2024)
Y538	FdhKO Z$^+$	RIY232, f*dh1*Δ, Zeo$^+$	This work
RIY539	FdhKO	RIY538, *fdh1*Δ	This work
RIY540	eGfp	RIY536, *fdh1*Δ, p*AOX1-eGFP*, Zeo$^-$	(Bustos et al., 2024)
RIY657	*g*SER1-eGfp	RIY540, *fdh1*Δ, p*GAP-SER1*, p*AOX1-eGFP*, Zeo$^+$	This work
RIY658	*m*SER1-eGfp	RIY540, *fdh1*Δ, p*MDH3-SER1*, p*AOX1-eGFP*, Zeo$^+$	This work
RIY659	*g*SER2-eGfp	RIY540, *fdh1*Δ, p*GAP-SER2*, p*AOX1-eGFP*, Zeo$^+$	This work
RIY660	*m*SER2-eGfp	RIY540, *fdh1*Δ, p*MDH3-SER2*, p*AOX1-eGFP*, Zeo$^+$	This work
RIY661	*g*SER3-eGfp	RIY540 *fdh1*Δ, p*GAP-SER3*, p*AOX1-eGFP,* Zeo$^+$	This work
RIY662	*m*SER3-eGfp	RIY540, *fdh1*Δ, p*MDH3-SER3*, p*AOX1-eGFP*, Zeo$^+$	This work
RIY663	*m*SER3-*g*SER1-eGfp	RIY662, *fdh1*Δ, p*MDH3-SER3*, p*GAP-SER1*, p*AOX1-eGFP*, Zeo$^+$, Hyg$^+$	This work
RIY664	*m*SER3-*m*SER1-eGfp	RIY662, *fdh1*Δ, p*MDH3-SER3*, p*MDH3-SER1*, p*AOX1-eGFP*, Zeo$^+$, Hyg$^+$	This work
RIY655	GOX	RIY539, f*dh1*Δ, p*AOX1-αMF-GOX*, Zeo$^+$	This work
RIY665	GOX-SER3	RIY655, *fdh1*Δ, p*AOX1-αMF-GOX*, p*MDH3-SER3*, Zeo$^+$, NAT$^+$	This work

Each primer pair annealed to the 5′ and 3′ regions of the integrated cassette, confirming correct integration.

A schematic representation of the strain genotype is presented in Supplementary Information Figure A4-7. Monocopy integration of the SER and GOX gene expression cassettes in the yeast genome was assessed for the different constructed strains (Figures A4-7 and A4-8). For clarity and readability, plasmids, primers used

and strains are listed in Tables A4-1, A4-2 and Table 4-7, respectively, while only strain codes are used throughout the 4th chapter.

2.2 Medium composition and cultures conditions.

E. coli was grown at 37°C in Luria-Bertani medium (LB), supplemented with antibiotics as follows: 100 µg·mL^{-1} ampicillin, 50 µg·mL^{-1} kanamycin, 25 µg·mL^{-1} zeocin, or 50 µg·mL^{-1} nourseothricin. *K. phaffii* was grown at 30 °C either on YPD medium (20 g·L^{-1} glucose, 10 g·L^{-1} Difco yeast extract, and 10g·L^{-1} Difco bacto peptone) or in YNB medium (1.7 g·L^{-1} Difco YNB w/o ammonium chloride and amino acids, 5 g·L^{-1} NH_4Cl and, 0.4 mg L^{-1} biotin, 100 mM sodium/potassium phosphate buffer, pH 6.0) supplemented 1.75 g·L^{-1} glycerol and 3.5 g·L^{-1} sorbitol (YNBGS4), 20 g·L^{-1} sorbitol (YNBS) or 20 g·L^{-1} glycerol and 20 g·L^{-1} sorbitol (YNBGS). *K. Phaffii* transformants were selected on YPD agar plates, supplemented with 25 µg·mL^{-1} zeocin (YPD-Zeo), 200 µg·mL^{-1} Hygromycin (YPD-Hyg), 500 µg·mL^{-1} geneticin (YPD-Genet) or 100 µg·mL^{-1} nourseothricin (YPD-NAT).

All *K. phaffii* cultures were performed at 30 °C. Precultures were operated as previously described (Bustos et al., 2024)(Bustos et al., 2024). Shake flask cultures were performed either in a 250 ml Erlenmeyer flask containing 25 ml of YNBS with agitation of 150 rpm. Cultures in microbioreactors (BioLector 2, m2p-labs, Baesweiler, Germany), were operated at 1000 rpm with relative humidity of 85 % using 48-well Flower plates (M2P-MTP-48B, Beckman Coulter) containing 1 ml of YNBS or YNBGS4 medium. Stirred tank bioreactor cultivations were performed in 155 ml YNBGS medium in 200-ml DASGIP bioreactors (DASGIP DASbox Mini Bioreactors SR0250ODLS, Eppendorf, Hamburg, Germany at 30°C) as described previously (Theron et al., 2019). Operating parameters were as follows: aeration at 0.5 vvm, stirring at 900 rpm and pH automatically controlled at 6 by addition of 3N KOH.

2.3 Calculations.

The specific growth rate was calculated as

$$\mu = \frac{1}{X}\frac{dX}{dt}$$

Where X is the biomass (gDCW·L^{-1}) and t is the time (h)

The specific sorbitol up-take rate (qSor) was calculated as:

$$qSor = \frac{d[sorbitol]}{dX.t}$$

Where [sorbitol] is the sorbitol concentration, X the biomass ($gDCW \cdot L^{-1}$) and t is the time (h).

The oxygen transfer rate was calculated as

$$OTR = K_La\ (C_0\text{-}C_L)$$

Where K_La is the volumetric oxygen transfer coefficient determined using the dynamic method of desroption-absorpion of oxygen (Garcia-Ochoa & Gomez, 2009), C_0 is the oxygen concentration at equilibrium, which according to Henry's law equals 7.6 $mg \cdot L^{-1}$ (Berrios et al., 2017) and C_L is the measured dissolved oxygen concentration ($DO \cdot C_0$, $mg\ L^{-1}$)

The specific oxygen consumption rate (qO_2) was calculated as:

$$qO_2 = \frac{OTR}{dX} = \frac{K_La\ (C_0\text{-}C_L)}{X}$$

Where C_0 is the oxygen concentration at equilibrium, C_L is the measured dissolved oxygen concentration ($mg \cdot L^{-1}$) and X is the biomass ($gDCW \cdot L^{-1}$).

2.4 Analytical methods.

The cell growth was monitored either by optical density at 600nm (OD600) or dry cell weight (DCW) as previously described (Carly et al., 2016). Sorbitol and glycerol concentrations were determined using high-performance liquid chromatography (Agilent 1100 series equipped with UV (210 nm) and RID detector (Agilent Technologies, Santa Clara, CA, USA) using an Aminex HPX-87H column (300 × 7.8 mm Bio-Rad, Hercules, CA, USA). Compounds were eluted from the column at 65 °C with a flow rate of 0.5 mL min^{-1} and using a 5 mM H_2SO_4 solution as the mobile phase. During cultures in microbioreactors, biomass was monitored by light scattering at 600 nm (gain set at 2) while fluorescence was quantified at 520 nm (excitation 488 nm, gain set at 4) every 10 min. The eGFP fluorescence was expressed as specific fluorescence (sFU). For that purpose, fluorescence values were divided by the biomass values. The specific fluorescence value of the parental strain GS115pro (RIY232) was subtracted from the specific fluorescence of eGFP-producing strains to normalize the data.

Formate concentration in the culture supernatant were measured using the formic acid assay kit (Megazyme Inc., Bray, Ireland) according to the manufacturer's instructions. Briefly, formate is converted into carbon dioxide by formate dehydrogenase with the formation of NADPH which is quantified at 340 nm. Formate concentration is deduced from a calibration curve.

Glucose oxidase activity was monitored using a glucose oxidase assay kit (Megazyme Inc., Bray, Ireland) according to the manufacturer's instructions. Briefly, Gox catalyzes the oxidation of β-D-glucose to D-glucono-δ-lactone with the

concurrent release of hydrogen peroxide. In the presence of peroxidase, the H_2O_2 generated is converted, in the presence of p-hydroxybenzoic acid, into quinoneimine, which is measured at 510 nm. Gox activity is calculated based on a standard curve. For the formate and enzymatic assay, absorbances at specific wavelength were monitored over time using a SpectraMax M2 (Molecular Devices, San Jose, CA, USA). All assays were conducted in triplicates.

3. Results and discussion.

3.1 Overexpression of the 3-phosphoglycerate dehydrogenase-encoding gene in a FdhKO strain increases formate accumulation and pAOX1 induction.

Serine is a metabolic precursor in various anabolic pathways and serves as a donor of one-carbon units in the THF-C1 pathway, where formate is a key metabolite. We previously demonstrated that endogenous formate induces the p*AOX1* promoter in an FdhKO strain, and that supplementing the culture medium with serine positively influences p*AOX1* induction and, consequently, rProt (Bustos et al., 2024). We hypothesized that enhancing serine biosynthesis could increase intracellular formate levels in a FdhKO strain and thereby further potentiate p*AOX1* induction. To test this, genes involved in serine synthesis from 3-phosphoglycerate, namely *SER1* (PSat1), *SER2* (Psph), and *SER3* (Pgadh) (Supplementary information Table A4-3), were overexpressed in a FdhKO strain expressing eGFP under the control of the p*AOX1* promoter (*fdh1*Δ, p*AOX1-eGFP*, hereafter eGfp strains for simplicity; Table 4-7). Each gene was expressed under the control of constitutive promoters, either the strong p*GAP* (glyceraldehyde-3-phosphate dehydrogenase) promoter or the weak p*MDH3* (peroxisomal malate dehydrogenase 3 promoter) promoter. The resulting strains were designated as follows: *g*SER1-eGfp, *m*SER1-eGfp, *g*SER2-eGfp, *m*SER2-eGfp, *g*SER3-eGfp, *m*SER3-eGfp (Table 4-1). Monocopy integration of the *SER* gene expression cassettes in the yeast genome was assessed for the different constructed strains (see supplementary material and Figure A4-8 for details). They were cultivated in microbioreactors in sorbitol medium (YNBS), and specific eGFP fluorescence (i.e. normalized to biomass) was monitored as a proxy to estimate p*AOX1* induction.

For strains overexpressing *SER1* (Psat1) and *SER2* (Psph), no marked difference in cell growth was observed compared with the parental strain (Figure 4-6), whereas the specific fluorescence was lower than that of the parental eGFP strain, regardless of the promoter strength used (Figure 4-5A, B). In contrast, overexpression of *SER3* encoding 3-phosphoglycerate dehydrogenase (Pgadh) resulted in an increase in specific fluorescence and consequently p*AOX1* induction, particularly when expressed under the p*MDH3* (1.28-fold vs. 1.18-fold for p*GAP* after 48 h; Figure 4-5C). This strain also presented reduced growth ability, with a 38 % lower biomass at 48 h, (Figure 4-6). Pgadh catalyzes the first reaction of the serine biosynthesis pathway, which has been identified as the rate-limiting step of serine synthesis in *S.*

cerevisiae (Esch et al., 2020). Based on our observation, this step is also the rate limiting for serine anabolism in *K. phaffii*.

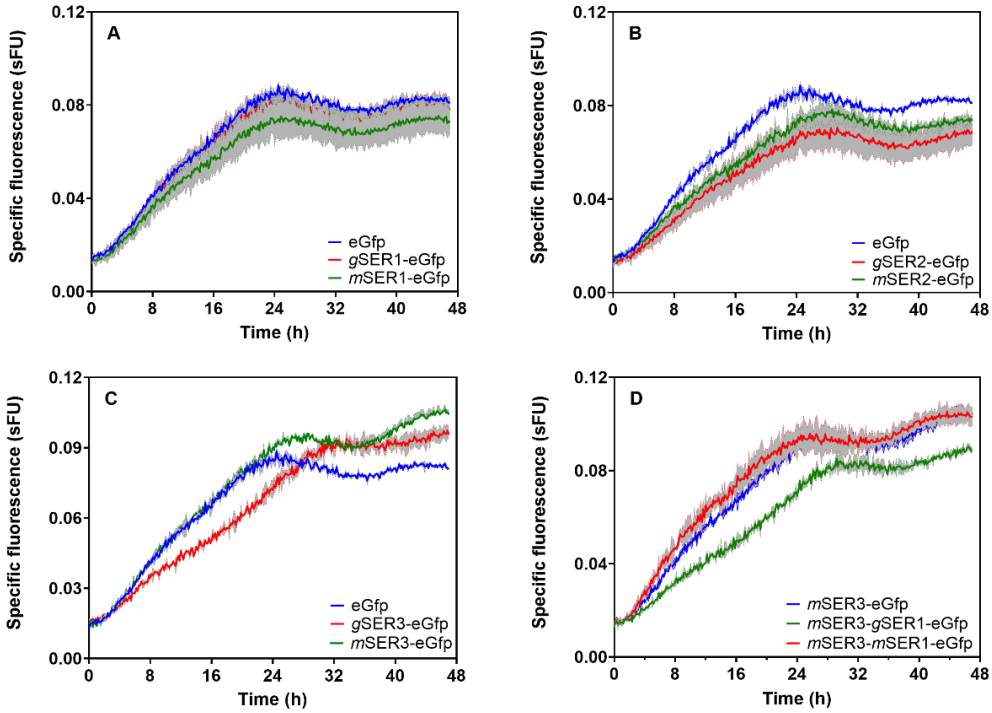

Figure 4-5: Specific eGFP fluorescence for eGfp strain (FdhKO p*AOX1*-e*GFP*) expressing gene *SER1* (panel A), *SER2* (panel B), *SER3* (panel C) and *SER1-SER3* (panel D) under the control the p*GAP* (strains marked with *g*) and p*MDH3* (strains marked with *m*) during growth in sorbitol medium (YNBS). The cells were grown in microbioreactors in batch mode as described in Materials and Methods. Specific fluorescence is the mean value (coloured lines) and standard deviation (grey shades) of biological triplicates. sFU: Specific fluorescence unit.

As *SER1* expression is downregulated by serine in *K. phaffii* (Delic et al., 2013), the gene was co-expressed in the *m*SER3-eGfp background using both p*GAP* and p*MDH3* promoters. The resulting strains, namely *m*SER3-*g*SER1-eGfp and *m*SER3-*m*SER1-eGfp were cultivated in microbioreactor under the same experimental conditions (YNBS medium). Compared to the parental *m*SER3-eGfp strain, the specific fluorescence signal decreased when *SER1* was expressed under the p*GAP* promoter (i.e., in the *m*SER3-*g*SER1-eGfp strain), whereas no significant change was observed when the p*MDH3*-driven expression (Figure 4-5D). The strain overexpressing *SER1* and *SER3* exhibited comparable growth to that of the parental strain, indicating that the expression of these genes does not cause any apparent metabolic imbalance. Taken together, these results suggest that the overexpression of *SER3* exerts a positive indirect effect on p*AOX1* induction while overexpression of *SER1* in the *m*SER3–eGfp background does not further enhance p*AOX1* induction.

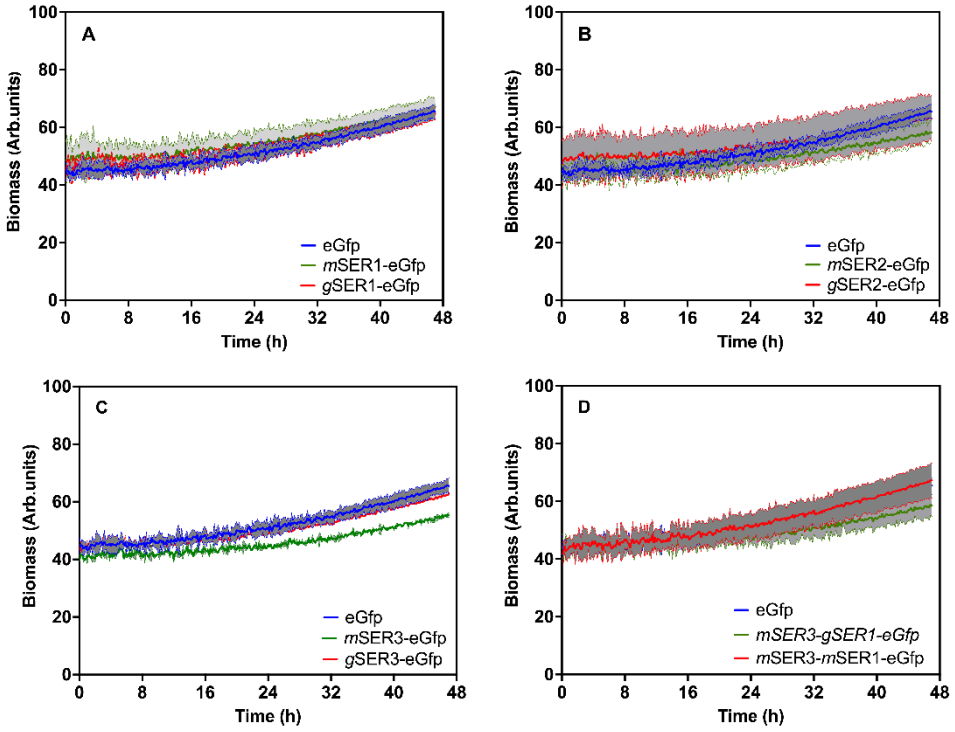

Figure 4-6: Biomass for eGfp strain (FdhKO p*AOX1*-eGFP) expressing gene *SER1* (panel A), *SER2* (panel B), *SER3* (panel C) and *SER1-SER3* (panel D) under the control the p*GAP* (strains marked with g) and p*MDH3* (strains marked with m) during growth in sorbitol medium (YNBS). Cells were grown in microbioreactors in batch mode as described in Materials and Methods. Biomass is the mean value (colored lines) and standard deviation (grey shades) of biological triplicates. Arb units: arbitrary unit.

In industrial rProt production processes based on p*AOX1*-driven expression systems, glycerol is commonly used during the cell growth phase, while a p*AOX1* non-repressive carbon source, such as sorbitol, is preferred during the rProt production stage (Carly et al., 2016; Ergün et al., 2022; Niu et al., 2013). Biomass and eGFP fluorescence were therefore monitored for the eGfp *m*SER3-eGfp grown in microbioreactors on glycerol and sorbitol at a 1:2 ratio (YNBGS4). Both strains exhibited diauxic growth, consuming glycerol within the first 8 hours of culture, followed by a sorbitol consumption phase (Figure 4-7A). However, marked differences were observed between the two strains regarding the specific fluorescence levels and thus p*AOX1* induction. Upon glycerol depletion, eGFP-specific fluorescence markedly increased for both strains. The strain overexpressing *SER3* (i.e., *m*SER3-eGfp) exhibited a 1.5-fold increase in specific fluorescence on average between 18 h and 48 h compared to eGfp strain (0.106 vs. 0.072 sFU, respectively). The fluorescence level then tended to decrease slightly as the biomass value reached a plateau (i.e., after 40 h) (Figure 4-7B). Although not regulated, the pH of the culture

medium only slightly decreased from 6 to 5.7 at the end of the culture (data not shown).

During those cultures, secreted formate in the culture supernatant was monitored over time as a proxy for intracellular accumulation (Bustos et al., 2024, 2025). It increased for both strains after glycerol depletion and peaked at 10 h of culture. Thereafter, the formate concentration gradually decreased for both strains and became nearly undetectable in the culture supernatant by 48 h for the eGFP strain (Figure 4-7C). At any time point, the formate content was consistently higher for the *m*SER3-eGFP strain compared to the eGFP strain, with the greatest difference observed at 10 h (2-fold, 29 µM vs 14 µM, respectively). As both strains grew similarly, the accumulation of formate did not affect cell fitness. Furthermore, the formate concentration in the *m*SER3-eGfp strain remained nearly an order of magnitude lower than the concentration reported as cell toxic (20 mM (Singh & Narang, 2020))

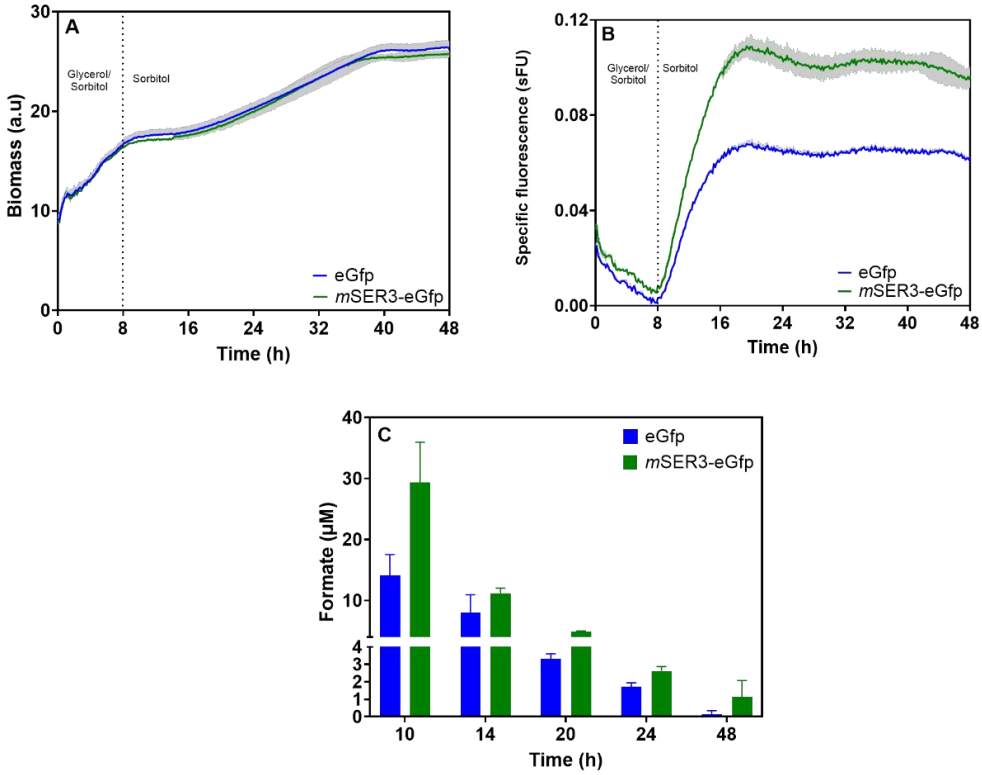

Figure 4-7: Biomass (panel A), specific eGFP (panel B) and extracellular formate concentration (Panel C) for eGfp (fdh1Δ, p*AOX1*-e*GFP*, blue color) and m*SER3*-eGfp (fdh1Δ, p*AOX1*-e*GFP*, p*MDH3*-*SER3*, green color) strains grown in YNB minimal media containing glycerol and sorbitol at a 1:2 ratio (YNBGS4). The cells were grown in microbioreactors in batch mode as described in Materials and Methods in glycerol-sorbitol media (YNBGS4), and data represent the mean and standard deviation of triplicate cultures. sFU: specific fluorescence unit; a.u: arbitrary units. µM: micromolar. In panel A and B, the dotted line highlights the point at which glycerol was depleted from the medium.

3.2 Enhancing serine metabolism in FdhKO strains increases the synthesis of secreted proteins.

The FdhKO p*MDH3-SER3* strain (hereafter *m*SER3) was further considered for its ability to produce a secretory protein, namely glucose oxidase (Gox) from *A. niger*. Gox is an industrially relevant enzyme widely used in food processing, biosensing, and biocatalysis (Bankar et al., 2009). It is also a well-established model for secretory protein (Ahmad et al., 2014; Çelik & Çalık, 2012; Yu et al., 2020). The corresponding codon optimized sequence transcriptionally fused with the signal peptide from the α-mating factor from *S. cerevisiae* was cloned under the control of the p*AOX1* and expressed in a FdhKO and in the *SER3* strain (Figure A4-5 and A4-6). As a first characterisation, the resulting GOX and GOX-SER3 strains were characterized for monocopy integration (see supplementary material for details, Figure A4-9) and were grown in shake flasks on sorbitol medium (YNBS) at medium OTC (K_La 50 h^{-1}) based on previous results (Bustos et al., 2025). Cell growth, Gox activity and extracellular formate concentration were measured at various time points for 72h. At the end point of cultivation, the GOX-SER3 strain exhibited a 1.4-fold increased Gox activity compared to the GOX strain, with respective values of 450 $U{\cdot}L^{-1}$ and 316 $U{\cdot}L^{-1}$. Both strains showed similar growth kinetics (Figure 4-8A). Both strains exhibited similar growth kinetics, confirming that *SER3* overexpression does not impair cell growth in those experimental conditions (Figure 4-8C). As observed for the eGFP-expressing strains (Figure 4-8), formate accumulated in both the GOX and GOX–SER3 strains (Figure 4-8B), with higher levels detected in the *SER3*-overexpressing strain. After 12 h of cultivation, formate concentrations reached 55 µM and 62 µM in the GOX and GOX–SER3 strains, respectively. Subsequently, formate levels gradually decreased for both strains and became nearly undetectable after 72 h, despite continued cell growth and the presence of approximately 70% of the initial sorbitol in the culture medium (Figure 4-8D). These results for secreted proteins production are consistent with the trend observed with the eGFP strains (i.e., eGfp and *m*SER3-eGfp strains, Figure 4-7).

The GOX and GOX-SER3 strains were further cultivated in batch mode in stirred-tank bioreactors with pH control using YNBGS medium containing glycerol and sorbitol at a 1:2 ratio. Biomass, GOX-specific activity, dissolved oxygen (DO) and carbon source concentrations were measured over 62h. Culture conditions were set at 800 rpm agitation and 1 vvm aeration, corresponding to an experimentally determined K_La of 48 h^{-1} (see supplementary material for details, table A4-4). Both strains exhibited diauxic growth, consuming glycerol during the first 15 h, followed by sorbitol over the subsequent 35 h (Figure 4-9A, 4-9B). Glycerol depletion was indicated by a sharp increase in DO at 15 h (Figure 4-9C). At this time point, glycerol was no longer detectable in the culture supernatant, whereas sorbitol consumption had not yet started (Figure 4-9B). During the sorbitol consumption phase (i.e., between 25h and 50 h), DO levels remained stable at approximately 85% air saturation, particularly for the GOX-SER3 strain (Figure 4-9C). Under these conditions, a pseudo-steady state with respect to DO can be assumed, such that the oxygen uptake

rate (OUR) equals the oxygen transfer rate (OTR) (J. Liang & Yuan, 2007). This assumption allowed calculation of the cell-specific oxygen consumption rate (qO_2) by normalizing OTR values to the corresponding biomass. Based on biomass measurements obtained at multiple time points between 25 and 50 h of culture, the average qO_2 for the GOX-SER3 strain was 3.4 mg $O_2 \cdot gDCW^{-1} \cdot h^{-1}$. Upon sorbitol depletion, DO increased to 100% saturation (Figure 4-9C). Throughout the sorbitol consumption phase, both strains exhibited continuous growth with an average specific growth rate of 0.016 h^{-1} and a sorbitol uptake rate (qSor) of 0.025 $g \cdot gDCW^{-1} \cdot h^{-1}$. Since oxygen was not limiting during rProt production on sorbitol, the calculated qO_2 and qSor values can be considered reference parameters for future process design. In particular, they can be used to estimate qO_2 at high cell densities (typically 60–100 $gDCW \cdot L^{-1}$) and to define the operational conditions required to meet OTR demands and to establish appropriate sorbitol feeding strategies.

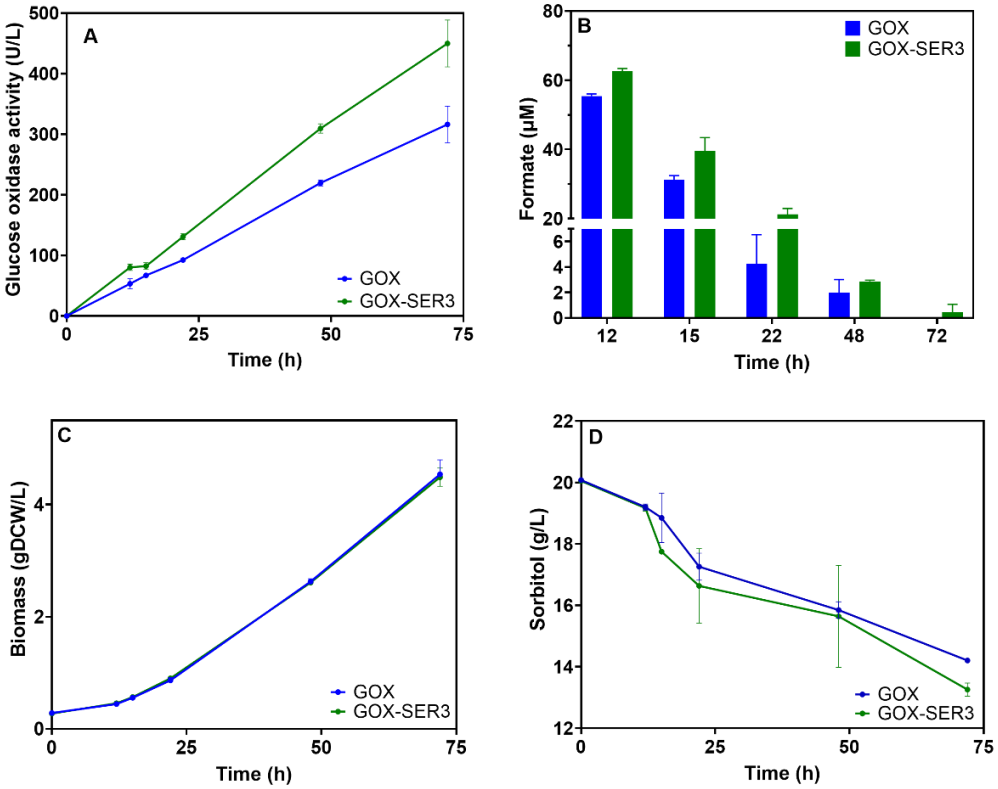

Figure 4-8: Glucose oxidase activity (panel A), extracellular formate concentration (panel B), biomass (panel C) and sorbitol concentration (panel D) during growth of GOX (blue color) and GOX-SER3 (green color) strains in sorbitol media (YNBS). The data are presented as the means and standard deviations of triplicate cultures conducted in shake flasks as described in Materials and Methods. Glucose oxidase assays were performed in triplicate, sorbitol and formate assays were performed in duplicate.

Most importantly, no Gox activity was detected in the culture supernatant during the glycerol consumption phase, confirming that the p*AOX1* promoter is tightly repressed by glycerol. Upon glycerol depletion, Gox-specific activity increased almost linearly in both strains, reaching a plateau after 40 h. At the end of the culture, the Gox-specific activity of the GOX-SER3 strain was 1.3-fold higher than that of the GOX strain (Figure 4-9D). The enzymatic productivities calculated over a 47-h production period were 0.31 and 0.39 U·gDCW-1·h-1 for strains GOX and GOX-SER3, respectively.

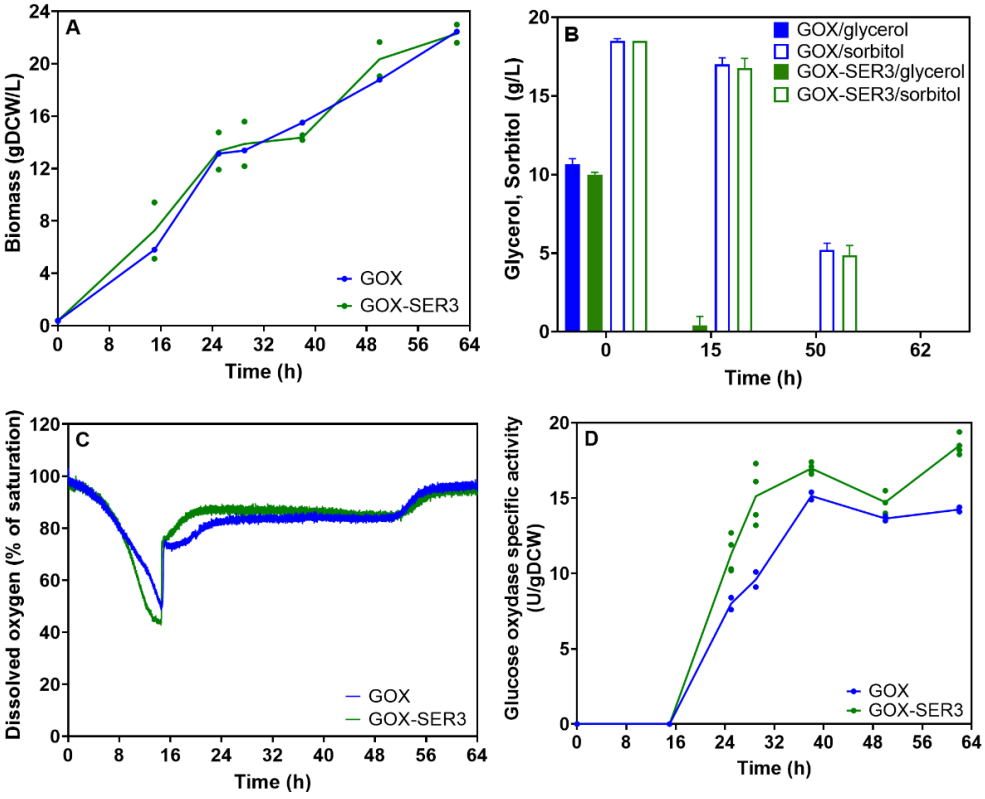

Figure 4-9: Biomass (panel A), glycerol (filled histograms) and sorbitol (empty histograms) concentrations (panel B), dissolved oxygen (panel C) glucose oxidase specific activity (panel D) during growth of GOX (blue colour) and GOX-SER3 (green colour) strains in a stirred-tank bioreactor in batch mode as described in Materials and Methods in glycerol-sorbitol media (YNBGS). In panel A and D, the dots represent all the measurements while the lines connect the mean values.

These observations have important implications for future process development. In most processes, rProt production is temporally separated from biomass formation. Typically, cells are first grown in batch or fed-batch under conditions that repress p*AOX1*, with glycerol as the primary carbon source. The rProt production phase is then initiated by shifting to permissive culture conditions, most commonly through

methanol supplementation. The main technical challenge lies in determining the optimal timing and methodology for transitioning from repressive to inducible conditions. In addition, cells must adapt to methanol, a process that requires extensive metabolic reorganization. Formate has been proposed and successfully tested, in combination with an FdhKO strain, as an alternative inducer to methanol (Bustos et al., 2024). Using CalB as a model secreted protein, a maximum specific activity of 136 $U \cdot mgDCW^{-1}$ was achieved on sorbitol with a FdhKO CalB strain, compared to 113 $U \cdot mgDCW^{-1}$ obtained with a Fdh CalB strain using methanol as the inducer. In addition, this maximum specific activity was reached 2.4-fold faster with the FdhKO CalB strain on sorbitol medium.

Therefore, the limitations associated with methanol-based induction can be overcome by cultivating FdhKO strains in media containing both glycerol and sorbitol, with the glycerol supply adjusted to reach the desired biomass. Upon glycerol depletion, p*AOX1* repression is relived, and sorbitol becomes the primary carbon and energy source. In contrast to methanol, sorbitol catabolism requires only minor metabolic adaptation. Under these conditions, formate generated via THF-C1 pathway accumulates intracellularly in FdhKO strains, inducing p*AOX1* and initiating the rProt production phase. In such a way, no external inducer is requested as the p*AOX1* is auto-induced by endogenous formate. Overexpression of *SER3* further enhance this autoinduction effect. Importantly, compared to methanol-based processes, optimal culture performance can be achieved at lower OTR, a highly advantageous feature for large-scale bioprocess development, where oxygen transfer is often a key limitation. Consistently, the qO_2 values determined in this study for sorbitol (≈4 $mgO_2 \cdot gDCW^{-1} \cdot h^{-1}$) are substantially lower than those reported for methanol-based processes [120-170 $mgO_2 \cdot gDCW^{-1} \cdot h^{-1}$;(Berrios et al., 2017; Velastegui et al., 2023)].

4. Conclusion.

In *K. phaffii*, *AOX1* promoter–based expression systems have proven highly effective for rProt production. However, the use of methanol at industrial scale is associated with several challenges that increase process complexity and cost. Consequently, methanol-free induction strategies have been actively explored. These include the use of derepressed promoters, such as the recently reported p*DH*, which is induced under the so-called pseudo-starvation conditions (Bernat-Camps et al., 2023; Ebner et al., 2025), as well as the use of alternative inducers for p*AOX1*, notably formate (Singh & Narang, 2020). Nevertheless, due to the low energy content of formate, its use as an inducer requires the presence of a permissive carbon source, such as sorbitol. In addition, formate-based induction presents further challenges, as formate becomes toxic to cells at concentrations above approximately 20 mM (Singh & Narang, 2020).

Recently, we reported that disruption of the formate dehydrogenase gene in *K. phaffii* leads to formate accumulation when FdhKO cells are grown on sorbitol, but not on glycerol. This enables *AOX1* promoter–based expression systems to operate in a self-inducible manner, thereby eliminating the need for methanol as an external

inducer and its associated issues. Specifically, for FdhKO cells cultivated in a glycerol–sorbitol mixture, p*AOX1* induction is triggered only after glycerol depletion. The low growth rate of the FdhKO strain on sorbitol favors the accumulation of endogenous formate required for p*AOX1* activation, while sorbitol provides the necessary energy supply for rProt synthesis.

In the present study, we aimed to further enhance endogenous formate accumulation by engineering serine metabolism. Overexpression of the gene encoding 3-phosphoglycerate dehydrogenase in a formate dehydrogenase-deficient *K. phaffii* strain significantly increased formate accumulation without compromising cell fitness and markedly enhanced p*AOX1* induction under derepressed culture conditions. This strategy further improved recombinant protein productivity, as exemplified by a 30% increase in Gox secretion under bioreactor process conditions.

Chapter 5

Yarrowia lipolytica, Komagataella phaffii and secretory proteins: recombinant laccase as a case study

Description of Chapter 5.

Previous studies have shown that signal peptide selection is a key determinant of secretion efficiency and that optimal performance depends on both the host organism and the target protein.(Gasser & Mattanovich, 2018; Puxbaum et al., 2015). In *Komagataella phaffii*, protein secretion has been widely reported as an additional limiting step in this host. (Zahrl et al., 2018).

The present chapter addresses a complementary aspect of recombinant protein (rProt) production by evaluating the effect of different signal peptide regions combination on laccase secretion in *Yarrowia lipolytica* compared with *Komagataella phaffii*.

This chapter complements the general objective of the doctoral project. While the main chapters investigate how methanol-free metabolic engineering strategies performed on FDH-deficient strain affecting p*AOX1* induction and protein production, this study addresses the secretion step, representing an additional layer of optimization within the same production pipeline.

In this context, this work contributes to understanding secretion-level determinants that influence overall production efficiency.

This work represents a complementary extension of my doctoral research and is based on a co-authored publication. The study was carried out in close collaboration with Contance Keller, with joint involvement throughout all stages of the work.

Within this framework, my contribution encompassed the experimental design, execution of molecular biology related to qPCR measurements and secretion experiments, data analysis, and interpretation of results. The study reflects a shared intellectual and experimental contribution between both authors.

This work is an original contribution adapted from:

- Keller, C., Cozmar, R., Alcalde, M., & Fickers, P. (2026). *Yarrowia lipolytica, Komagatoella phaffii* and secretory proteins: recombinant laccase as a case study. Journal of Biotechnology, 412, 1-4. https://doi.org/10.1016/j.jbiotec.2026.01.015

Chapter 5: *Yarrowia lipolytica*, *Komagataella phaffii* and secretory proteins: recombinant laccase as a case study.

1. Short communication.

For more than three decades, the methylotrophic yeast *Komagataella phaffii* has been a workhorse to produce recombinant secretory proteins (rsProt). The classical expression system, combining the tightly regulated promoter from alcohol oxidase 1 (p*AOX1*) with the *Saccharomyces cerevisiae* α-factor signal peptide, remains a benchmark in industrial biotechnology (Bustos et al., 2022). Despite its advantages, including high cell density cultivation and the possibility to express recombinant genes under the control of p*AOX1* at high level upon methanol induction, *K. phaffii* faces limitations in protein folding and secretion machinery. Under conditions of high rsProt synthesis, the endoplasmic reticulum (ER) becomes saturated, leading to protein misfolding, ER stress, and reduced secretion efficiency (Zahrl et al., 2018).

Secretion efficiency depends critically on N-terminal signal peptides (SP), which typically consist of a pre-sequence (Pre) that directs proteins into the ER and a pro-sequence (Pro) that increases protein solubility in the ER, assists protein folding, maturation, and trafficking to the Golgi compartment. The pre-sequence is cleaved in the ER by a signal peptidase, whereas the pro-sequence is removed later in the Golgi by Kex-like proteases. While the presence of a pro-sequence is not essential for protein secretion, the specific amino acid sequence of the pre- sequence is a critical determinant of rsProt productivity (Celińska et al., 2018; Celińska & Nicaud, 2019). We previously compared the production of lipase B from *Candida antarctica* (CalB), *Yarrowia lipolytica,* and *K. phaffii* hosts and found that, despite a seven-fold higher mRNA level in *K. phaffii*, enzyme production was significantly higher in *Y. lipolytica*, a discrepancy attributed to the CalB protein proteasomal degradation before secretion in *K. phaffii* due to a strong endoplasmic reticulum (ER) stress response during rsProt production, leading to substantial protein loss through ER-associated degradation (ERAD) (Theron et al., 2020).

In contrast, *Y. lipolytica* naturally secretes large amounts of hydrolytic enzymes (lipases, proteases, laccases) and exhibits a filamentous fungi-like secretory pathway, which provides superior protein export (Celińska & Nicaud, 2019; Darvishi et al., 2018; Nicaud, 2012).

To extend these findings, we evaluated herein the engineered laccase LacVader (Mateljak & Alcalde, 2021) as a model rsProt. Large-scale fermentation of laccases remains challenging due to low secretion efficiency, improper folding, proteolytic degradation, variability in post-translational modifications (Bannach-Machado et al., 2026), their size (60–100 kDa), extensive glycosylation, and the requirement for copper incorporation into multiple active sites (Mateljak & Alcalde, 2021). Unlike commonly used model proteins such as eGFP or Gox

used in the previous chapter, which are relatively robust and are often efficiently secreted in *K. phaffii* (Bankar et al., 2009; Tsien, 1998). Laccases are particularly sensitive to limitations in protein folding, trafficking, and secretion efficiency, making them well-suited to reveal subtle but functionally relevant differences in signal peptide performance (Bannach-Machado et al., 2026; Sodhi et al., 2024).

Nevertheless, laccases have diverse industrial applications, including organic synthesis, pulp bleaching, dye decolorization, beverage stabilization, flavor enhancement, and baking additives (Mateljak & Alcalde, 2021).

In *K. phaffii* strain RIY667 (Table 5.1), the LacVader coding sequence under the control of the p*AOX1* promoter was transcriptionally fused to an evolved pre-pro-sequence from *S. cerevisiae* α-factor and integrated at the *AOX1* locus (Mate et al., 2013). In the different constructed *Y. lipolytica* strains, the LacVader expression cassettes were driven by the constitutive p*TEF* promoter and targeted to the *LIP2* locus. Four pre-sequences were tested, namely αPre from *S. cerevisiae* α-factor, Yps3Pre from the *Y. lipolytica* GPI-anchored protease Yps3, Lip2Pre from the extracellular lipase Lip2, and SoAmyPre, a codon-optimized pre-sequence from the insect *Sitophilus oryzae* α-amylase SoAmy. These pre-sequences were selected based on their demonstrated secretory potential for heterologous proteins, namely α-amylase from *S. oryzae* and a glucoamylase from the fungus *Thermomyces lanuginosus* (Celińska et al., 2018). Two pro-sequences were also evaluated, namely the αPro from the *S. cerevisiae* α-factor and the Lip2Pro from the highly secreted *Y. lipolytica* Lip2 lipase (Celińska et al., 2018). A total of nine combinations of pre- and pro-sequences transcriptionally fused to the LacVader coding sequence were assembled using Golden Gate cloning and integrated into the *Y. lipolytica* genome at the *LIP2* locus (Fig. 5.1, Table 5.1). Biomass and laccase activity based on ABTS oxidation were measured at 60 h and 72 h, and specific activity was calculated. The methods related to plasmids and strains construction; cultures conditions and enzyme assay are detailed in Appendix 21-24; Table 5A-1, Table 5A-2, Figure 5A-3 and Appendix 28-33. Integration consistency check among the constructed strains led to the selection of those carrying a single copy of the LacVader expression cassette (Appendix 31, Figure 5A-4). Since all constructs were driven by the constitutive p*TEF* promoter and integrated at the same *LIP2* locus, it was assumed that LacVader expression levels were comparable across the different *Y. lipolytica* strains. Cultivations were performed in 24-square deepwell plates under oxygen transfer conditions comparable to those of stirred tank reactors (i.e., 30-40 mmol O_2 L^{-1} h^{-1}, (Duetz et al., 2000; Duetz & Witholt, 2001).

Table 5-1. Yeast strains used in 5th chapter

Strain	Parental strain, plasmid, genotype	Reference
RIY146	*Y. lipolytica*, Po1d, eyk1::Leu2ex, Ura$^-$	(Vandermies et al., 2017)
RIY667	*K. phaffii*, (pJRoC30), p*PDF*-αfactor-LacVader	(Mateljak & Alcalde, 2021)
RIY668	RIY146, (RIP534), p*TEF*-αPre-LacVader-*LIP2*tt	This work
RIY670	RIY146, (RIP535), p*TEF* -Yps3Pre-LacVader-*LIP2*tt	This work
RIY672	RIY146, (RIP536), p*TEF*-Lip2Pre-LacVader-*LIP2*tt	This work
RIY674	RIY146, (RIP537), p*TEF*-SoAmyPre-LacVader-Lip2tt	This work
RIY676	RIY146, (RIP538), p*TEF*-αPre-αPro-LacVader-*LIP2*tt	This work
RIY678	RIY146, (RIP539), p*TEF*-Yps3Pre-αPro-LacVader-Lip2tt	This work
RIY680	RIY146, (RIP540), p*TEF*-Lip2Pre-αPro-LacVader-*LIP2*tt	This work
RIY682	RIY146, (RIP541), p*TEF*-SoAmyPre-αPro-LacVader-*LIP2*tt	This work
RIY684	RIY146, (RIP542), p*TEF*-αPre-Lip2Pro-LacVader-*LIP2*tt	This work
RIY686	RIY146, (RIP543), p*TEF*-Yps3Pre-Lip2Pro-LacVader-*LIP2*tt	This work
RIY688	RIY146, (RIP544), p*TEF*- Lip2Pre-Lip2Pro-LacVader-*LIP2*tt	This work
RIY690	RIY146, (RIP545), p*TEF*-SoAmy-Lip2Pro-LacVader-*LIP2*tt	This work

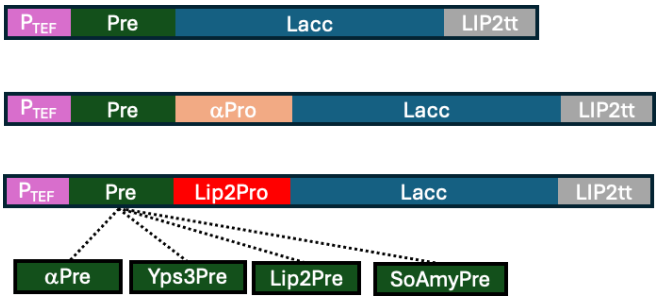

Figure 5-1. Schematic representation of the constructed expression systems obtained by Golden Gate (GG) assembly (Supporting information A). Abbreviations are as follow: p*TEF*, promoter p*TEF*-4UA (GGE146); Pre, presequence of α factor (αPre); Yps3 protease, (Yps3Pre); LIP2 lipase, (Lip2Pre); SoAmy α-amylase (SoAmyPre); Lacc, LacVader laccase encoding gene; LIP2tt; *LIP2* transcriptional terminator. All constructs were integrated at the *LIP2* locus of *Y. lipolytica* strain RIY146.

At both sampling times, most *Y. lipolytica* constructs outperformed *K. phaffii* (Fig. 5.2). Only αPre, αPre-αPro, and Yps3Pre-αPro yielded lower laccase specific

activities. These findings confirm our earlier observations with CalB (Theron et al., 2020) on the superior secretion capacity of *Y. lipolytica*. In *Y. lipolytica*, both pre- and pro-sequences modulated laccase specific activity, with clear evidence of synergistic effects. Specifically, laccase specific activity was minimal when the αPre sequence was used alone without a pro-sequence (NoPro, 0.3 ± 0.2 U·gCDW^{-1}, data at 72h). Specific activity increased eight-fold upon combination with the αPro sequence (2.5 ± 0.7 U·gCDW^{-1}), and more than 110-fold when combined with the Lip2Pro sequence (34.9 ± 3.5 U·gCDW^{-1}). In contrast, the Yps3Pre sequence displayed a distinct behavior. Laccase specific activity was markedly reduced when Yps3Pre was combined with the αPro sequence compared with Yps3Pre alone (NoPro. 4.7 ± 2.2 U·gCDW-^{1} and 18.2 ± 3.1 U·gCDW-1 at 72h, respectively). Conversely, a significant enhancement of laccase specific activity was observed when the Yps3Pre sequence was combined with the Lip2Pro sequence. At 72h, the Yps3Pre-Lip2Pro construct yielded the highest laccase specific activity (58 ± 4 U·gCDW^{-}1) that is eight-fold higher than the specific laccase activity obtained for *K. phaffii* (7.3± 0.8 U·gCDW^{-}1). To further investigate the differences in laccase specific activities observed for constructs based on the Yps3Pre with or without a Pro-sequence, the LacVader expression levels were quantified in strains Yps3Pre, Yps3Pre-αPro and Yps3Pre-Lip2Pro during both the exponential growth and stationary phases (i.e. at 24h and 48 h, Fig. 5.3). Although the LacVader gene was expressed under the constitutive p*TEF* promoter, the modest variations in transcript abundance observed among the strains are most likely attributable to post- transcriptional effects rather than differences in promoter activity. In particular, the nucleotide sequence encoding the Pre- and Pro-sequence can influence mRNA secondary structure, translation efficiency, and ribosome dynamics, thereby modulating transcript stability independently of transcriptional control (Harigaya & Parker, 2016; Presnyak et al., 2015). However, the difference in LacVader mRNA relative quantification cannot support the differences observed in laccase specific activity. SoAmyPre and Lip2Pre based constructs showed no increase of laccase specific activity when combined with αPro, but it significantly increases with Lip2Pro. Across all pre-sequences, Lip2Pro consistently outperformed αPro, with improvements ranging from 1.7-fold for Lip2Pre to 14-fold for αPre at 72 h.

Surprisingly, the dynamics of laccase specific activity between 60 h and 72 h were not consistent across all pre- and pro-sequence combinations. For most tested strains, the specific laccase activity increased during this interval; however, for certain constructs, namely SoAmyPre-αPro and αPre-Lip2Pro, the increase was less pronounced. In contrast, the combination of pre- and pro-sequences had no significant effect on cell growth with an average biomass of 4.6 ± 0.6 gDCW·L^{-1} at 72 h across all *Y. lipolytica* strains tested (Fig.5A-5).

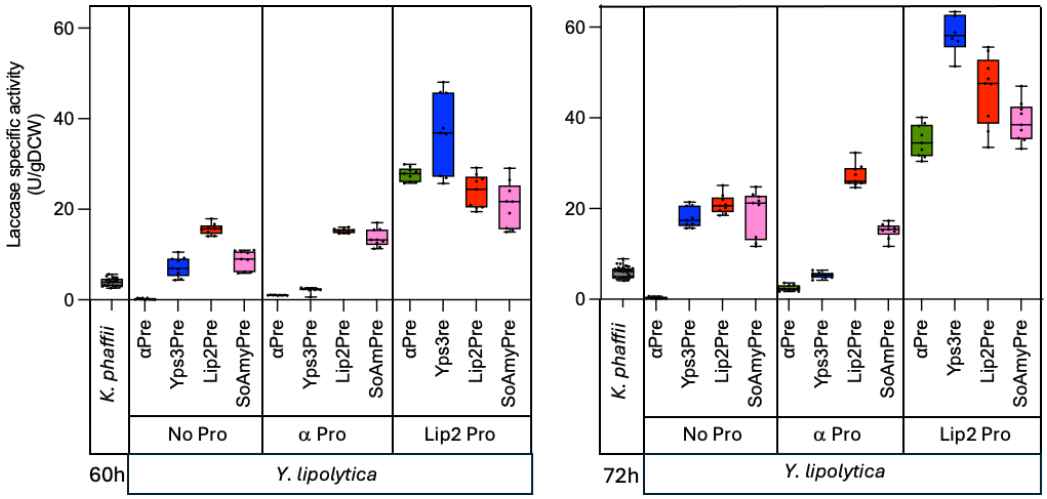

Figure 5-2. Laccase specific activity after 60 h and 72 h of growth in BMD1 medium for *K. phaffii* and YNBG-Cu for *Y. lipolytica* strains. Data are for biological triplicate cultures and technical duplicate of enzyme assays.

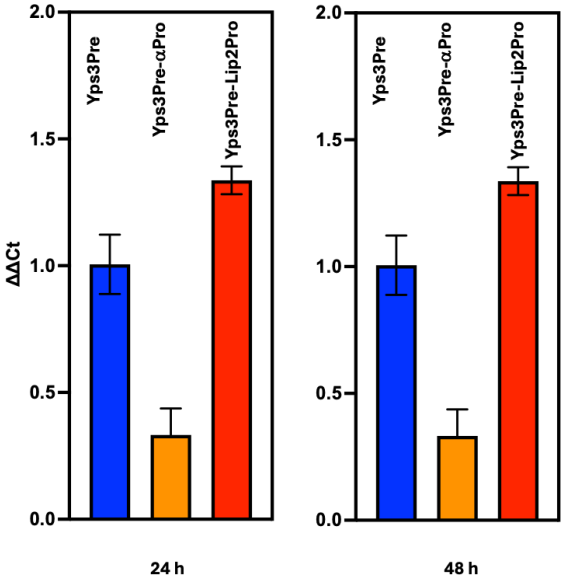

Figure 5-3. LacVader expression level for *Y. lipolytica* Yps3Pre, Yps3Pre-αPro and Yps3Pre-Lip2Pro strains grown in YNBG-Cu after 24 h and 48 h. Data are means and standard deviation of triplicate cultures. Expression levels were first normalized to that of Actin (ΔCt) and to the mean expression level of Yps3Pre (ΔΔCt).

Therefore, the nature of the pre- and pro-sequences did not appear to impose a differential metabolic burden. These findings demonstrate that the appropriate combination of pre- and pro-sequences is critical for efficient secretion, with the nature of the pro-sequence playing a decisive role in either enhancing or impairing enzyme production. Notably, the best- performing strain, Yps3Pre–Lip2Pro, achieved an eightfold higher specific activity than the *K. phaffii* reference strain. The synergistic effect of Yps3Pre-Lip2Pro highlights the potential of rational signal peptide optimization to overcome long-standing challenges in rsProt production

The present work reinforces the central role of signal peptide engineering as a key determinant of recombinant protein secretion efficiency. In *K. phaffii*, secretion performance is strongly dependent on the nature of the signal peptide, and optimal secretion is known to be highly protein-specific rather than universally transferable. While the S. cerevisiae α-mating factor remains the most widely used secretion signal, numerous studies have demonstrated that alternative heterologous and endogenous signal peptides can significantly enhance secretion yields in *K. phaffii*. For example, systematic screening approaches have shown that signal peptides derived from different yeast species (L. Wang et al., 2024; Xu et al., 2025) and endogenous signals peptides (G. Duan et al., 2019; Q. Shen et al., 2022; Zou et al., 2022). Likewise, *K. phaffii* secretory proteins can outperform the classical α-MF leader sequence in the secretion of heterologous proteins and industrial enzymes, sometimes achieving several-fold improvements in extracellular production, engineered or non-conventional signal peptides have been reported to improve secretion efficiency in a protein-dependent manner, highlighting the modular and transferable nature of signal peptide design in this host (Celińska et al., 2018; Celińska & Nicaud, 2019)..

Collectively, these findings support the concept that *K. phaffii* is not limited to a single optimal secretion signal, but rather represents a flexible platform where heterologous signal peptides from diverse biological origins can be systematically exploited to enhance rsProt production. In this context, the results presented in this chapter are consistent with and extend the established literature, further supporting signal peptide optimization as a transferable strategy for improving secretion efficiency in *K. phaffii*.

Chapter 6

General Discussion

Chapter 6: General discussion.

The background presented in Chapters 1 and 2 establishes *Komagataella phaffii* as a methylotrophic expression platform with biotechnological relevance (Lv & Cai, 2025), which is fundamentally linked to the methanol utilization pathway (MUT) and its tight transcriptional regulation via the *AOX1* promoter (J. Wang et al., 2017). This system has been extensively exploited for recombinant protein (rProt) production due to its strong inducibility and high expression capacity under methanol-based cultivation conditions.

However, the same chapters also highlight that MUT is not an isolated linear pathway but rather a highly interconnected metabolic network in which carbon assimilation, peroxisomal oxidation, and cytosolic detoxification are tightly coupled. In this context, methanol metabolism generates formaldehyde as a central intermediate, which is partitioned between assimilatory and dissimilatory routes, ultimately converging on formate and CO_2 production (Cregg et al., 1989; Berrios et al., 2022). This metabolic architecture implies that p*AOX1* regulation is not solely dependent on methanol presence but is embedded in a broader metabolic network integrating carbon flux distribution, peroxisomal activity, and cellular redox balance, as mediated by transcriptional regulators such as Mxr1 and Mit1 (G. P. Lin-Cereghino et al., 2006; Zhan et al., 2017). This context provides the conceptual framework for interpreting alternative induction mechanisms based on endogenous C1 metabolite formate in FDH-deficient strain of *K. phaffii*.

Recent studies have proposed formate as an alternative inducer of p*AOX1* (Feng et al., 2022; B. Liu, Zhao, et al., 2022a; Singh & Narang, 2020)**.** In agreement with this concept, the present work and previous results from our group Bustos et al., (2024) demonstrate that formate can induce p*AOX1* in FDH-deficient *K. phaffii* strains cultivated on sorbitol as sole carbon source (Figure 2-7, Figure 3-7D and Figure 4-5B). In chapter 3, enhanced sorbitol assimilation through *SOR1* overexpression increased carbon flux through the THF–C1 cycle in the FdhKO SdOE strain, and therefore increased the growth rate (Figure 3-5A). Nevertheless, an opposite trend is observed for formate accumulation and rProt production, and p*AOX1* induction (Figure 3-5 and 3-6B and Figure 3-6D). In chapter 3, enhanced sorbitol assimilation through *SOR1* overexpression increased carbon flux through the THF–C1 cycle in the FdhKO SdOE strain, and therefore increased the growth rate (Figure 3-5A). Nevertheless, an opposite trend is observed for formate accumulation and rProt production, and p*AOX1* induction (Figure 3-5 and 3-6B and Figure 3-6D). This result contrasts with the baseline FDH-deficient phenotype (FdhKO) reported by Bustos et al., (2024), highlighting a general principle in metabolic engineering: whereby increased substrate uptake does not necessarily translate into flux toward the desired product but depends on intracellular flux partitioning.

This observation suggests that intracellular formate accumulation emerges as a consequence of carbon flux redistribution, respiratory capacity, and redox balance. When sorbitol is used as the sole carbon source, carbon enters central metabolism through glycolysis and is channelled toward biomass formation via the 3-

phosphoglycerate node. His intermediate connects sorbitol assimilation with one-carbon metabolism through the serine biosynthesis pathway, which supplies C1 units to the tetrahydrofolate (THF) cycle (Figure 2-8). In this way, additional carbon generated by *SOR1* overexpression may have been redistributed within the THF-dependent C1 network through this node, potentially favouring biomass-associated metabolic routes such as 10-formyl-THF formation, such as purine pathway, during exponential growth (22h) of FdhKO SdOE eGfp strain (Figure 3-5A). Consequently, the flux toward serine-derived C1 metabolism in this strain is reduced, limiting intracellular formate accumulation. In contrast, FdhKO strains under limited carbon flux appear to favour induction-associated metabolic states.

In both strains, formate oxidation to CO_2 is blocked. This process is tightly coupled to redox metabolism, as oxidation of C1 units generates reducing equivalents that must be re-oxidized via the respiratory chain. Coordinated shifts in respiratory capacity, fermentative fluxes, and cofactor handling under low oxygen conditions have been demonstrated by transcriptional and proteomic analyses, which have been associated with increased intracellular NADH (Jouhten et al., 2008; Rintala et al., 2009).

The initial values established for low and high oxygen transfer coefficient (OTC) should be interpreted as initial benchmark conditions rather than constant physiological parameters throughout cultivation. In shake flask cultures, O_2 transfer changes during cultivation as a consequence of metabolism, which alters the liquid–gas interfacial area and oxygen demand (Maier & Büchs, 2001; Meier et al., 2016). This effect is particularly relevant for the FdhKO SdOE strain, which exhibited the highest growth rate (Figure 3-7A), suggesting a larger increase in oxygen demand and the most pronounced shift in effective oxygen availability over time. Considering that *K. phaffii* is a Crabtree-negative yeast and thus relies strictly on respiratory metabolism, oxygen availability becomes a primary determinant of growth performance (Bernauer et al., 2021). Accordingly, the condition with the highest OTC provides the greatest oxygen supply, which is consistent with the higher growth rates observed under these conditions (Figure 3-7A).

Across shake flask experiments, reduced oxygen transfer conditions (OTC) consistently increased p*AOX1* induction in both control and engineered strains. Improved p*AOX1* induction under low oxygen availability has been reported Velastegui et al., (2023), in agreement with improved recombinant protein yields under oxygen-limited conditions (Vogl et al., 2018). Under these conditions of low OTC, the electron transport chain becomes the main limiting NADH sink, increasing the intracellular NADH/NAD^+ ratio and creating a respiratory bottleneck. (Figure 3-7D and 3-8A). In methylotrophic and related yeasts, elevations in the NADH/NAD^+ ratio and alterations in NAD-dependent enzyme activities have been documented under oxygen limitation, conditions under which accumulation of reduced C1 intermediates or overflow metabolites implicated in promoter regulation has been observed (Jayachandran et al., 2017a; Vemuri et al., 2007). Cellular redox homeostasis can be perturbed by this condition, limiting respiratory reoxidation of NADH at the electron transport chain, thereby increasing the cellular NADH/NAD^+

ratio; this alteration in redox cofactor balance has immediate consequences for dehydrogenase activities, glycolytic flux, and one-carbon metabolism (Tomàs-Gamisans et al., 2020). This redox imbalance reduces respiratory ATP generation, slows growth, and forces metabolic rerouting toward alternative oxidative pathways, including THF-linked C1 metabolism, thereby explaining the simultaneous increase in intracellular formate and p*AOX1* induction observed under oxygen limitation. Alterations in redox potential across multiple organelles (cytosol, ER, mitochondria, peroxisomes) under hypoxic conditions have been measured using glutathione GS(H)/GSSG redox sensors, and increased rProt secretion has been observed under these conditions (Kostopoulou et al., 2025). Altogether, these findings support that, in methanol-free induction, oxygen limitation increases *pAOX1* induction via redox cofactor shifts (e.g., higher NADH/NAD^+) and altered GS(H)/GSSG ratio, which favors formate accumulation. Hypoxia creates a physiological state analogous to respiratory overflow metabolism, where reduced energy yield and redox imbalance promote carbon redistribution away from biomass formation toward C1 oxidation.

In contrast to sorbitol assimilation engineering, in chapter 4, serine metabolism is closely connected to the C1 cycle, as serine catabolism via serine hydroxymethyltransferase generates glycine and 5,10-methylene-THF, thereby directly contributing to one-carbon units and formate. Serine metabolism therefore feeds the tetrahydrofolate (THF)-dependent C1 cycle and plays a central role in supplying one-carbon units. Consequently, *SER3* overexpression enhances the upstream supply of serine-derived C1 units and increases flux through the THF–C1 network without compromising central carbon metabolism. This explains the simultaneous increase in formate levels and the maintenance of robust growth. Bustos et al., (2024) demonstrated that exogenous serine supplementation increased *pAOX1* induction compared to sorbitol alone, strongly implicating serine metabolism in C1-driven induction. *SER3*, which encodes the phosphoglycerate dehydrogenase catalysing the first and limiting step of serine biosynthesis. This modification produced the strongest performance among tested strains (Figure 4-5C). This observation is correlated with previous reports in *Saccharomyces cerevisiae* for *SER3* and the paralog gene *SER33,* which has been reported as a critical step for the serine biosynthesis pathway (Kobayashi et al., 2022) The *m*SER3 strain showed a strong increase in induction and rProt production relative to the parent strain, achieving 86% of fold-increase eGFP obtained with the reported in minimal media with sorbitol and added serine (Bustos et al., 2024). Moreover, *m*SER3 strain grown in mixed glycerol–sorbitol cultures achieved 100% of this value without adding serine to the culture medium (Figure 4-7B).

The observed correlation between intracellular formate accumulation and p*AOX1* induction suggests that formate contributes to promoter activation through regulatory pathways that may involve transcription factors acting on the p*AOX1* upstream activating sequences (UAS). The presence of formate is an indicator of the dissimilatory pathway; therefore, some of the MUT pathway signals would be active, which may be related to the regulation of transcription factors that regulate p*AOX1*, such as Mrx1 or Mit1 transcriptional network toward a methylotrophic-like

expression state. Instead, the current evidence supports an indirect mechanism in which formate reflects the global metabolic state of the cell, integrating carbon flux distribution, redox balance, and one-carbon (C1) availability. Furthermore, to date, no transcription factor has been identified in this organism.

Most strikingly, in this strategy, the growth rate remained essentially unchanged, maintaining the same cell growth throughout cultivation (Figure 4-7A and 4-8C). *SER3* overexpression also increased formate levels in *m*SER3 and GOX-SER3 strains (Figure 4-3C and 4-4B), indicating enhanced flux through the serine pathway. This increase suggests higher flux of the serine–THF–C1 cycle than the FdhKO strains, which increases 5,10-methylene-THF and formate pools without draining central metabolism. C1 flux is tightly connected to cellular redox homeostasis, since interconversion of C1 intermediates is coupled to NAD(P)H-dependent reactions. However, the relationship between formate accumulation, redox balance, and p*AOX1* induction remains to be elucidated. In *S. cerevisiae, SER3* overexpression has been associated with a 1.8-fold increase in glutathione content (Kobayashi et al., 2022). In agreement with this, increased serine biosynthesis is suggested to expand the pool of C1 units without depleting carbon skeletons or cofactors required for biomass formation, contributing to improved redox buffering capacity in the engineered strains, enhancing resistance to oxidative stress associated with increased metabolic activity. Enhanced serine biosynthesis is expected to increase the availability of glycine and subsequently feed the methionine cycle, thereby supporting S-adenosylmethionine (SAM)-dependent reactions and contributing to glutathione biosynthesis. Glutathione acts as an antioxidant (Ianshina et al., 2023; Kostopoulou et al., 2025), which may contribute to the improved phenomenon observed. Based on this premise, serine metabolism is closely linked to glycine synthesis and one-carbon metabolism, increased flux through this pathway could potentially influence glutathione biosynthesis. Although glutathione levels were not measured in the present study, these observations suggest that *SER3* overexpression may have broader metabolic consequences beyond formate accumulation. Further studies would be required to determine the possible contribution of glutathione metabolism to p*AOX1* induction in *K. phaffii* and whether they contribute to the observed phenotype, which remains unclear.

Regarding formate accumulation, although no evidence suggests acute toxicity under the tested conditions. The formate concentration in the *m*SER3 strains background were low (29 μM, Figure 4-7C and 62 μM, Figure 4-8B), which are well below the concentration considered toxic to cells (20 mM (Singh & Narang, 2020)).

The absence of growth impairment in the *m*SER3 strains suggests that the increased intracellular formate levels did not reach concentrations that adversely affected growth under the conditions tested. However, a quantitative limit for tolerance remains undefined in *K. phaffii* strains tests in this study. In this context, future studies should systematically evaluate formate-dependent stress responses, including intracellular pH regulation, NADH/NAD^+ ratios, reactive oxygen species formation, glutathione redox state (GSH/GSSG), and mitochondrial performance, in order to define the physiological boundaries of FDH-deficient systems. Although p*AOX1*

regulation was not directly engineered in this work, the observed association between enhanced serine metabolism, increased formate accumulation, and improved p*AOX1* induction indicates a functional link between these processes. The molecular mechanisms underlying this relationship remain unknown and warrant further investigation. This interaction is most likely indirect. The C1 metabolite availability rather than by direct sensing of formate itself, providing a mechanistic basis for methanol-free modulation of p*AOX1* induction. This interpretation aligns with observations of (Bustos et al., 2024) and provides a mechanistic basis for future investigation of methanol-free induction systems.

Compared with other methanol-free strategies, the FDH-deficient/*m*SER3 strain occupies a distinct conceptual space. As mentioned earlier in Chapter 2, constitutive promoters such as p*GAP* enable continuous expression but generally show lower induction compared to p*AOX1*, lacking tight regulatory control desirable for industrial applications (Prielhofer et al., 2017). Alternative inducible promoters such as p*FLD1* (induced by methylamine) (S. Shen et al., 1998) and *pPEX8* (induced by methylamine or oleate) (H. Liu et al., 1995) have been investigated; however, they remain less widely used than p*AOX1* in the industry. Co-feeding strategies combining glycerol or sorbitol with small amounts of methanol provide partial solutions (Berrios et al., 2022; Carly et al., 2016; Niu et al., 2013) do not fully eliminate methanol. In contrast, this work maintains p*AOX1* regulation while decoupling it from methanol dependence, exploiting endogenous C1 metabolism to achieve methanol-free p*AOX1*-driven expression.

Beyond metabolic effects, the *SER3* overexpression provides strain-specific physiological parameters that can be directly translated into process design criteria. In high-cell-density cultivations of *K. phaffii*, oxygen transfer and carbon feeding represent key operational constraints, particularly at high biomass concentrations (60–100 gDCW·L^{-1}), where volumetric oxygen demand increases significantly (Cos et al., 2006; Potvin et al., 2012; Stratton et al., 1998). Particularly in SER3-strain, dissolved oxygen remained non-limiting during sorbitol consumption under the conditions tested. The experimentally determined specific oxygen uptake rate (qO_2: 3.4 mg O_2·gDCW^{-1}·h^{-1}) and sorbitol uptake rate (qSor: 0.025 g·gDCW^{-1}·h^{-1}) can be condition-dependent physiological parameters of the SER3-GOX strain. These relatively low consumption rates are favorable from a process economics perspective, as they reduce oxygen demand at industrial scale. A theoretical extrapolation to 80 gDCW·L^{-1} predicts an OUR value of approximately 270 mg O_2·L^{-1}·h^{-1} (~8.5 mmol·L^{-1}·h^{-1}), which can be used to estimate the required oxygen transfer capacity according to classical bioreactor design relationships ($OUR = OTR = kLa \cdot (C^* - CL)$) (Garcia-Ochoa & Gomez, 2009). In parallel, the projected sorbitol consumption rate (~2 g·L^{-1}·h^{-1} at 80 gDCW·L^{-1}) provides a quantitative basis for implementing a biomass-proportional, carbon-limited feeding strategy, a condition known to support metabolic stability and prevent substrate accumulation in high-cell-density *K. phaffii* processes (Cos et al., 2006; Potvin et al., 2012; Stratton et al., 1998). Thus, the physiological characterization of the SER3-GOX strain enables rational definition of aeration capacity, agitation regime, and feeding profile under realistic industrial

operating conditions, bridging metabolic engineering outcomes with scalable bioprocess design.

However, rProt production in yeast is inherently complex. Multi-step processes depend not only on transcriptional control and metabolism but also other factors such as protein folding, processing, and secretion (Gasser et al., 2008; Delic et al., 2013). Among these factors, signal peptides play a critical role by directing proteins into the secretory pathway, thereby influencing secretion efficiency and final product yield (Puxbaum et al., 2015; Spohner et al., 2015). From an integrated bioprocess engineering perspective, optimal protein production requires coordination of promoter regulation, metabolic flux, and secretory capacity (Gasser et al., 2008). The combined consideration of these factors enables the rational design of improved expression systems. The selection of nine combinations of pre- and pro-sequences of signal peptides (SPs) in Chapter 5 was guided by a systematic design-of-variations strategy rather than a single-target optimization. The rationale was to capture the combinatorial nature of secretory efficiency, where SPs influence multiple sequential steps including endoplasmic reticulum (ER) targeting, translocation, pro-peptide processing, and secretion kinetics (Delic et al., 2013; Gasser et al., 2008). Because these processes are highly context-dependent and protein-specific, the goal was not only to identify a "best performer" but to map functional compatibility between secretion signals and heterologous proteins under the engineered *K. phaffii* FDH-deficient.

In this regard, the superior performance observed with *Yarrowia lipolytica*-derived SPs for laccase secretion does not undermine the relevance of the methanol-free *K. phaffii* platform; rather, it highlights that secretion bottlenecks remain protein- and host-dependent even in optimized expression systems. While *Y. lipolytica* is a well-established industrial microorganism*, K. phaffii* remains more established as a platform for recombinant protein production due to its highly standardized expression and fermentation systems*,* such as p*AOX1* use, and well-established regulatory and safety frameworks for recombinant protein manufacturing, particularly for secreted enzymes and pharmaceutical proteins, where process robustness and genetic tractability are critical (Cregg et al., 2000; Delic et al., 2013; Gasser et al., 2013; Vogl & Glieder, 2013).

Conversely, *Y. lipolytica* may outperform in specific secretion-heavy cases such as oxidoreductases or native-like folding-dependent enzymes (Madzak, 2018) but lacks the same level of industrial standardization and promoter engineering depth available in *K. phaffii* (Cereghino & Cregg, 2000; Gasser et al., 2013; Prielhofer et al., 2013). Therefore, rather than weakening the conclusions of the previous chapters, these results reinforce the concept that optimal recombinant protein production cannot be attributed to a single engineering layer (metabolic, transcriptional, or secretory), emerging from their integration.

Regarding the absence pre- and pro-peptide testing on *K. phaffi* was a deliberate scope decision: the study aimed to evaluate whether heterologous secretion signals could expand the secretion landscape beyond the canonical *K. phaffii* toolkit, rather than performing an exhaustive re-optimization of endogenous signal peptides already extensively characterized in the literature (G. Duan et al., 2019; Zou et al., 2022).

Nonetheless, the results strongly suggest that incorporating systematic pre/pro-peptide engineering within *K. phaffii* itself would be a logical extension to further close the gap between metabolic engineering and secretion efficiency in future work.

Overall, exploring signal peptides derived from *Y. lipolytica* in *K. phaffi* FDH-deficient, such as the SPs tested for laccase production in Chapter 5, may expand the scope of the strategy developed by addressing a key downstream bottleneck in recombinant protein production. Together with the methanol-free induction approach developed through metabolic engineering, signal peptide optimization contributes to the establishment of more efficient and industrially relevant yeast expression platforms

The implications of these findings are relevant for economic investment. The global enzyme market is projected to surpass USD 20.4 billion by 2029, driven by applications in food, feed, textiles, detergents, and bioenergy (MarketsandMarkets, 2024). In therapeutic and industrial protein production, there is increasing interest in avoiding methanol-based induction systems due to safety, handling, and regulatory considerations, creating demand for methanol-free systems. The developed approach in this work offers advantages in safety and regulatory compliance, as facilities would no longer require methanol storage or handling infrastructure. Methanol-free systems, therefore, represent a valuable alternative for simplifying process infrastructure. Furthermore, such systems may broaden the applicability of *K. phaffii*-based production platforms. The increased induction levels achieved through serine pathway engineering, without compromising cellular fitness, are particularly relevant for large-scale implementation, as they suggest improved scalability without metabolic burden trade-offs.

To summarize, this study provides a promising framework for methanol-free induction of *pAOX1* in *K. phaffii*. The *SOR1* overexpression highlighted the sensitivity of induction to metabolic flux redistribution, whereas the *SER3* overexpression demonstrated that changes in serine metabolic fluxes can enhance induction without fitness penalties. Oxygen transfer conditions further emphasize the importance of integrating metabolic and process engineering perspectives. Compared with other methanol-free systems, this approach preserves the regulatory advantages of p*AOX1* while eliminating methanol feeding, positioning it as a potentially valuable strategy for industrial applications. Expressing outcomes in terms of fold-changes facilitates generalization beyond specific recombinant proteins. Collectively, these findings contribute to a deeper understanding of C1 metabolism in *K. phaffii* and support the development of methanol-free bioprocess strategies.

Chapter 7

Conclusions and perspectives

Chapter 7: Conclusions and Perspectives.

1. Conclusions.

This research has focused on the use of an FDH-deficient *Komagataella phaffii* yeast strain to develop strategies aimed at enhancing *AOX1* promoter (p*AOX1*) induction as a means of reducing the risks associated to methanol use. The proposed strategies have led to the development of new strains with noteworthy features for recombinant protein (rProt) production, which has allowed it to continue exploring and deepening our understanding of p*AOX1* induction. The following conclusions can be drawn from this study:

Formate accumulation correlates with p*AOX1* induction in FDH-deficient strains, yet formate itself likely does not function as a directly sensed inducer. Instead, it behaves as a metabolic state indicator reflecting the activity of the dissimilatory C1 pathway and the global redox configuration of the cell. This supports an indirect regulatory model in which C1 flux, NADH/NAD^+ balance, and respiratory capacity converge to shape p*AOX1* regulation.

Increased substrate uptake does not necessarily enhance induction. Overexpression of *SOR1* improved sorbitol assimilation and growth rate but reduced formate accumulation and rProt production and p*AOX1* induction. This demonstrates that carbon flux redistribution toward biomass-associated pathways can dilute induction-associated metabolic states. Thus, intracellular flux partitioning, rather than absolute carbon uptake, determines induction efficiency.

The oxygen transfer conditions (OTC) play a decisive role in modulating induction. Reduced OTC consistently enhanced p*AOX1* induction and rProt production. Oxygen limitation appears to reinforce C1-associated metabolic states that favor formate accumulation and p*AOX1* induction.

Engineering of the serine biosynthesis pathway represents a more effective strategy than carbon assimilation enhancement. Overexpression of *SER3* increased flux through the serine–THF–C1 cycle, elevated intracellular formate levels, and enhanced rProt production without impairing growth, reinforcing induction-associated metabolic states. The results position serine metabolism as a metabolic control node linking central carbon metabolism, redox balance, and C1 flux.

Formate accumulation in the tested range was not toxic and remained within physiological tolerance limits. The absence of growth impairment indicates that the engineered system operates within a buffered metabolic regime, supporting its potential scalability.

The physiological characterization of the SER3-GOX strain demonstrates that the methanol-free platform is compatible with industrial bioprocess requirements. The qO_2 and qSor rates provide realistic parameters for estimating aeration capacity and biomass-proportional feeding strategies at high cell density, directly linking strain engineering with scalable process design. This strain enables a clear decoupling of the growth and induction phases, allowing biomass accumulation on glycerol followed by

controlled p*AOX1* induction without methanol. This preserves the classical process architecture of *K. phaffii* while improving safety and process sustainability.

Signal Peptides (SPs) engineering demonstrated that secretion efficiency is protein- and host-dependent. Although *Yarrowia lipolytica*-derived SPs outperformed native configurations in specific cases, methanol-free *K. phaffii* retains strategic industrial advantages, including established high-cell-density fermentation processes, regulatory familiarity, and well-characterized promoter systems. The secretory pathway optimization can be considered a complementary strategy.

2. Perspectives.

This work has provided valuable insights into the development of new methanol-free p*AOX1* induction systems. The mechanism underlying formate-mediated induction on non-repressive carbon sources in an FDH-deficient strain was elucidated, highlighting sorbitol as an optimal carbon source for this newly proposed system. Nevertheless, several research directions could further enhance this platform:

The FdhKO SdOE strain, despite accumulating less formate than FdhKO, represents an interesting system for further study. The strategy developed in chapter 4 (*SER3* overexpression) can complement this strain to accumulate formate to improve p*AOX1* induction.

It has been experimentally documented by various authors that formate can act as an inducer of the p*AOX1* in *K. phaffi* (Bustos et al., 2024; Feng et al., 2022; Jayachandran et al., 2017b; B. Liu, Li, et al., 2022b; B. Liu, Zhao, et al., 2022b; Singh & Narang, 2020). Until today, the molecular mechanisms involved in these related elements have not been reported yet. Although formate accumulation correlates with p*AOX1* induction, the molecular sensing mechanism remains undefined. Future studies should: Characterize transcription factor dynamics (Mxr1, Mit1) under varying C1 fluxes and perform transcriptomic and metabolomic analyses to identify regulatory signatures associated with induction. Elucidation of these mechanisms represents a key step toward rational improvement of this system.

SER3 strains showed a 48% increase in specific eGFP fluorescence in microreactor cultivations and a 30% increase in specific Gox activity in bioreactor cultivations compared with the parental strain. These improvements highlight the potential for further strategies to enhance recombinant protein yields under methanol-free conditions to define oxygen transfer thresholds for optimal induction, establish scalable feeding strategies, and quantify volumetric productivity under high-cell-density conditions focused on bioreactor optimization and subsequent scale-up to industrial operating conditions. Integration of metabolic and process engineering will be critical for industrial translation. This approach will aim to identify optimal parameters for recombinant protein production and evaluate their applicability for the industrial production of valuable compounds.

Future work should incorporate systematic pre- and pro- SPs investigated in chapter 5 to use directly in the FDH-deficient *K. phaffii* background optimized with the strategies developed in this project to enable host-consistent comparisons and eliminate secretion as a potential bottleneck.

Appendix

Appendix.

Appendix 1.

Table A3-1. *Escherichia coli strains list used in the 3rd chapter.*

Strain name (plasmid)	Plasmid - genotype	Source/Reference
A2	BB1_23	(Prielhofer et al., 2017)
D12	BB3aZ_14	(Prielhofer et al., 2017)
A4	BB1_12_p*GAP*	(Prielhofer et al., 2017)
C1	BB1_34_*ScCYC1*tt	(Prielhofer et al., 2017)
C9	BB1_34_*RPS3*tt	(Prielhofer et al., 2017)
C12	BB3aK_AC	(Prielhofer et al., 2017)
D4	BB2_AB	(Prielhofer et al., 2017)
D5	BB2_BC	(Prielhofer et al., 2017)
RIE341 (RIP341)	A2_BB1_23_*SOR1*	This work
RIE343 (RIP343)	A2_BB1_23_Pp*HXT1*	This work
RIE354 (RIP354)	BB3-p*GAP*- Pp*HXT1-ScCYC1*tt	This work
RIE355 (RIP355)	BB3-p*GAP-SOR1-ScCYC1*tt	This work
RIE370 (RIP370)	BB3-AC-LoxP-Zeo-loxP	This work
RIE372 (RIP372)	BB2(AB)-p*GAP-SOR1- ScCYC1*tt	This work
RIE374 (RIP374)	BB2(BC1)-p*GAP*-Pp*HXT1-RPS3*tt	This work
RIE378 (RIP378)	BB3a-p*GAP-SOR1-ScCYC1*tt, p*GAP*-Pp*HXT1-RPS3*tt	This work

Appendix 2.

***Table A3-2**. Primer list used in the 3rd chapter.*

Name	Sequence 5´to 3´	Restriction site/gene
M13-Fw	gtaaaacgacggccagt	
M13-RV	aacagctatgaccatg	
pGAP.Int-Fw	cgtcgctggcaataatagcgg	
ScCYC1tt.Int-Rv	gggacctagacttcaggttgtc	
Rps3tt.Int-Rv	gacgagtccagggctatcttaag	
SOR1-Fw	c**ggtctc**acatgtccgataacccaagtgttatcttaaaaggattaatgagatt gtcatagaagatagaccaattccagccattgaggatcctcactatgtgaaa atagcaatcaaaagaccggaatttg	*Bsa*I
SOR1-Rv	c**ggtctc**caagctttactctgggccgtcaatgatag	*Bsa*I
qAct-F	agatggctccgagaagttca	*ACT1*
qAct-R	gttgctcagagggcttcaac	*ACT1*
qeGFP-F	atcatggccgacaagcagaa	e*GFP*
qeGFP-R	tctcgttggggtctttgctc	e*GFP*
ST_qPCR_Fo	ccaggtgttttcgtcgttgt	Pp*HXT1*
ST_qPCR_Rev	aggcgaacagagtacatccc	Pp*HXT1*
SDH_qPCR_Fo	cccgtctcgttacagcaatg	*SOR1*
SDH_qPCR_Rev	gcatggacagcaacactcaa	*SOR1*

*Bsa*I site is in bold.

Appendix 3.

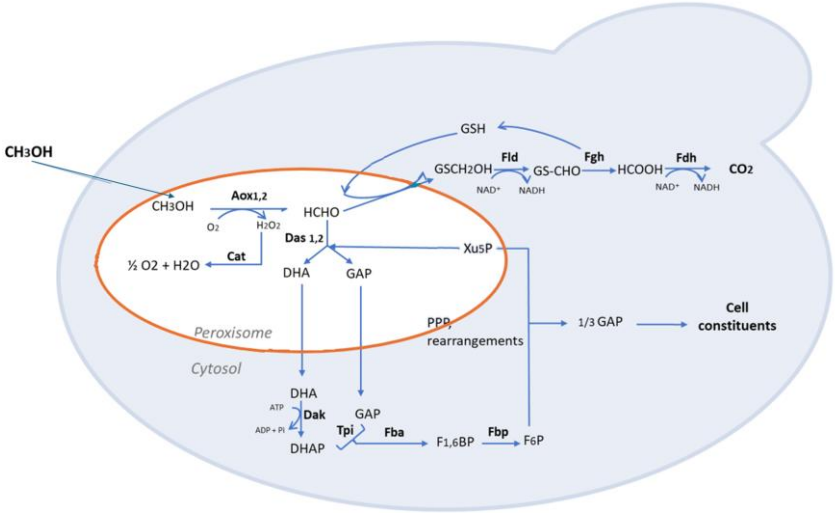

Figure A3-3. Methanol utilization pathway in *Komagataella phaffii*. Aox1, 2: alcohol oxidase1 and 2; Cat: catalase; Das1, 2: dihydroxyacetone synthase; Fld: formaldehyde dehydrogenase; Fgh: S-formylglutathione hydrolase; Fdh: formate dehydrogenase; Dak: dihydroxyacetone kinase; Tpi: triose phosphate isomerase; Fba: fructose-1,6-bisphosphate aldolase; Fbp: fructose-1,6-bisphosphatase; GS(H): glutathione; DHA: dihydroxyacetone; DHAP: dihydroxyacetone phosphate; GAP: glyceraldehyde-3-phosphate; F1,6BP: fructose-1,6-bisphosphate; F6P: fructose-6-phosphate; Xu5P: xylulose 5-phosphate.

Appendix 4.

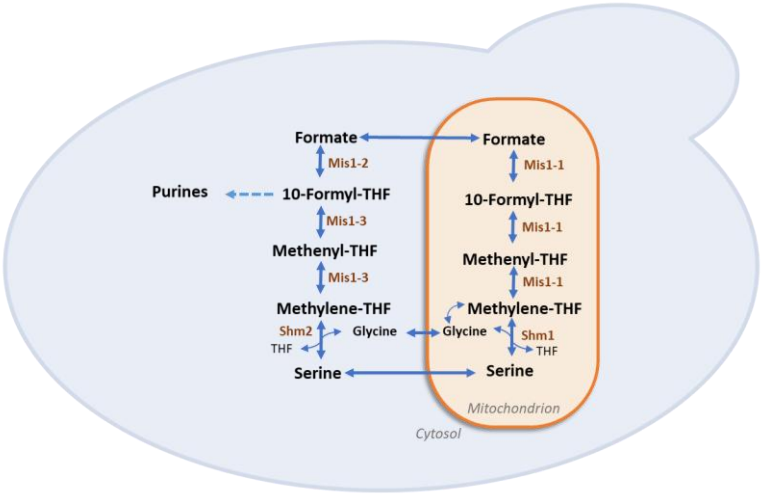

Figure A3-4. Tetrahydrofolate (THF) mediated one-carbon (THF-C1) metabolism in yeast. Fdh, formate dehydrogenase; Shm1, mitochondrial serine hydroxymethyltransferase; Shm2, cytosolic serine hydroxymethyltransferase; Mis1-2, formate-tetrahydrofolate ligase; Mis1-3, methylenetetrahydrofolate dehydrogenase & methenyltetrahydrofolate cyclohydrolase; Mis1-1, trifunctional enzyme: formate-tetrahydrofolate ligase, methenyltetrahydrofolate cyclohydrolase and methylenetetrahydrofolate reductase; THF, tetrahydrofolate. Figure adapted from (Bustos, et al.2024).

Appendix 5.

```
XP_002489933 - K. phaffii GS115   1   MS--DNPSVILKRINEIVIEDRPIPAIEDPHYVKIAIKKTGICGSDVHFYTDGCCGSFKL  58
                                      MS   NP+V+L+++ +I IE RPIP I+DPHYVK+AIK TGICGSD+H+Y  G  G + L
XKU26523.1 - S. cerevisiae        1   MSQNSNPAVVLEKVGDIAIEQRPIPTIKDPHYVKLAIKATGICGSDIHYYRSGGIGKYIL  60

XP_002489933 - K. phaffii GS115   59  ESPMVLGHESAGIVVEVGSEVKSLRVGDKVACEPGIPSRYSNAYKSGHYNLCPEMAFAAT  118
                                      ++PMVLGHES+G VVEVG  V  ++VGD+VA EPG+PSRYS+  K G YNLCP MAFAAT
XKU26523.1 - S. cerevisiae        61  KAPMVLGHESSGQVVEVGDAVTRVKVGDRVAIEPGVPSRYSDETKEGRYNLCPHMAFAAT  120

XP_002489933 - K. phaffii GS115   119 PPIDGTLCRYFLLPEDFCVKLPEHVSLEEGALVEPLSVAVHAARLAKITFGDSVVVFGAG  178
                                      PPIDGTL +Y+L PEDF VKLPE VS EEGA VEPLSV VH+ +LA + FG  VVVFGAG
XKU26523.1 - S. cerevisiae        121 PPIDGTLVKYYLSPEDFLVKLPEGVSYEEGACVEPLSVGVHSNKLAGVRFGTKVVVFGAG  180

XP_002489933 - K. phaffii GS115   179 PVGLLVAATARAYGATNVLIVDIFDDKLTLAKDTLQVATHSFNS--------KNGMDNLL  230
                                      PVGLL  A ARA+GAT+V+ VD+FD+KL  AKD    AT++FNS         ++  D +
XKU26523.1 - S. cerevisiae        181 PVGLLTGAVARAFGATDVIFVDVFDNKLQRAKDF--GATNTFNSSQFSTDKAQDLADGVQ  238

XP_002489933 - K. phaffii GS115   231 ESFEGKHPNVSIDCTGVESCIAAGINALAPRGVHVQVGMGKSEYNNFPLGLICEKECIVK  290
                                      +   G H +V  +C+G + CI A +      G  VQVGMGK+ Y NFP+  +  KE  +
XKU26523.1 - S. cerevisiae        239 KLLGGNHADVVFECSGADVCIDAAVKTTKVGGTMVQVGMGKN-YTNFPIAEVSGKEMKLI  297

XP_002489933 - K. phaffii GS115   291 GVFRYCYNDYNLAVELIASGKVEVKGLVTHRFKFTEAVDAYD--TVRQGKAIKAIIDGPE  348
                                      G FRY + DY  AV L+A+GKV VK L+TH+FKF +A  AYD      G+ +K II GPE
XKU26523.1 - S. cerevisiae        298 GCFRYSFGDYRDAVNLVATGKVNVKPLITHKFKFEDAAKAYDYNIAHGGEVVKTIIFGPE  357
```

Figure A3-5. Sorbitol Dehydrogenase enzyme. Protein alignment. XP_002489933.1 corresponds to (gene PAS_chr1-1_0490) protein sequence *K. phaffii*, and XKU26523.1 corresponds to *Saccharomyces cerevisiae*.

Appendix 6.

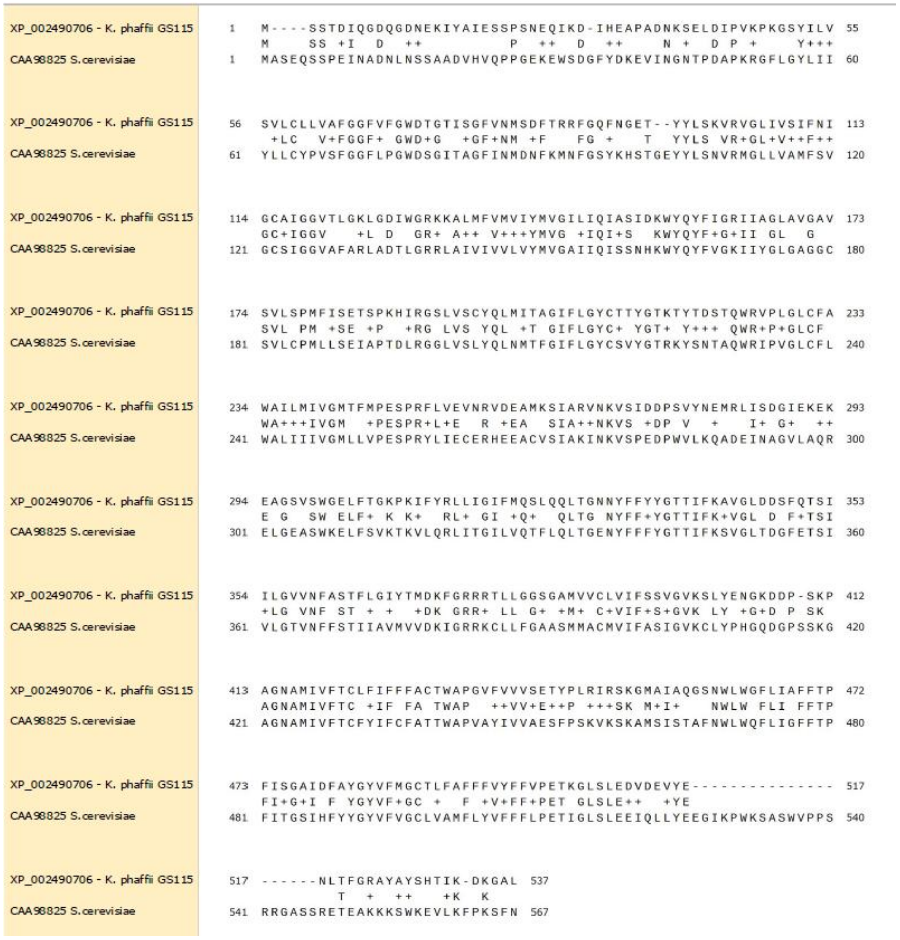

Figure A3-6. Hexose transporter protein. Protein alignment. XP_002490706.1 corresponds to (gene PAS_chr1-4_0570) protein sequence *K. phaffii*, and CAA98825.1 corresponds to *Saccharomyces cerevisiae*.

Appendix 7.

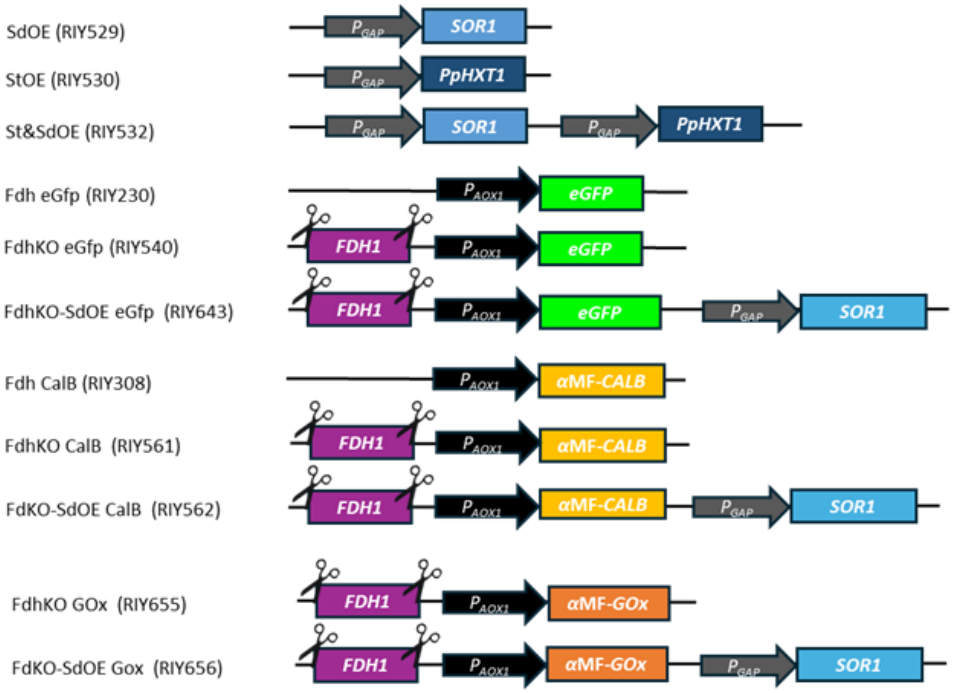

Figure A3-7. Schematic representation of the genotype of yeast strains used in 3rd chapter.

Appendix 8.

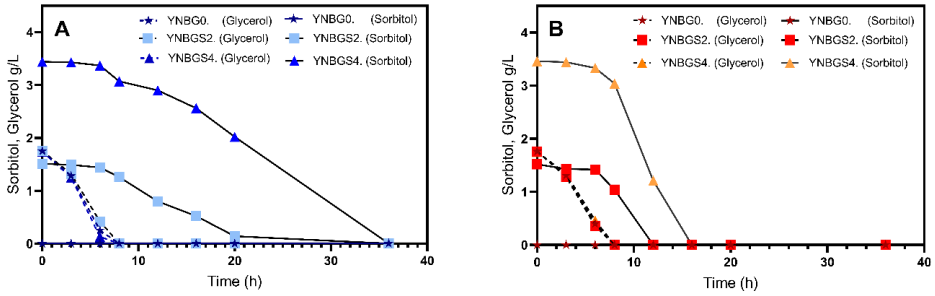

Figure A3-8. Glycerol and sorbitol concentration during the growth of FdhKO eGfp strain (blue colors, Panel A) and FdhKO SdOE eGfp strain (orange colors, Panel B) in YNB minimal medium containing different mixtures of glycerol and sorbitol (YNBG0, 1.75 g·L^{-1} glycerol; YNBGS2, 1.75 g·L^{-1} glycerol and 1.75 g·L^{-1} sorbitol; YNBGS4, 1.75 g·L^{-1} glycerol and 3.5 g·L^{-1} sorbitol). The data show one representative culture.

Appendix 9.

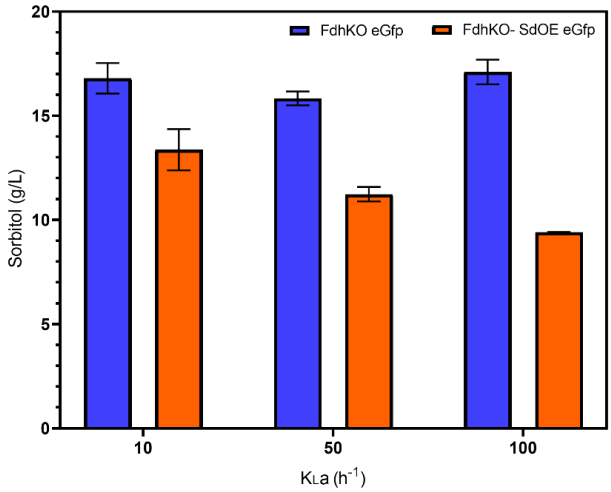

Figure A3-9. Sorbitol concentration after 22 h of growth of strains SdhKO eGfp (blue) and SdhKO SdOE eGfp (orange) in the YNBS2 medium under different OTC (low, K_La 10 h^{-1}; medium, K_La 10 h^{-1}; high, K_La 100 h^{-1}). Data are the mean and standard deviation of triplicate cultures conducted in in shake flasks.

Appendix 10.

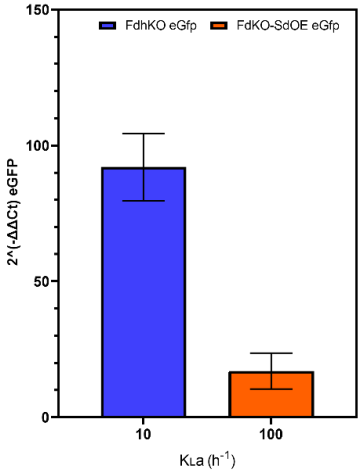

Figure A3-10. e*GFP* gene expression level for FdhKO eGfp and FdhKO-SdOE eGfp strains cultured strains grown under different OTC (low, K_La 10 h^{-1}; high, K_La 100 h^{-1}), in shake-flask cultures. Culture samples were taken at the mid-exponential growth phase (i.e. after 22 h). Data are means and standard deviations of triplicate cultures. Gene expression levels were normalized according to that of actin gene.

Apendix 11.

Table A4-1. *Escherichia coli strains list used in the 4th chapter.*

Strain name (plasmid)	Plasmid, genotype, (integration locus)	Source/Reference
A2, GoldenPiCS kit	BB1_23	(Prielhofer et al., 2017)
D12, GoldenPiCS kit	BB3aZ_14 (*AOX1*tt, *AOX1* terminator PP7435_Chr4-013)	(Prielhofer et al., 2017)
E1, GoldenPiCS kit	BB3eH_14 (*ENO1*, PP7435_Chr3-1154)	(Prielhofer et al., 2017)
E8, GoldenPiCS kit	BB3rN_14 (*RGI2*, PP7435_Chr1-0725)	(Prielhofer et al., 2017)
A4, GoldenPiCS kit	BB1_12_p*GAP*	(Prielhofer et al., 2017)
A9, GoldenPiCS kit	BB1_12_p*MDH3*	(Prielhofer et al., 2017)
B8, GoldenPiCS kit	BB1_12_p*AOX1*	(Prielhofer et al., 2017)
C1, GoldenPiCS kit	BB1_34_*ScCYC1*tt	(Prielhofer et al., 2017)
RIE396 (RIP396)	pKTAC-Cre	(Bustos et al., 2024)
RIE457 (RIP457)	pUC57-*aMF* (codon optimized)	This work
RIE485 (RIP485)	pGEM®-T-*GOX* (codon optimized)	This work
RIE504 (RIP504)	A2_BB1_23_*aMFGOX*	This work
RIE507 (RIP507)	BB3aZ_14-p*AOX1-aMFGOX-ScCYC1*tt, integration at *AOX1*tt locus	This work
RIE508 (RIP508)	TOPO_*SER1*	This work
RIE509 (RIP509)	TOPO_*SER2*	This work
RIE510 (RIP510)	TOPO_*SER3*	This work
RIY511 (RIP511)	BB3aZ_14-p*GAP-SER1-ScCYC1*tt, assembly of parts 1, 8,14, D12	This work
RIE512 (RIP512)	BB3aZ_14-p*MDH3-SER1-ScCYC1*tt, assembly of parts 4, 9, 14, D12	This work
RIE513 (RIP513)	BB3aZ_14-p*GAP-SER2-ScCYC1*tt, assembly of parts 2, 10, 16, D12	This work
RIE514 (RIP514)	BB3aZ_14-p*MDH3-SER2-ScCYC1*tt, assembly of parts 5, 11, 16, D12	This work
RIE515 (RIP515)	BB3aZ_14-p*GAP-SER3-ScCYC1*tt, assembly of parts 1, 12, 17, D12	This work
RIE516 (RIP516)	BB3aZ_14-p*MDH3-SER3-ScCYC1*tt, assembly of parts 6, 13, 17, D12	This work
RIE517 (RIP517)	BB3eH_14-p*GAP-SER1-ScCYC1*tt, assembly of parts 1, 8, 15, E1	This work
RIE518 (RIP518)	BB3eH_14-p*MDH3-SER1-ScCYC1*tt, assembly of parts 4, 9, 15, E1	This work
RIE519 (RIP519)	BB3rN_14-p*MDH3-SER3-ScCYC1*tt, assembly of parts 7, 4, 18, E8	This work

Appendix 12.

Table A4-2. *Primer list used in the 4th chapter.*

Name	Sequence 5´to 3´
M13-Fw	Gtaaaacgacggccagt
M13-Rv	Aacagctatgaccatg
SER1-Fw	Atggcaaaaactttggaaagagaa
SER1-Rv	Tcaagaatgagcttcagcaa
SER2-Fw	Atgagttatcgtttaactgc
SER2-Rv	Ctattcgttaagaaatccct
SER3-Fw	Atggcttctccccaagatat
SER3-Rv	Ctagtatagcagacgggtga
1.pGAP.SER1-Rv	**Caaagtttttgccatggtgttttgatag**ttgttcaattgatt
2.pGAP.SER1-Fw	**ctatcaaaacaccatggcaaaaactttg**gaaagagaagaacca
1.pMDH3.SER1-Rv	**caaagtttttgccatgttgttattgttc**gttggttgtaactctaaagtct
2.pMDH3.SER1-Fw	**gaacaataacaacatggcaaaaactttg**gaaagagaagaacca
3.SER1.C1-Rv	**aaaaggggcctgaagctcaagaatgagcttc**agcaaattcgatg
4.SER1.C1-Fw	**gaagctcattcttgagcttcaggcccctttt**cctttgtcgatatca
1.pGAP.SER2-Rv	**taaacgataactcatggtgttttgatag**ttgttcaattgatt
2.pGAP.SER2-Fw	**ctatcaaaacaccatgagttatcgttta**actgctatttcaaag
1.pMDH3.SER2-Rv	**taaacgataactcatgttgttattgttc**gttggttgtaactctaaagtct
2.pMDH3.SER2-Fw	**gaacaataacaacatgagttatcgttta**actgctatttcaaag
3.SER2.C1-Rv	**aaaaggggcctgaagctctattcgttaaga**aatccctcaatttcg
4.SER2.C1-Fw	**cttaacgaatagagcttcaggcccctttt**cctttgtcgatatcat
1.pGAP.SER3-Rv	**tggggagaagccatggtgttttgatag**ttgttcaattgatt
2.pGAP.SER3-Fw	**ctatcaaaacaccatggcttctcccca**agatattaagcagtta
1.pMDH3.SER3-Rv	**ttggggagaagccatgttgttattgttc**gttggttgtaactctaaagtct
2.pMDH3.SER3-Fw	**gaacaataacaacatggcttctccccaa**gatattaagcagtta
3.SER3.C1-Rv	**aaaaggggcctgaagctctagtatagcaga**cgggtga
4.SER3.C1-Fw	**tctgctatactagagcttcaggcccctttt**cctttgtcgatatcat
4.BB3rN14.C1-Rv	**cattatacgaagttatggcatgccggagcg**agcgagcttgcaaattaaagcc
1.BB3rN14pMDH3-Fw	**cagggcgggtttttttcgcgatcggaggt**agcttgggtaggacttgacaagt
4.BB3eH14.C1-Rv	**attctgggcctccatgtccatgccggagcg**agcgagcttgcaaattaaagcc
2.pGAP-Fw	**gggcggggttttttcgcgatcggag**gatccttttttgtagaaatgtctt
2.pMDH3-Fw	**gggcggggttttttcgcgatcggag**tagcttgggtaggacttgacaagt
4.CYC1-Rv	**tcgacctgcagcgtaccatgccggagcg**agcttgcaaattaaagccttc
CkBB3aZ14-Fw	tgacagggcggggttttttcgcgatcggag
CkBB3aZ14-Rv	tcgacctgcagcgtaccatgccggagcg
1.BB3rN14-Rv	ctccgatcgcgaaaaaaccccgccctgtca
4.BB3rN14-Fw	cgctccggcatgccataacttcgtataat
1BB3aZ14-Rv	ctccgatcgcgaaaaaaccccgccctgtcaggggcggggttttttg
4.BB3eH14-Fw	cgctccggcatggacatggaggcccagaataccctccttgaca

Overlap sequence for hifi assembly is in bold.

Appendix 13.

***Table A4-3**: Enzymes involved in serine biosynthesis pathway in GS115 Komagataella phaffi strain of 4th chapter.*

Enzyme	Gene name	uniProtID GS115	Gene ID
PGADH	*SER3*	C4R1C8_KOMPG	PAS_chr2-1_0657
PSAT1	*SER1*	F2QSD3_KOMPC	PAS_chr3_0566
PSPH	*SER2*	C4R7E7_KOMPG	PAS_chr4_0285

Appendix 14.

***Table A4-4:** Values of experimental K_La obtained for DASGIP system determined by the dynamic method of desroption-absorpion of oxygen in 4th chapter.*

vvm	rpm	K_La (h^{-1})	R^2	vvm	rpm	K_La (h^{-1})	R^2
1	800	48.72	0.996	0.5	800	85.28	0.993
	400	17.56	0.998		400	12.87	0.999
	200	12.71	0.999		200	8.36	0.999
	100	4.91	0.997		100	2.17	0.997

Appendix 15.

Figure A4-5. Codon optimized sequence of the alfa mating factor (*α*MF) from *Saccharomyces cerevisiae* (NM_001184001.1). Modified codons are in red, *Bsa*I sequence is blue. Optimization was made using SnapGene software.

Appendix 16.

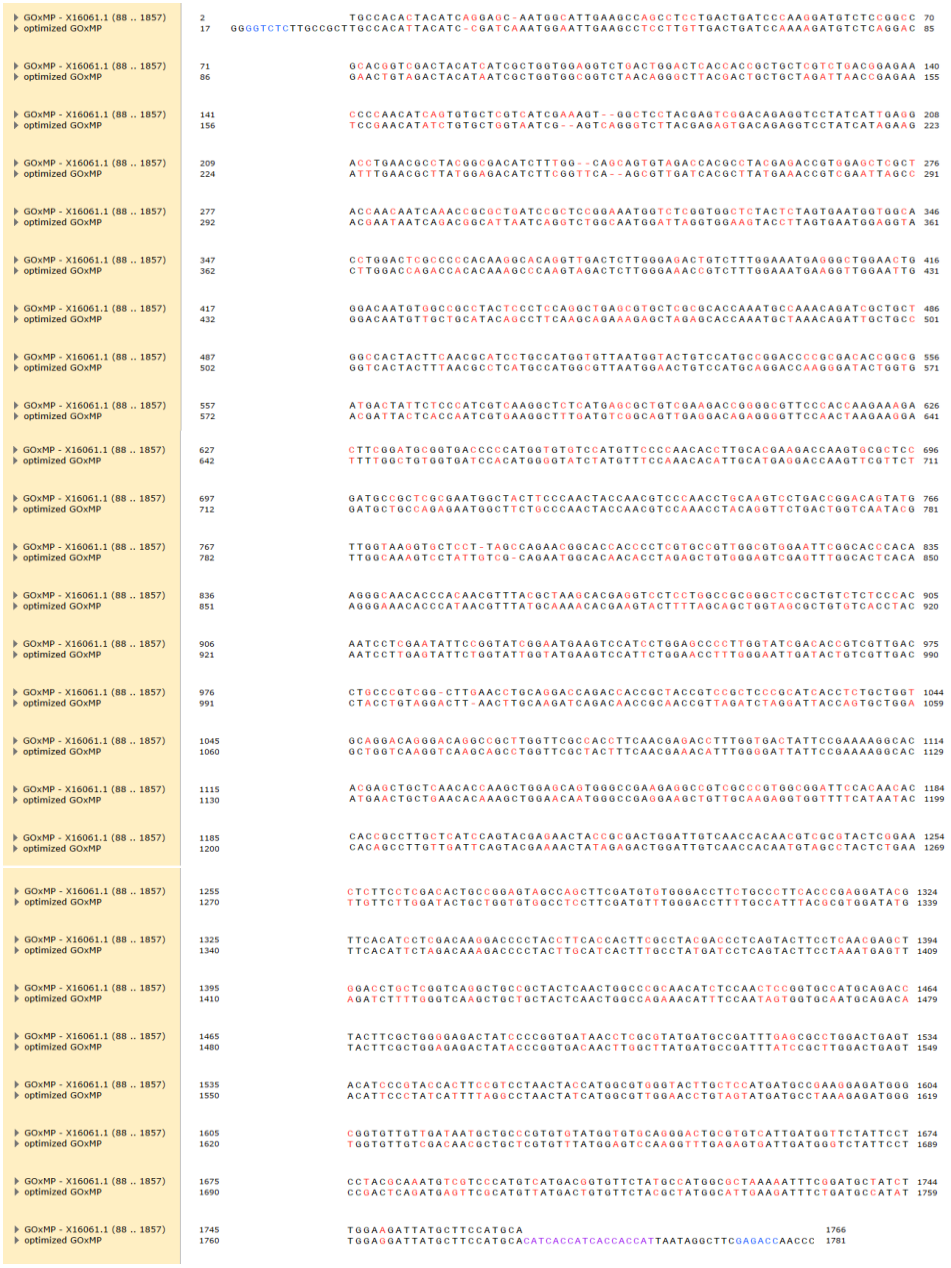

Figure A4-6. Codon optimized sequence of the intron less glucose oxidase gene from *Aspergillus niger* (x60601.1). Modified codons are in red. *Bsa*I sequence is blue. Sequence in purple corresponds to a histidine tag fuse to the Gox protein for purification. Optimization was made using SnapGene software.

Appendix 17.

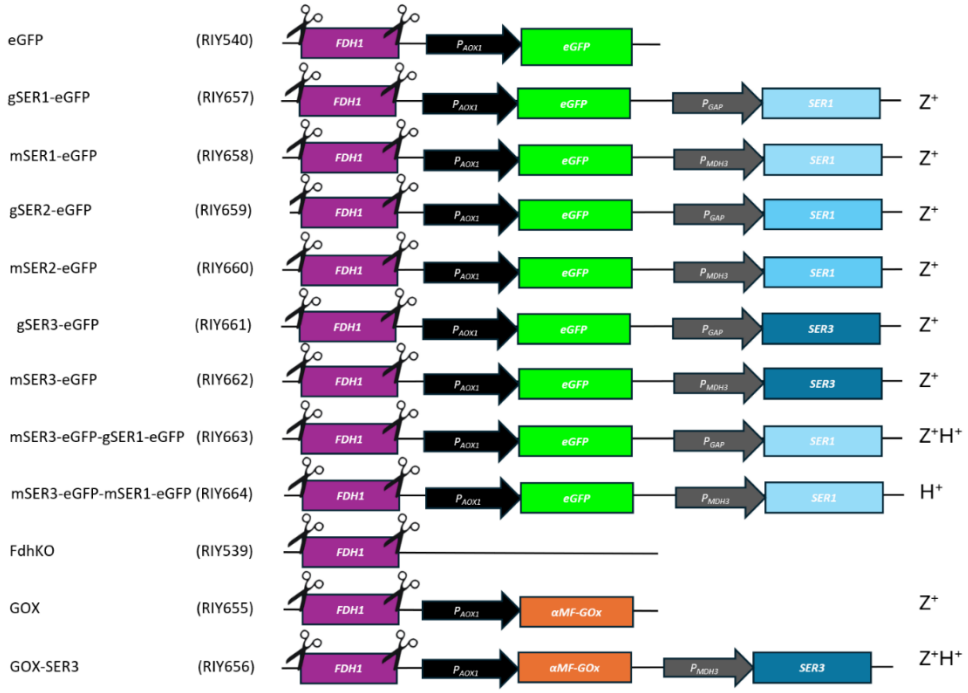

Figure A4-7. Schematic representation of the strain genotype used in 4th chapter.

Appendix 18.

Assessment of Single-Copy Integration of Recombinant Gene Expression Cassettes in the Yeast Genome of 4th chapter.

The occurrence of a single-copy integration of the GOX and the three SER genes expression cassette in the yeast genome was inferred indirectly, based on the assumption that variation in copy number among three randomly selected clones would result in different phenotypes, reflected by differences in eGFP fluorescence or GOX-specific activity, depending on the strain genotype. To test this, the relevant proxy was measured in three randomly selected transformants of a given strain after 48 h of growth in a microbioreactor in YNBS medium. The consistency of these signals indicates an identical number of insertion events across the transformants, most likely a single integration, since the probability of multiple independent integration events producing identical results in three randomly chosen clones is very low.

In practice, three randomly selected transformants of strains *g*SER1-eGfp (*fdh1*Δ, p*AOX1-eGFP*, p*GAP-SER1*), *m*SER1-eGfp (*fdh1*Δ, p*AOX1-eGFP*, p*MDH3-SER1*),

gSER2-eGfp (*fdh1*Δ, p*AOX1-eGFP*, p*GAP-SER2*), *m*SER2-eGfp (*fdh1*Δ, p*AOX1*-eGFP, p*MDH3-SER2*), gSER3-eGfp (*fdh1*Δ, p*AOX1-eGFP*, p*GAP-SER3*), *m*SER3-eGfp (*fdh1*Δ, p*AOX1-eGFP*, p*MDH3-SER3*), *m*SER3-*g*SER1 eGfp (*fdh1*Δ, p*AOX1-eGFP*, p*MDH3-SER3*, p*GAP-SER1*), and *m*SER3-*m*SER1-eGfp (*fdh1*Δ, p*AOX1-eGFP*, p*MDH3-SER3*, p*MDH3-SER1*) were cultivated for 48 h in a microbioreactor in YNBS medium, and their eGFP-specific fluorescence was measured. As shown in Figure A4-8, the consistent eGFP signals observed suggest monocopy integration of the SER gene expression cassettes. Similarly, GOX-specific activity was used as a proxy instead of eGFP fluorescence for strains RIY655 and RIY665 to evaluate GOX or *SER3* monocopy integration. As shown in Figure A4-9, the GOX expression cassette integrated as a single copy in the GOX strain, while one copy of the *SER3* expression cassette integrated in the GOX-SER3 strain. Based on this, one transformant of each strain was selected.

Appendix 19.

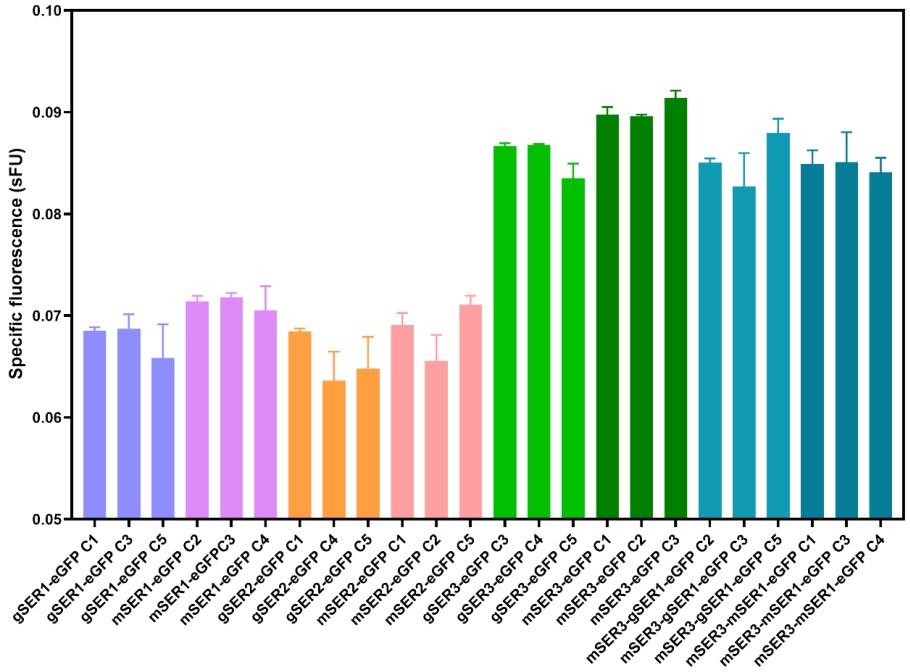

Figure A4-8. Specific eGFP fluorescence of the different eGFP constructed strains. Histogram color is specific for a constructed strain, each histogram bars representing one of the three transformants tested. Data represents the mean and standard deviation of triplicate cultures. sFU: specific fluorescence unit.

Appendix 20.

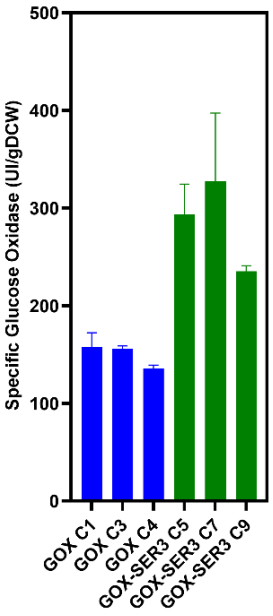

Figure A4-9. Specific glucose oxidase activity of the different GOX constructed strains. Histogram color is specific for a constructed strain, each histogram bars representing one of the three transformants tested. Data represents the mean and standard deviation of triplicate cultures.

Appendix 21.

Molecular biology techniques of 5th chapter.

E. coli was grown at 37°C in Luria-Bertani medium (LB), supplemented with antibiotics as follows: 100 $\mu g \cdot mL^{-1}$ ampicillin, 50 $\mu g \cdot mL^{-1}$ kanamycin. Golden gate assembly was as described elsewhere (Celińska et al., 2018). Vector TOPO Blunt II was from Invitrogen (Waltham, Massachusetts, United States). Q5 High-Fidelity DNA polymerase (New England Biolabs, Ipswich, Massachusetts, United States) was used for PCR amplification with annealing temperature of 65 °C and elongation time of 2 min. Restriction enzymes (*Not*I, *Bsa*I) and DNA ligase were from New England Biolabs. DNA fragments were purified from agarose gels using a NucleoSpin Gel and a PCR clean-up kit (Machery-Nagel, Düren, Germany). Plasmid purification was made using the NucleoSpin Plasmid EasyPure kit (Macherey-Nagel). Quantitative PCR (qPCR) were performed as described elsewhere (Bustos et al., 2024). Primer pairs LacqPCR-F/LacqPCR-R that hybridized withing the LacVader coding sequence,

and ACT-F/ACT-R specific for actin gene used as a reference were used (Table A5-1). Total RNA was extracted using the NucleoSpin RNA Plus kit (Machery-Nagel). qPCR was performed using the Luna Universal qPCR Master Mix and the Step OnePlus Real-Time PCR system (Thermo Scientific). SanpGene software (Dotmatics) was used for in silico plasmid construction and primer design.

Appendix 22.

Culture media of 5th chapter.

BMD1 medium contained 100 mM potassium phosphate buffer pH 6.0, 3.5 $g \cdot L^{-1}$ yeast nitrogen base without amino acids, 400 $\mu g \cdot L^{-1}$ biotin and 10 $g \cdot L^{-1}$ D-glucose. BMM2 medium contained 100 mM potassium phosphate buffer pH 6.0, 3.5 $g \cdot L^{-1}$ yeast nitrogen base without amino acids, 400 $\mu g \cdot L^{-1}$ biotin and 2% methanol (v: v). BMM10 medium contained 100 mM potassium phosphate buffer pH 6.0, 3.5 $g \cdot L^{-1}$ yeast nitrogen base without amino acids, 400 $\mu g \cdot L^{-1}$ biotin and 10% methanol (v: v). YNBDCu medium contained 50 mM potassium phosphate buffer pH 6.8, 1.7 $g \cdot L^{-1}$ yeast nitrogen base w/o NH_4SO_4 and amino acid, 20 $g \cdot L^{-1}$ glucose, 5 $g \cdot L^{-1}$ NH_4Cl 5 $g \cdot L^{-1}$, 2 $g \cdot L^{-1}$ casamino acids, 0.1 mM $CuSO_4$.

Appendix 23.

Yeast culture of 5th chapter.

Cultures were performed in 24-square deepwell plates (Enzyscreen, Bennebrroek, The Netherland) at an oxygen transfer rate in the range of 30-40 mmol $O_2 \cdot L^{-1} \cdot h^{-1}$, which is similar to that typically achieved in stirred tank reactors (Duetz et al., 2000; Duetz & Witholt, 2001). Culture of *Y. lipolytica* strains were performed in 1.5 ml of medium YNBDCu. *K. phaffii* was first grown in 550 µL of BMD1. Ater 36h of growth, the first induction was carried out with 700 µL of BMM2. Second and third inductions were performed at 48 and 60h by adding 215 µL of BMM10. All cultures were inoculated at an initial OD 600 nm of 0.5 from a 24h precultures in the same media. Sampling volume was equal to 150 µL.

Appendix 24.

Plasmid construction of 5th chapter.

The primers sequences used for PCR are listed in Table A5-1. The fusion constructs containing the pre-pro-α peptide and the LacVader mature DNA sequence was generated by overlap extension PCR in two steps to eliminate the internal *Bsa*I site present in the laccase coding sequence. In the first step, two PCR reactions were performed using primer pairs Lac01b/Lac04 and Lac03/Lac02, with plasmid pJRoC30 as the template. The resulting 0.6-kb and 1.1-kb fragments were purified and used as templates in a second PCR with primers Lac01b/Lac02. The resulting 1.75-kb fragment was cloned into a TOPO Blunt II vector and sequence-verified using

M13 primers. This construct was designated RIP528 (αPre-Pro-Lacc, Fig. A5-1). Primers Lac01b and Lac02 were designed to introduce D (AATG) and E (TCTA)-type overhangs, respectively.

The LacVader mature sequence was amplified from plasmid RIE528 using primers Lac05/Lac02. The resulting 1.5-kb fragment was cloned into a TOPO Blunt II vector and sequence-verified. This construct was designated RIE529 (Lacc biobrick, Fig. A5-1). Primer Lac05 was designed to introduce an X (TGCC)-type overhang.

The αPro-LacVader fusion was amplified from plasmid RIE528 using primers Lac06/Lac02. The resulting 1.75-kb fragment was cloned into a TOPO Blunt II vector and sequence-verified. This construct was designated RIE530 (αPro-Lacc biobrick, Fig. A5-1). Primer Lac06 was designed to introduce an X-type overhang.

The Lip2Pro-LacVader fusion was amplified from plasmid RIE528 using primers Lac07/Lac02. The resulting 1.75-kb fragment was cloned into a TOPO Blunt II vector and sequence-verified. This construct was designated RIE531 (Lip2Pro-Lacc biobrick, Fig. A5-1). Primer Lac07 was designed to introduce an X-type overhang and the Lip2Pro sequence.

For Golden Gate assemblies, the following vectors were used: GGE146 (promoter p*TEF*- 4UAS), GGE020 (LIP2 transcriptional terminator, *LIP2*tt), GGE083 (URA3 marker), GGE029 (backbone vector GB3), GGE255 (Lip2-*Not*I-up), and GGE254 (Lip2-*Not*I-down). These were combined with GGV0063 (Yps3Pre), GGV0069 (Lip2Pre), GGV0071 (SoAmyPre), RIP532 (αPre), RIE529 (Lacc biobrick), RIE530 (αPro-Lacc biobrick), or RIE532 (Lip2Pro- Lacc biobrick). The detailed assembly protocol was described previously (Celińska et al., 2018; Celińska & Nicaud, 2019). The resulting constructs are summarized in Table A5-2. The integrity of all constructs was confirmed by DNA sequencing (Whole plasmid sequencing, EuroFins, Germany).

Appendix 25.

***Table A5-1**. Primers used in 5th chapter.*

Name	Sequence 5´to 3´
Lac01B	ggg**ggtctctaatg**agatttccttcaatttttactgatgttttattcgc
Lac02	ccc**ggtctcttaga**tcagaggtcgctgggg
Lac03	ctgtgacggactcaggggtccg
Lac04	cggacccctgagtccgtcacag
Lac05	ggg**ggtctcttgccg**aattcagcattgggccagtcg
Lac06	ggg**ggtctcttgcc**gctccagcaacactacaacagaag
Lac07	**ggtctcttgcc**ctcccttccccatcactccttctgaggccgcagttctccagaagcgagaatt cagcattgggccagtcg
pTEF-Fo	gcgtagggtactgcagtctg
Lac-Rev	gaagggcacggatccagtag
LacqPCR-F	atgcgacccgaattacacgt
LAcqPCR-R	gaagggcacggatccagtag
ACT-F	tccaggccgtcctctccc
ACT_R	ggccagccatatcgagtcgca

*Bsa*I site is in bold, Lip2Pro sequence is underline

Appendix 26.

***Table A5-2**. Escherichia coli strains used in 5th chapter.*

Strain name (plasmid)	Plasmid, genotype, (integration locus)	Source/Reference
A1 (GGE029)	backbone vector GB3, overhang A:M (GCCT-TGCG)	(Celińska et al., 2018)
A3 (GGE083)	URA3 marker, overhangs B:C (AGGT-ACGG)	(Celińska et al., 2018)
B1 (GGE146)	Promoter p*TEF*-4UAS, overhangs C:D (ACGG-AATG)	(Celińska et al., 2018)
D12 (GGE020)	*LIP2*tt, overhangs E: L (TCTA: GAGT)	(Celińska et al., 2018)
E12 (GGE254)	Lip2-*Not*I-down, overhangs L:M (GAGT-TGCG)	(Celińska et al., 2018)
E11 (GGE255)	Lip2-*Not*I-up, overhangs A: B (GCCT-AGGT)	(Celińska et al., 2018)
GGE0063 (GGV0063)	Yps3Pre, overhangs D:X (AATG-TGCC)	(Celińska & Nicaud, 2019)
GGE0069 (GGV0069)	Lip2Pre, overhangs D:X (AATG-TGCC)	(Celińska & Nicaud, 2019)
GGE0071 (GGV0071)	SoAmy, overhangs D:X (AATG-TGCC)	(Celińska & Nicaud, 2019)
RIE528 (RIP528)	TOPO Blunt II vector, αpre-αpro-LacVader, overhangs D: E (AATG-TCTA)	This work
RIE529 (RIP529)	TOPO Blunt II vector, LacVader, overhangs X: E (TGCC- TCTA)	This work
RIE530 (RIP530)	TOPO Blunt II vector, αPro-LacVader, overhangs X: E (TGCC- TCTA)	This work
RIE531 (RIP531)	TOPO Blunt II vector, Lip2Pro-LacVader, overhangs X: E (TGCC- TCTA)	This work
RIE532 (RIP532)	pEX-K168-αPre from S. cerevisiae, synthetic DNA, overhangs D:X (AATG-TGCC)	This work
RIE535 (RIP535)	GG assembly, Yps3Pre-LacVader	This work
RIE536 (RIP536)	GG assembly, Lip2Pre-LacVader	This work
RIE537 (RIP537)	GG assembly, SoAmyPre-LacVader	This work
RIE538 (RIP538)	GG assembly, αPre-αPro-LacVader	This work
RIE539 (RIP539)	GG assembly, Yps3Pre-αPro-LacVader	This work
RIE540 (RIP540)	GG assembly, Lip2Pre-αPro-LacVader	This work
RIE541 (RIP541)	GG assembly, SoAmyPre-αPro-LacVader	This work
RIE542 (RIP542)	GG assembly, αPre-Lip2Pro-LacVader	This work
RIE543 (RIP543)	GG assembly, Yps3Pre-Lip2Pro-LacVader	This work
RIE544 (RIP544)	GG assembly, Lip2Pre-Lip2Pro-LacVader	This work
RIE545 (RIP545)	GG assembly, SoAmyPre-Lip2Pro-LacVader	This work
RIE546 (RIP546)	pJRoC30, pPDF-αPre-αPro-LacVader.	This work
A1 (GGE029)	backbone vector GB3, overhang A:M (GCCT-TGCG)	(Celińska et al., 2018)
A3 (GGE083)	URA3 marker, overhangs B:C (AGGT-ACGG)	(Celińska et al., 2018)
B1 (GGE146)	Promoter p*TEF*-4UAS, overhangs C:D (ACGG-AATG)	(Celińska et al., 2018)

All Golden Gate constructs contained in addition to the Pre-(Pro)-LacVader fusion the following biobricks A1, A3, B1, D12, E11 and E12.

Appendix 27.

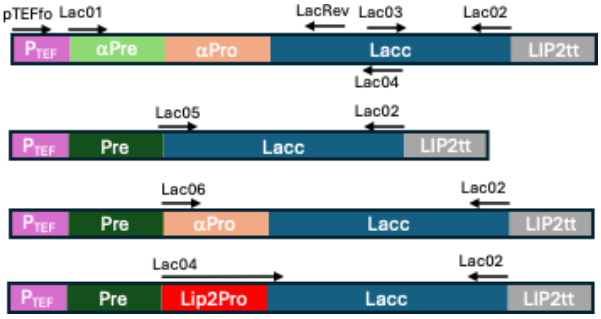

Figure A5-3. Schematic representation of the constructed expression systems obtained by Golden Gate (GG) assembly. Abbreviations are as follow: p*TEF*, promoter p*TEF*-4UA (GGE146); Pre, presequence (αPre, Yps3Pre, Lip2Pre or SoAmyPre); Lacc, LacVader laccase encoding gene; *LIP2*tt; LIP2 transcriptional terminator *LIP2*tt.

Appendix 28.

Y. lipolytica strain construction and verification.

Y. lipolytica RIY146 strain was transformed by the lithium acetate method (Barth & Gaillardin, 1996). The LacVader expression cassettes were released from the corresponding plasmids by *Not*I digestion and gel purified. Transformants were selected on YNBG plates after 48 h incubation at 28 °C. To verify the genotype of the yeast transformants, colony PCR were performed using Phire Plant Direct PCR Master Mix (Thermo Scientific) with primers pTEF-Fo and LacRev that anneal in the p*TEF* and Lacc region, respectively.

Appendix 29.

K. phaffii strain construction and verification.

For the expression of LacVader in *K. phaffii*, the strain BG11 and the plasmid pBSY5Z, containing the expression cassette under the control of the *PDF* promoter, were kindly provided by Bisy (Graz, Austria). An initial screening to select the best-performing transformants was conducted in deep-well plates. Individual colonies were used to inoculate 250 µL BMD medium per well. These cultures were grown for 60 hours at 28°C with shaking at 340 rpm and 80% humidity. Following this growth phase, protein expression was induced by the addition of 250 µL of BMM2. To sustain expression, cultures were further fed with 50 µL of BMM10 at 70, 82, and 106 hours

post-inoculation. All media used for induction in the deep-well plates were supplemented with 0.1 mM $CuSO_4$.

Appendix 30.

Laccase activity.

Laccase activity was determined as described elsewhere (Mate et al., 2013) using ABTS as a substrate (0.5 mM in 100 mM sodium acetate buffer pH 4.5; molar extinction coefficient of ABTS at 420 nm of 36 000 M^{-1} cm^{-1}).

Appendix 31.

Integration consistency check among constructed strain

To assess the consistency of the copy number of the LacVader cassette integration at the *LIP2* locus, two randomly selected transformants per construct were cultivated in triplicates in deep-well plates containing YNBCu medium, and the laccase activity was measured in triplicate after 48 h of growth. Specific laccase activity was then calculated from the corresponding biomass values and expressed as units per gram of cell dry weight ($U \cdot gDCW^{-1}$). When the nine activity values obtained for each transformant were within a comparable range (i.e., without significant differences) for both transformants, it was assumed that the LacVadder cassette copy number was identical and most likely equal to one. Indeed, the probability of independent multicopy integration at the same copy number in two randomly chosen transformants is low, especially when transformant selection is based on auxotrophy (here for uracil with URA3 marker). As shown in Fig. A5-2, the specific laccase activities were consistent for both transformant across all tested strains, except for the Lip2Pre-LacVader construct. In this case, activities of 6.8 ± 4.1 $U \cdot gDCW^{-1}$ and 26.1 ± 7.3 $U \cdot gDCW^{-1}$ were obtained, suggesting that one transformant carried two copies of the LacVadder expression cassette. For subsequent experiments, the Lip2Pre-LacVader transformant with the lower laccase activity was selected, while for all other constructed strains, one transformant was selected at random.

Appendix 32.

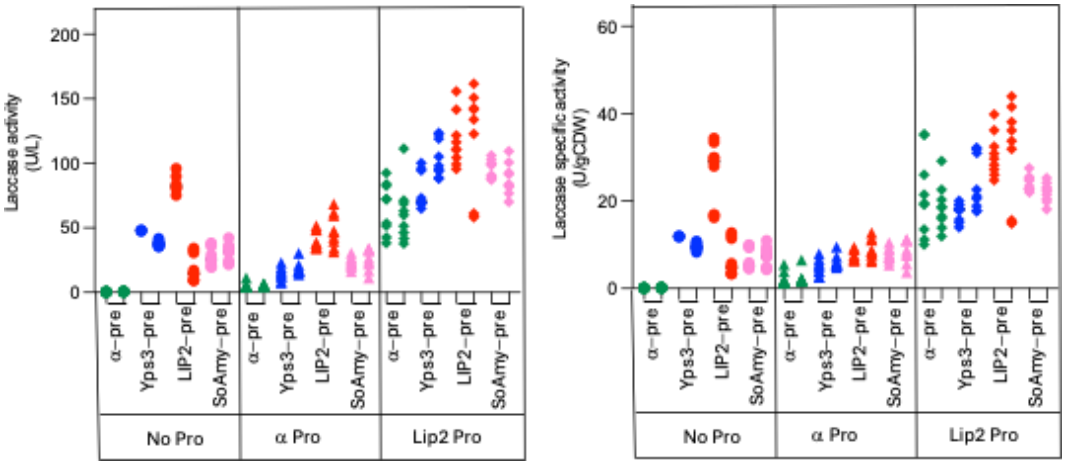

Figure A5-4. Assessment of gene integration consistency. For each construct, two transformants were cultivated in biological triplicates for 48h. The laccase activity was determined in triplicate and specific laccase activity calculated from the corresponding biomass. For both transformants per constructed strain, nine values are given.

Appendix 33.

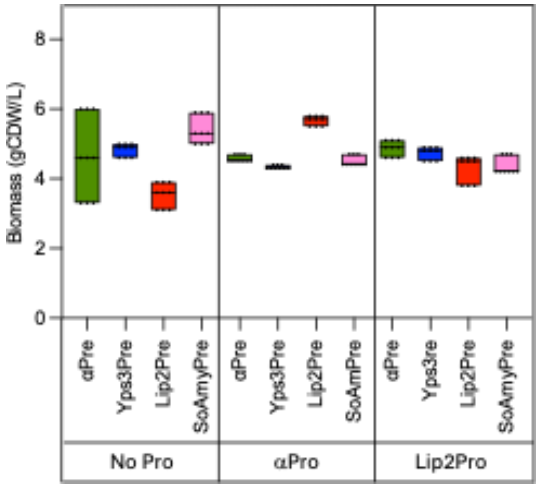

Figure A5-5. Biomass after 72 of growth of the different *Y. lipolytica* strains grown in deepweel plate in YNBCu medium in triplicate. Box represents the minimal and maximal value obtained. Black dots represent the obtained values.

References

References.

Ahmad, M., Hirz, M., Pichler, H., & Schwab, H. (2014). Protein expression in *Pichia pastoris*: Recent achievements and perspectives for heterologous protein production. In *Applied Microbiology and Biotechnology* (Vol. 98, Issue 12, pp. 5301–5317). Springer Verlag. https://doi.org/10.1007/s00253-014-5732-5

Ahn, J., Hong, J., Park, M., Lee, H., Lee, E., Kim, C., Lee, J., Choi, E. S., Jung, J. K., & Lee, H. (2009). Phosphate-responsive promoter of a *Pichia pastoris* sodium phosphate symporter. *Applied and Environmental Microbiology*, *75*(11), 3528–3534. https://doi.org/10.1128/AEM.02913-08

Akentyev, P., Sokolova, D., Korzhenkov, A., Gubaidullin, I., & Kozlov, D. (2023). Expression level of *SOR1* is a bottleneck for efficient sorbitol utilization by yeast *Komagataella kurtzmanii*. *Yeast*, *40*, 414–424. https://doi.org/10.1002/YEA.3884

Albacar, M., Casamayor, A., & Ariño, J. (2024). Harnessing alkaline-pH regulatable promoters for efficient methanol-free expression of enzymes of industrial interest in *Komagataella Phaffii*. *Microbial Cell Factories*, *23*(1). https://doi.org/10.1186/s12934-024-02362-9

Avcı, B., & Çalık, P. (2025). Dual-acting single-engineered hybrid-architectured promoters enhance and convert expressions into multi-carbon source-regulated systems in *Komagataella phaffii*. *Enzyme and Microbial Technology*, *191*. https://doi.org/10.1016/j.enzmictec.2025.110713

Bannach-Machado, Isabeli, et al. "Strategies for recombinant laccase expression and their roles in environmental remediation." World Journal of Microbiology and Biotechnology 42.5 (2026): 237. https://doi.org/10.1007/s11274-026-04978-y

Bankar, S. B., Bule, M. V., Singhal, R. S., & Ananthanarayan, L. (2009). Glucose oxidase — An overview. *Biotechnology Advances*, *27*(4), 489–501. https://doi.org/10.1016/j.biotechadv.2009.04.003

Barone, G. D., Emmerstorfer-Augustin, A., Biundo, A., Pisano, I., Coccetti, P., Mapelli, V., & Camattari, A. (2023). Industrial Production of Proteins with *Pichia pastoris—Komagataella phaffii*. In *Biomolecules* (Vol. 13, Issue 3). MDPI. https://doi.org/10.3390/biom13030441

Baumann, K., Maurer, M., Dragosits, M., Cos, O., Ferrer, P., & Mattanovich, D. (2008). Hypoxic fed-batch cultivation of *Pichia pastoris* increases specific and volumetric productivity of recombinant proteins. *Biotechnology and Bioengineering*, *100*(1), 177–183. https://doi.org/10.1002/bit.21763

Bernat-Camps, N., Ebner, K., Schusterbauer, V., Fischer, J. E., Nieto-Taype, M. A., Valero, F., Glieder, A., & Garcia-Ortega, X. (2023). Enabling growth-decoupled *Komagataella phaffii* recombinant protein production based on the methanol-free PDH promoter. *Frontiers in Bioengineering and Biotechnology*, *11*. https://doi.org/10.3389/fbioe.2023.1130583

Berrios, J., Flores, M.-O., Díaz-Barrera, A., Altamirano, C., Martínez, I., & Cabrera, Z. (2017). A comparative study of glycerol and sorbitol as co-substrates in methanol-induced cultures of *Pichia pastoris*: temperature effect and scale-up simulation. *Journal of Industrial Microbiology and Biotechnology*, *44*(3), 407–411. https://doi.org/10.1007/s10295-016-1895-7

Berrios, J., Theron, C. W., Steels, S., Ponce, B., Velastegui, E., Bustos, C., Altamirano, C., & Fickers, P. (2022). Role of Dissimilative Pathway of *Komagataella phaffii* (*Pichia pastoris*): Formaldehyde Toxicity and Energy Metabolism. *Microorganisms*, *10*(7). https://doi.org/10.3390/microorganisms10071466

Besleaga, M., Zimmermann, C., Ebner, K., Mach, R. L., Mach-Aigner, A. R., Geier, M., Glieder, A., Spadiut, O., & Kopp, J. (2024). Bi-directionalized promoter systems allow methanol-free production of hard-to-express peroxygenases with *Komagataella Phaffii*. *Microbial Cell Factories*, *23*(1). https://doi.org/10.1186/s12934-024-02451-9

Brierley, R. A., Bussineau, C., Kosson, R., Melton, A., & Siegel, R. S. (1990). Fermentation Development of Recombinant *Pichia pastoris* Expressing the Heterologous Gene: Bovine Lysozyme. *Annals of the New York Academy of Sciences*, *589*(1), 350–362. https://doi.org/10.1111/j.1749-6632.1990.tb24257.x

Bustos, C., Berrios, J., & Fickers, P. (2024). Formate from THF-C1 metabolism induces the *AOX1* promoter in formate dehydrogenase-deficient *Komagataella phaffii*. *Microbial Biotechnology*, *17*(10), e70022. https://doi.org/10.1111/1751-7915.70022

Carly, F., Niu, H., Delvigne, F., & Fickers, P. (2016). Influence of methanol/sorbitol co-feeding rate on p*AOX1* induction in a *Pichia pastoris* Mut+ strain in bioreactor with limited oxygen transfer rate. *Journal of Industrial Microbiology and Biotechnology*, *43*(4), 517–523. https://doi.org/10.1007/s10295-015-1722-6

Carnicer, M., Baumann, K., Töplitz, I., Sánchez-Ferrando, F., Mattanovich, D., Ferrer, P., & Albiol, J. (2009). Macromolecular and elemental composition analysis and extracellular metabolite balances of *Pichia pastoris* growing at different oxygen levels. *Microbial Cell Factories*, *8*(1), 1–14. https://doi.org/10.1186/1475-2859-8-65

Casal, M., Paiva, S., Queirós, O., & Soares-Silva, I. (2008). Transport of carboxylic acids in yeasts. *FEMS microbiology reviews*, *32*(6), 974-994. https://doi.org/10.1111/j.1574-6976.2008.00128.x

Çelik, E., & Çalık, P. (2012). Production of recombinant proteins by yeast cells. *Biotechnology Advances*, *30*(5), 1108–1118. https://doi.org/10.1016/j.biotechadv.2011.09.011

Çelik, E., Çalık, P., & Oliver, S. G. (2009). Fed-batch methanol feeding strategy for recombinant protein production by *Pichia pastoris* in the presence of co-substrate sorbitol. *Yeast*, *26*(9), 473–484. https://doi.org/10.1002/yea.1679

Cereghino, J. L., & Cregg, J. M. (2000). Heterologous protein expression in the methylotrophic yeast *Pichia pastoris*. *FEMS Microbiology Reviews*, *24*(1), 45–66. https://doi.org/10.1111/j.1574-6976.2000.tb00532.x

Christensen, K. E., & MacKenzie, R. E. (2006). Mitochondrial one-carbon metabolism is adapted to the specific needs of yeast, plants and mammals. *BioEssays*, *28*(6), 595–605. https://doi.org/10.1002/bies.20420

Cooney, C. L., Wang, D. I. C., & Mateles, R. I. (2000). Measurement of heat evolution and correlation with oxygen consumption during microbial growth. *Biotechnology and Bioengineering*, *67*(6), 691–703. https://doi.org/10.1002/(SICI)1097-0290(20000320)67:6<691::AID-BIT7>3.0.CO;2-R

Couderc, R., & Baratti, J. (1980). Oxidation of Methanol by the Yeast, *Pichia pastoris*. Purification and Properties of the Alcohol Oxidase. *Agricultural and Biological Chemistry*, *44*(10), 2279–2289. https://doi.org/10.1080/00021369.1980.10864320

Cregg, J. M., Barringer, K. J., Hessler, A. Y., & Madden, K. R. (1985). *Pichia pastoris* as a Host System for Transformations. In *MOLECULAR AND CELLULAR BIOLOGY* (Vol. 5, Issue 12).

Cregg, J. M., Cereghino, J. L., Shi, J., & Higgins, D. R. (2000). Recombinant Protein Expression in *Pichia pastoris. Molecular Biotechnology*, *16*(1), 23–52. https://doi.org/10.1385/MB:16:1:23

Cregg, J. M., Madden, K. R., Barringer, K. J., Thill, G. P., & Stillman, C. A. (1989). Functional characterization of the two alcohol oxidase genes from the yeast *Pichia pastoris*. *Molecular and Cellular Biology*, *9*(3), 1316–1323. https://doi.org/10.1128/mcb.9.3.1316-1323.1989

Cregg, J. M., Tolstorukov, I., Kusari, A., Sunga, J., Madden, K., & Chappell, T. (2009). Chapter 13 Expression in the Yeast *Pichia pastoris*. In *Methods in Enzymology* (Vol. 463, Issue C, pp. 169–189). Academic Press Inc. https://doi.org/10.1016/S0076-6879(09)63013-5

Daly, R., & Hearn, M. T. W. (2005). Expression of heterologous proteins in *Pichia pastoris*: a useful experimental tool in protein engineering and production. *Journal of Molecular Recognition*, *18*(2), 119–138. https://doi.org/10.1002/jmr.687

de Sá Magalhães, S., & Keshavarz-Moore, E. (2021). *Pichia pastoris* (*Komagataella phaffii*) as a Cost-Effective Tool for Vaccine Production for Low- and Middle-Income Countries (LMICs). *Bioengineering*, *8*(9), 119. https://doi.org/10.3390/bioengineering8090119

Delic, M., Mattanovich, D., & Gasser, B. (2013). Repressible promoters - A novel tool to generate conditional mutants in *Pichia pastoris*. *Microbial Cell Factories*, *12*(1). https://doi.org/10.1186/1475-2859-12-6

Duan, G., Ding, L., Wei, D., Zhou, H., Chu, J., Zhang, S., & Qian, J. (2019). Screening endogenous signal peptides and protein folding factors to promote the secretory

expression of heterologous proteins in *Pichia pastoris*. *Journal of biotechnology*, *306*, 193-202. https://doi.org/10.1016/j.jbiotec.2019.06.297

Duan, H., Umar, S., Hu, Y., & Chen, J. (2009). Both the *AOX1* promoter and the *FLD1* promoter work together in a *Pichia pastoris* expression vector. *World Journal of Microbiology and Biotechnology*, *25*(10), 1779–1783. https://doi.org/10.1007/s11274-009-0077-4

Ellis, S. B., Brust, P. F., Koutz, P. J., Waters, A. F., Harpold, M. M., & Gingeras, T. R. (1985). Isolation of alcohol oxidase and two other methanol regulatable genes from the yeast *Pichia pastoris*. *Molecular and Cellular Biology*, *5*(5), 1111–1121. https://doi.org/10.1128/mcb.5.5.1111

Enzymes Market Size And Share | Industry Report, 2033. (2025). Https://Www.Grandviewresearch.Com/Industry-Analysis/Enzymes-Industry.

Erden-Karaoğlan, F., Karaoğlan, M., Yılmaz, G., Yılmaz, S., & İnan, M. (2022). Deletion analysis of *Pichia pastoris* alcohol dehydrogenase 2 (*ADH2*) promoter and development of synthetic promoters. *Biotechnology Journal*, *17*(2). https://doi.org/10.1002/biot.202100332

Ergün, B. G., Demir, İ., Özdamar, T. H., Gasser, B., Mattanovich, D., & Çalık, P. (2020). Engineered Deregulation of Expression in Yeast with Designed Hybrid-Promoter Architectures in Coordination with Discovered Master Regulator Transcription Factor. *Advanced Biosystems*, *4*(4). https://doi.org/10.1002/adbi.201900172

Ergün, B. G., Laçın, K., Çaloğlu, B., & Binay, B. (2022). Second generation *Pichia pastoris* strain and bioprocess designs. *Biotechnology for Biofuels and Bioproducts*, *15*(1), 150. https://doi.org/10.1186/s13068-022-02234-7

Esch, B. M., Limar, S., Bogdanowski, A., Gournas, C., More, T., Sundag, C., Walter, S., Heinisch, J. J., Ejsing, C. S., André, B., & Fröhlich, F. (2020). Uptake of exogenous serine is important to maintain sphingolipid homeostasis in *Saccharomyces cerevisiae. PLoS Genetics*, *16*(8). https://doi.org/10.1371/JOURNAL.PGEN.1008745

Feng, A., Zhou, J., Mao, H., Zhou, H., & Zhang, J. (2022). Heterologous protein expression enhancement of *Komagataella phaffii* by ammonium formate induction based on transcriptomic analysis. *Biochemical Engineering Journal*, *185*. https://doi.org/10.1016/j.bej.2022.108503

Fickers, P., Nicaud, J. M., Destain, J., & Thonart, P. (2003). Overproduction of lipase by *Yarrowia lipolytica* mutants. *Applied Microbiology and Biotechnology*, *63*(2), 136–142. https://doi.org/10.1007/s00253-003-1342-3

Gasser, B., Prielhofer, R., Marx, H., Maurer, M., Nocon, J., Steiger, M., Puxbaum, V., Sauer, M., & Mattanovich, D. (2013). *Pichia Pastoris*: Protein Production Host and Model Organism for Biomedical Research. *Future Microbiology*, *8*(2), 191–208. https://doi.org/10.2217/fmb.12.133

Gasser, B., Saloheimo, M., Rinas, U., Dragosits, M., Rodríguez-Carmona, E., Baumann, K., Giuliani, M., Parrilli, E., Branduardi, P., Lang, C., Porro, D., Ferrer, P., Tutino, M., Mattanovich, D., & Villaverde, A. (2008). Protein folding

and conformational stress in microbial cells producing recombinant proteins: A host comparative overview. In *Microbial Cell Factories* (Vol. 7). https://doi.org/10.1186/1475-2859-7-11

Gorczyca, M., Kaźmierczak, J., Steels, S., Fickers, P., & Celińska, E. (2020). Impact of oxygen availability on heterologous geneexpression and polypeptide secretion dynamics in *Yarrowia lipolytica* -based protein production platforms. *Yeast*, *37*(9–10), 559–568. https://doi.org/10.1002/yea.3499

Gu, L., Zhang, J., Liu, B., Du, G., & Chen, J. (2015). High-Level Extracellular Production of Glucose Oxidase by Recombinant *Pichia Pastoris* Using a Combined Strategy. *Applied Biochemistry and Biotechnology*, *175*(3), 1429–1447. https://doi.org/10.1007/s12010-014-1387-z

Haghighi Poodeh, S., Ranaei Siadat, S. O., Arjmand, S., & Khalifeh Soltani, M. (2022). Improving *AOX1* promoter efficiency by overexpression of Mit1 transcription factor. *Molecular Biology Reports*, *49*(10), 9379–9386. https://doi.org/10.1007/s11033-022-07790-7

Hamaker, K. H., Johnson, D. C., Bellucci, J. J., Apgar, K. R., Soslow, S., Gercke, J. C., Menzo, D. J., & Ton, C. (2011). Design of a novel automated methanol feed system for pilot-scale fermentation of *Pichia pastoris*. *Biotechnology Progress*, *27*(3), 657–667. https://doi.org/10.1002/btpr.560

Hartner, F. S., & Glieder, A. (2006). Regulation of methanol utilisation pathway genes in yeasts. In *Microbial Cell Factories* (Vol. 5). https://doi.org/10.1186/1475-2859-5-39

Hausjell, J., Schendl, D., Weissensteiner, J., Molitor, C., Halbwirth, H., & Spadiut, O. (2020). Recombinant production of a hard-to-express membrane-bound cytochrome P450 in different yeasts—Comparison of physiology and productivity. *Yeast*, *37*(2), 217–226. https://doi.org/10.1002/yea.3441

Heistinger, L., Gasser, B., & Mattanovich, D. (2020). Microbe Profile*: Komagataella phaffii*: a methanol devouring biotech yeast formerly known as *Pichia pastoris*. *Microbiology*, *166*(7), 614–616. https://doi.org/10.1099/mic.0.000958

Huang, Y., Jia, S., Lin, Y., Wang, J., Nong, L., Ye, L., & Liang, S. (2025). High-efficiency patatin expression strategies in *Komagataella phaffii* (*Pichia pastoris*): Expression cassette toolbox and regulation of protein secretion. *Synthetic and Systems Biotechnology*, *10*(2), 463–473. https://doi.org/10.1016/j.synbio.2025.01.003

Ianshina, T., Sidorin, A., Petrova, K., Shubert, M., Makeeva, A., Sambuk, E., Govdi, A., Rumyantsev, A., & Padkina, M. (2023). Effect of Methionine on Gene Expression in *Komagataella phaffii* Cells. *Microorganisms*, *11*(4), 877. https://doi.org/10.3390/microorganisms11040877

Inan, M., & Meagher, M. M. (2001). Non-repressing carbon sources for alcohol oxidase (*AOX1*) promoter of *Pichia pastoris*. *Journal of Bioscience and Bioengineering*, *92*(6), 585–589. https://doi.org/10.1016/S1389-1723(01)80321-2

Jayachandran, C., Palanisamy Athiyaman, B., & Sankaranarayanan, M. (2017a). Cofactor engineering improved CalB production in *Pichia pastoris* through heterologous expression of NADH oxidase and adenylate kinase. *PLOS ONE*, *12*(7), e0181370. https://doi.org/10.1371/journal.pone.0181370

Jayachandran, C., Palanisamy Athiyaman, B., & Sankaranarayanan, M. (2017b). Formate co-feeding improved *Candida antarctica* Lipase B activity in *Pichia pastoris*. In *Research Journal of Biotechnology* (Vol. 12, Issue 12).

Jia, L., Li, T., Wu, Y., Wu, C., Li, H., & Huang, A. (2021). Enhanced human lysozyme production by *Pichia pastoris* via periodic glycerol and dissolved oxygen concentrations control. *Applied Microbiology and Biotechnology*, *105*(3), 1041–1050. https://doi.org/10.1007/s00253-021-11100-9

Jordan, P., Choe, J.-Y., Boles, E., & Oreb, M. (2016). Hxt13, Hxt15, Hxt16 and Hxt17 from *Saccharomyces cerevisiae* represent a novel type of polyol transporters. *Scientific Reports*, *6*(1), 23502. https://doi.org/10.1038/srep23502

Jouhten, P., Rintala, E., Huuskonen, A., Tamminen, A., Toivari, M., Wiebe, M., Ruohonen, L., Penttilä, M., & Maaheimo, H. (2008). Oxygen dependence of metabolic fluxes and energy generation of *Saccharomyces cerevisiae* CEN.PK113-1A. *BMC Systems Biology*, *2*(1), 60. https://doi.org/10.1186/1752-0509-2-60

Juturu, V., & Wu, J. C. (2018). Heterologous Protein Expression in *Pichia pastoris*: Latest Research Progress and Applications. *ChemBioChem*, *19*(1), 7–21. https://doi.org/10.1002/cbic.201700460

Karbalaei, M., Rezaee, S. A., & Farsiani, H. (2020). *Pichia pastoris*: A highly successful expression system for optimal synthesis of heterologous proteins. Journal of cellular physiology, 235(9), 5867-5881. https://doi.org/10.1002/jcp.29583

Karaoglan, M., Karaoglan, F. E., & Inan, M. (2016a). Comparison of *ADH3* promoter with commonly used promoters for recombinant protein production in *Pichia pastoris*. *Protein Expression and Purification*, *121*, 112–117. https://doi.org/10.1016/j.pep.2016.01.017

Karaoglan, M., Karaoglan, F. E., & Inan, M. (2016b). Functional analysis of alcohol dehydrogenase (*ADH*) genes in *Pichia pastoris*. *Biotechnology Letters*, *38*(3), 463–469. https://doi.org/10.1007/s10529-015-1993-z

Kern, A., Hartner, F. S., Freigassner, M., Spielhofer, J., Rumpf, C., Leitner, L., Fröhlich, K. U., & Glieder, A. (2007). *Pichia pastoris* "just in time" alternative respiration. *Microbiology*, *153*(4), 1250–1260. https://doi.org/10.1099/mic.0.2006/001404-0

Kobayashi, J., Sasaki, D., Hara, K. Y., Hasunuma, T., & Kondo, A. (2022). Metabolic engineering of the l-serine biosynthetic pathway improves glutathione production in *Saccharomyces cerevisiae*. *Microbial Cell Factories*, *21*(1), 153. https://doi.org/10.1186/s12934-022-01880-8

Koller, A., Valesco, J., & Subramani, S. (2000). The *CUP1* promoter of *Saccharomyces cerevisiae* is inducible by copper in *Pichia pastoris*. *Yeast*,

16(7), 651–656. https://doi.org/10.1002/(SICI)1097-0061(200005)16:7<651::AID-YEA580>3.0.CO;2-F

Kostopoulou, A., Rebnegger, C., Ferrero-Bordera, B., Mattanovich, M., Maaß, S., Becher, D., Gasser, B., & Mattanovich, D. (2025). Impact of Oxygen Availability on the Organelle-Specific Redox Potentials and Stress in Recombinant Protein Producing *Komagataella phaffii*. *Microbial Biotechnology*, *18*(2). https://doi.org/10.1111/1751-7915.70106

Koutz, P., Davis, G. R., Stillman, C., Barringer, K., Cregg, J., & Thill, G. (1989). Structural comparison of the *Pichia pastoris* alcohol oxidase genes. *Yeast*, *5*(3), 167–177. https://doi.org/10.1002/yea.320050306

Krainer, F. W., Dietzsch, C., Hajek, T., Herwig, C., Spadiut, O., & Glieder, A. (2012). Recombinant protein expression in *Pichia pastoris* strains with an engineered methanol utilization pathway. *Microbial Cell Factories*, *11*. https://doi.org/10.1186/1475-2859-11-22

Küberl, A., Schneider, J., Thallinger, G. G., Anderl, I., Wibberg, D., Hajek, T., Jaenicke, S., Brinkrolf, K., Goesmann, A., Szczepanowski, R., Pühler, A., Schwab, H., Glieder, A., & Pichler, H. (2011). High-quality genome sequence of *Pichia pastoris* CBS7435. *Journal of Biotechnology*, *154*(4), 312–320. https://doi.org/10.1016/j.jbiotec.2011.04.014

Kumar, N. V., & Rangarajan, P. N. (2012). The zinc finger proteins Mxr1p and repressor of phosphoenolpyruvate carboxykinase (ROP) have the same DNA binding specificity but regulate methanol metabolism antagonistically in *Pichia pastoris*. *Journal of Biological Chemistry*, *287*(41), 34465–34473. https://doi.org/10.1074/jbc.M112.365304

Kumar, P., & Singh, J. (2024). Industrial Microbial Bioprocess Development: Strategies, Applications, Environmental Management, and Challenges. In *Industrial Microbiology and Biotechnology* (pp. 3–34). Springer Nature Singapore. https://doi.org/10.1007/978-981-97-6270-5_1

Kurtzman, C. P. (2005). Description *of Komagataella phaffii* sp. nov. and the transfer of *Pichia pseudopastoris* to the methylotrophic yeast genus *Komagataella*. *International Journal of Systematic and Evolutionary Microbiology*, *55*(2), 973–976. https://doi.org/10.1099/ijs.0.63491-0

Kurtzman, C. P. (2009). Biotechnological strains of *Komagataella* (*Pichia*) *pastoris* are *Komagataella phaffii* as determined from multigene sequence analysis. *Journal of Industrial Microbiology & Biotechnology*, *36*(11), 1435–1438. https://doi.org/10.1007/s10295-009-0638-4

Li, J., Yang, M., Zhao, F., Zhang, Y., & Han, S. (2024). Efficient expression of an alkaline pectin lyase from *Bacillus licheniformis* in *Pichia pastoris*. *Bioresources and Bioprocessing*, *11*(1). https://doi.org/10.1186/s40643-024-00752-w

Li, P., Sun, H., Chen, Z., Li, Y., & Zhu, T. (2015). Construction of efficient xylose utilizing *Pichia pastoris* for industrial enzyme production. *Microbial Cell Factories*, *14*(1). https://doi.org/10.1186/s12934-015-0206-8

Lin-Cereghino, G. P., Godfrey, L., de la Cruz, B. J., Johnson, S., Khuongsathiene, S., Tolstorukov, I., Yan, M., Lin-Cereghino, J., Veenhuis, M., Subramani, S., & Cregg, J. M. (2006). Mxr1p, a Key Regulator of the Methanol Utilization Pathway and Peroxisomal Genes in *Pichia pastoris*. *Molecular and Cellular Biology*, *26*(3), 883–897. https://doi.org/10.1128/MCB.26.3.883-897.2006

Lin-Cereghino, J., Wong, W. W., Xiong, S., Giang, W., Luong, L. T., Vu, J., Johnson, S. D., & Lin-Cereghino, G. P. (2005). Condensed Protocol for Competent Cell Preparation and Transformation of the Methylotrophic Yeast *Pichia Pastoris*. *BioTechniques*, *38*(1), 44–48. https://doi.org/10.2144/05381BM04

Liu, B., Cong, W., Zhao, Y., Zhou, H., & Zhang, J. (2023). An inducible *Komagataella phaffii* system for protein expression using sorbitol dehydrogenase promoter. *Biotechnology Letters*, *45*(5–6), 667–677. https://doi.org/10.1007/s10529-023-03370-2

Liu, B., Li, H., Zhou, H., & Zhang, J. (2022). Enhancing xylanase expression by *Komagataella phaffii* by formate as carbon source and inducer. *Applied Microbiology and Biotechnology*, *106*(23), 7819–7829. https://doi.org/10.1007/s00253-022-12249-7

Liu, B., Zhao, Y., Zhou, H., & Zhang, J. (2022). Enhancing xylanase expression of *Komagataella phaffii* induced by formate through Mit1 co-expression. *Bioprocess and Biosystems Engineering*, *45*(9), 1515–1525. https://doi.org/10.1007/s00449-022-02760-6

Liu, H., Tan, X., Russell, K. A., Veenhuis, M., & Cregg, J. M. (1995). PER3, a Gene Required for Peroxisome Biogenesis in *Pichia pastoris*, encodes a Peroxisomal Membrane Protein Involved in Protein Import. *Journal of Biological Chemistry*, *270*(18), 10940–10951. https://doi.org/10.1074/jbc.270.18.10940

Liu, L., Redden, H., & Alper, H. S. (2013). Frontiers of yeast metabolic engineering: Diversifying beyond ethanol and *Saccharomyces*. In *Current Opinion in Biotechnology* (Vol. 24, Issue 6, pp. 1023–1030). https://doi.org/10.1016/j.copbio.2013.03.005

Lodder, J., Acomina, A., & Kreger-van Rij, N. J. W. (1952). The yeasts-a taxonomic study. *North- Holland Publishing*.

Looser, V., Bruhlmann, B., Bumbak, F., Stenger, C., Costa, M., Camattari, A., Fotiadis, D., & Kovar, K. (2015). Cultivation strategies to enhance productivity of *Pichia pastoris*: A review. *Biotechnology Advances*, *33*(6), 1177–1193. https://doi.org/10.1016/j.biotechadv.2015.05.008

Lv, W., & Cai, M. (2025). Advancing Recombinant Protein Expression in *Komagataella phaffii*: Opportunities and Challenges. *FEMS Yeast Research*, *25*, 10. https://doi.org/10.1093/femsyr/foaf010

Macreadie, I. G., Horaitis, O., Verkuylen, A. J., & Savin, K. W. (1991). Improved shuttle vectors for cloning and high-level Cu^{2+}-mediated expression of foreign genes in yeast. In *Gene* (Vol. 104). https://doi.org/10.1016/0378-1119(91)90474-P

Madzak, C. (2018). Engineering *Yarrowia lipolytica* for Use in Biotechnological Applications: A Review of Major Achievements and Recent Innovations. *Molecular biotechnology*, *60*(8), 621-635.https://doi.org/10.1007/s12033-018-0093-4

Meier, K., Klöckner, W., Bonhage, B., Antonov, E., Regestein, L., & Büchs, J. (2016). Correlation for the maximum oxygen transfer capacity in shake flasks for a wide range of operating conditions and for different culture media. *Biochemical Engineering Journal*, *109*, 228-235. https://doi.org/10.1016/j.bej.2016.01.014

Maier, U., & Büchs, J. (2001). Characterisation of the gas–liquid mass transfer in shaking bioreactors. *Biochemical Engineering Journal*, *7*(2), 99-106.MarketsandMarkets. (2024). *Enzymes Market Trends, Growth, and Forecast*. https://doi.org/10.1016/S1369-703X(00)00107-8

MarketsandMarkets. https://www.marketsandmarkets.com/Market-Reports/enzyme-market-46202020.html

Martens, J. A., Wu, P. Y. J., & Winston, F. (2005). Regulation of an intergenic transcript controls adjacent gene transcription in *Saccharomyces cerevisiae*. *Genes and Development*, *19*(22), 2695–2704. https://doi.org/10.1101/gad.1367605

Menendez, J., Valdes, I., & Cabrera, N. (2003). The ICLI gene of *Pichia pastoris*, transcriptional regulation and use of its promoter. *Yeast*, *20*(13), 1097–1108. https://doi.org/10.1002/yea.1028

Meng, Y., Zhao, M., Yang, M., Zhang, Q., Hao, J., & Meng, Y. (2014). Production and characterization of recombinant glucose oxidase from *Aspergillus niger* expressed in *Pichia pastoris*. *Letters in Applied Microbiology*, *58*(4), 393–400. https://doi.org/10.1111/lam.12202

Ndayambaje, J. B., & S., M. (2014). Co-feeding strategy to enhance phytase production in *Pichia pastoris*. *African Journal of Biotechnology*, *13*(21), 2181–2187. https://doi.org/10.5897/AJB2013.12986

Nielsen, J., & Keasling, J. D. (2016). Engineering Cellular Metabolism. In *Cell* (Vol. 164, Issue 6, pp. 1185–1197). Cell Press. https://doi.org/10.1016/j.cell.2016.02.004

Niu, H., Jost, L., Pirlot, N., Sassi, H., Daukandt, M., Rodriguez, C., & Fickers, P. (2013). A quantitative study of methanol/sorbitol co-feeding process of a *Pichia pastoris* Mut^{+}/p*AOX*1-lacZ strain. *Microbial Cell Factories*, *12*(1), 33. https://doi.org/10.1186/1475-2859-12-33

Ogata, K., Nishikawa, H., & Ohsugi, M. (1969). A Yeast Capable of Utilizing Methanol. *Agricultural and Biological Chemistry*, *33*(10), 1519–1520. https://doi.org/10.1080/00021369.1969.10859497

Parua, P. K., Ryan, P. M., Trang, K., & Young, E. T. (2012). *Pichia pastoris* 14-3-3 regulates transcriptional activity of the methanol inducible transcription factor Mxr1 by direct interaction. *Molecular Microbiology*, *85*(2), 282–298. https://doi.org/10.1111/j.1365-2958.2012.08112.x

Phaff, H. J., Miller, M. W., & Shifrine, M. (1956). The taxonomy of yeasts isolated from *Drosophila* in the Yosemite region of California. *Antonie van Leeuwenhoek*, *22*(1), 145–161. https://doi.org/10.1007/BF02538322

Potvin, G., Ahmad, A., & Zhang, Z. (2012). Bioprocess engineering aspects of heterologous protein production in *Pichia pastoris*: A review. *Biochemical Engineering Journal*, *64*, 91–105. https://doi.org/10.1016/j.bej.2010.07.017

Prielhofer, R., Barrero, J. J., Steuer, S., Gassler, T., Zahrl, R., Baumann, K., Sauer, M., Mattanovich, D., Gasser, B., & Marx, H. (2017). GoldenPiCS: a Golden Gate-derived modular cloning system for applied synthetic biology in the yeast *Pichia pastoris*. *BMC Systems Biology*, *11*(1), 123. https://doi.org/10.1186/s12918-017-0492-3

Prielhofer, R., Maurer, M., Klein, J., Wenger, J., Kiziak, C., Gasser, B., & Mattanovich, D. (2013). Induction without methanol: Novel regulated promoters enable high-level expression in *Pichia pastoris*. *Microbial Cell Factories*, *12*(1). https://doi.org/10.1186/1475-2859-12-5

Prielhofer, R., Reichinger, M., Wagner, N., Claes, K., Kiziak, C., Gasser, B., & Mattanovich, D. (2018). Superior protein titers in half the fermentation time: Promoter and process engineering for the glucose-regulated *GTH1* promoter of *Pichia pastoris*. *Biotechnology and Bioengineering*, *115*(10), 2479–2488. https://doi.org/10.1002/bit.26800

Pruneski, J. A., Hainer, S. J., Petrov, K. O., & Martens, J. A. (2011). The Paf1 Complex Represses *SER3* Transcription in *Saccharomyces cerevisiae* by Facilitating Intergenic Transcription-Dependent Nucleosome Occupancy of the SER3 Promoter ∇. *Eukaryotic Cell*, *10*(10), 1283–1294. https://doi.org/10.1128/EC.05141-11

Püllmann, P., & Weissenborn, M. J. (2021). Improving the Heterologous Production of Fungal Peroxygenases through an Episomal *Pichia pastoris* Promoter and Signal Peptide Shuffling System. *ACS Synthetic Biology*, *10*(6), 1360–1372. https://doi.org/10.1021/acssynbio.0c00641

Rajak, N., Dey, T., Sharma, Y., Bellad, V., & Rangarajan, P. N. (2024). Unlocking Nature's Toolbox: glutamate-inducible recombinant protein production from the *Komagatella phaffii* PEPCK promoter. *Microbial Cell Factories*, *23*(1). https://doi.org/10.1186/s12934-024-02340-1

Rebnegger, C., Flores-Villegas, M., Kowarz, V., De, S., Pusterla, A., Holm, H., Adelantado, N., Kiziak, C., Mattanovich, D., & Gasser, B. (2024). Knock-out of the major regulator Flo8 in *Komagataella phaffii* results in unique host strain performance for methanol-free recombinant protein production. *New Biotechnology*, *84*, 105–114. https://doi.org/10.1016/j.nbt.2024.10.001

Recombinant Proteins Market (2025, January). Https://Www.Novaoneadvisor.Com/Report/Recombinant-Proteins-Market.

Resina, D. (2004). Expression of a *Rhizopus oryzae* lipase in *Pichia pastoris* under control of the nitrogen source-regulated formaldehyde dehydrogenase promoter.

Journal of Biotechnology, *109*(1–2), 103–113. https://doi.org/10.1016/j.jbiotec.2003.10.029

Resina, D., Maurer, M., Cos, O., Arnau, C., Carnicer, M., Marx, H., Gasser, B., Valero, F., Mattanovich, D., & Ferrer, P. (2009). Engineering of bottlenecks in Rhizopus oryzae lipase production in *Pichia pastoris* using the nitrogen source-regulated *FLD1* promoter. *New Biotechnology*, *25*(6), 396–403. https://doi.org/10.1016/j.nbt.2009.01.008

Rintala, E., Toivari, M., Pitkänen, J.-P., Wiebe, M. G., Ruohonen, L., & Penttilä, M. (2009). Low oxygen levels as a trigger for enhancement of respiratory metabolism in *Saccharomyces cerevisiae*. *BMC Genomics*, *10*(1), 461. https://doi.org/10.1186/1471-2164-10-461

Sahu, U., Krishna Rao, K., & Rangarajan, P. N. (2014). Trm1p, a Zn(II)2Cys6-type transcription factor, is essential for the transcriptional activation of genes of methanol utilization pathway, in *Pichia pastoris*. *Biochemical and Biophysical Research Communications*, *451*(1), 158–164. https://doi.org/10.1016/j.bbrc.2014.07.094

Sassi, H., Delvigne, F., Kar, T., Nicaud, J. M., Coq, A. M. C. Le, Steels, S., & Fickers, P. (2016). Deciphering how *LIP2* and *POX2* promoters can optimally regulate recombinant protein production in the yeast *Yarrowia lipolytica*. *Microbial Cell Factories*, *15*(1), 159. https://doi.org/10.1186/s12934-016-0558-8

Schotte, P., Dewerte, I., Groeve, M., Keyser, S., Brabandere, V., & Stanssens, P. (2016). *Pichia pastoris* Mut^S strains are prone to misincorporation of O-methyl-l-homoserine at methionine residues when methanol is used as the sole carbon source. *Microbial Cell Factories*, *15*(1). https://doi.org/10.1186/s12934-016-0499-2

Shen, Q., Zhou, X. T., Guo, Q., Xue, Y. Z., Xue, Y. P., & Zheng, Y. G. (2022). Potential of the signal peptide derived from the PAS_chr3_0030 gene product for secretory expression of valuable enzymes in *Pichia pastoris*. Applied and Environmental Microbiology, 88(9), e00296-22. https://doi.org/10.1128/aem.00296-22

Shen, W. K., Chen, S. Y., Gan, Z. Q., Zhang, Y. Z., Yue, T., Chen, M. M., ... & Guo, A. Y. (2023). AnimalTFDB 4.0: a comprehensive animal transcription factor database updated with variation and expression annotations. *Nucleic acids research*, *51*(D1), D39-D45. https://doi.org/10.1093/nar/gkac907

Shen, S., Sulter, G., Jeffries, T. W., & Cregg, J. M. (1998). A strong nitrogen source-regulated promoter for controlled expression of foreign genes in the yeast *Pichia pastoris*. *Gene*, *216*(1), 93–102. https://doi.org/10.1016/S0378-1119(98)00315-1

Shen, W., Xue, Y., Liu, Y., Kong, C., Wang, X., Huang, M., Cai, M., Zhou, X., Zhang, Y., & Zhou, M. (2016). A novel methanol-free *Pichia pastoris* system for recombinant protein expression. *Microbial Cell Factories*, *15*(1). https://doi.org/10.1186/s12934-016-0578-4

Singh, A., & Narang, A. (2020). https://doi.org/10.1128/EC.05141-11The Mut+ strain of *Komagataella phaffii* (*Pichia pastoris*) expresses p*AOX1* 5 and 10 times faster than Mut^s and Mut^- strains: evidence that formaldehyde or/and formate are true inducers of p*AOX1*. *Applied Microbiology and Biotechnology*, *104*(18), 7801–7814. https://doi.org/10.1007/s00253-020-10793-8

Singh, A., & Narang, A. (2023). p*AOX1* expression in mixed-substrate continuous cultures of *Komagataella phaffii* (*Pichia pastoris*) is completely determined by methanol consumption regardless of the secondary carbon source. *Frontiers in Bioengineering and Biotechnology*, *11*. https://doi.org/10.3389/fbioe.2023.1123703

Sodhi, A. S., Bhatia, S., & Batra, N. (2024). Laccase: Sustainable production strategies, heterologous expression and potential biotechnological applications. *International Journal of Biological Macromolecules*, *280*, 135745. https://doi.org/10.1016/j.ijbiomac.2024.135745

Spohner, S. C., Müller, H., Quitmann, H., & Czermak, P. (2015). Expression of enzymes for the usage in food and feed industry with *Pichia pastoris*. *Journal of Biotechnology*, *202*, 118–134. https://doi.org/10.1016/j.jbiotec.2015.01.027

Stadlmayr, G., Mecklenbräuker, A., Rothmüller, M., Maurer, M., Sauer, M., Mattanovich, D., & Gasser, B. (2010). Identification and characterisation of novel *Pichia pastoris* promoters for heterologous protein production. *Journal of Biotechnology*, *150*(4), 519–529. https://doi.org/10.1016/j.jbiotec.2010.09.957

Takagi, S., Tsutsumi, N., Terui, Y., Kong, X. Y., Yurimoto, H., & Sakai, Y. (2019). Engineering the expression system for *Komagataella phaffii* (*Pichia pastoris*): an attempt to develop a methanol-free expression system. *FEMS Yeast Research*, *19*(6). https://doi.org/10.1093/femsyr/foz059

Theron, C. W., Berrios, J., Steels, S., Telek, S., Lecler, R., Rodriguez, C., & Fickers, P. (2019). Expression of recombinant enhanced green fluorescent protein provides insight into foreign gene-expression differences between Mut^+ and Mut^S strains of *Pichia pastoris*. *Yeast*, *36*(5), 285–296. https://doi.org/10.1002/yea.3388

Thorpe, E. D., d'Anjou, M. C., & Daugulis, A. J. (1999). Sorbitol as a non-repressing carbon source for fed-batch fermentation of recombinant *Pichia pastoris*. *Biotechnology Letters*, *21*(8), 669–672. https://doi.org/10.1023/A:1005585407601

Toivari, M. H., Salusjärvi, L., Ruohonen, L., & Penttilä, M. (2004). Endogenous xylose pathway in *Saccharomyces cerevisiae*. *Applied and Environmental Microbiology*, *70*(6), 3681–3686. https://doi.org/10.1128/AEM.70.6.3681-3686.2004

Tomàs-Gamisans, M., Andrade, C. C. P., Maresca, F., Monforte, S., Ferrer, P., & Albiol, J. (2020). Redox Engineering by Ectopic Overexpression of NADH Kinase in Recombinant *Pichia pastoris* (*Komagataella phaffii*): Impact on Cell Physiology and Recombinant Production of Secreted Proteins. *Applied and Environmental Microbiology*, *86*(6). https://doi.org/10.1128/AEM.02038-19

Tsien, R. Y. (1998). The green fluorescent protein. Annual review of biochemistry, 67(1), 509-544. https://doi.org/10.1146/annurev.biochem.67.1.509

Tschopp, J. F., Brust, P. F., Cregg, J. M., Stillman, C. A., & Gingeras, T. R. (1987). Expression of the lacZ gene from two methanol-regulated promoters in *Pichia pastoris*. In *Nucleic Acids Research* (Vol. 15). https://academic.oup.com/nar/article/15/9/3859/2382885

Türkanoğlu Özçelik, A., Yılmaz, S., & Inan, M. (2019). *Pichia pastoris* Promoters. In *Methods in Molecular Biology* (Vol. 1923, pp. 97–112). Humana Press Inc. https://doi.org/10.1007/978-1-4939-9024-5_3

Tyurin, O. V., & Kozlov, D. G. (2015). Deletion of the FLD gene in methylotrophic yeasts *Komagataella phaffii* and *Komagataella kurtzmanii* results in enhanced induction of the *AOX1* promoter in response to either methanol or formate. *Microbiology*, *84*(3), 408–411. https://doi.org/10.1134/S0026261715030212

Unver, Y., & Dagci, I. (2024). *Komagataella phaffii* (*Pichia pastoris*) as a Powerful Yeast Expression System for Biologics Production. *Frontiers in Bioscience-Elite*, *16*(2). https://doi.org/10.31083/j.fbe1602019

van der Klei, I. J., Yurimoto, H., Sakai, Y., & Veenhuis, M. (2006). The significance of peroxisomes in methanol metabolism in methylotrophic yeast. In *Biochimica et Biophysica Acta - Molecular Cell Research* (Vol. 1763, Issue 12, pp. 1453–1462). https://doi.org/10.1016/j.bbamcr.2006.07.016

Vanz, A. L., Lünsdorf, H., Adnan, A., Nimtz, M., Gurramkonda, C., Khanna, N., & Rinas, U. (2012). Physiological response of *Pichia pastoris* GS115 to methanol-induced high-level production of the Hepatitis B surface antigen: Catabolic adaptation, stress responses, and autophagic processes. *Microbial Cell Factories*, *11*. https://doi.org/10.1186/1475-2859-11-103

Veenhuis, M., Salomons, F. A., & Van Der Klei, I. J. (2000). Peroxisome biogenesis and degradation in yeast: A structure/function analysis. *Microscopy Research and Technique*, *51*(6), 584–600. https://doi.org/10.1002/1097-0029(20001215)51:6<584::AID-JEMT8>3.0.CO;2-W

Velastegui, E., Quezada, J., Altamirano, C., Berrios, J., & Fickers, P. (2023). Co-feeding strategy alleviates hypoxic stress in large-scale bioreactor for optimal production of secretory recombinant proteins in *Pichia pastoris*. *Journal of Biotechnology*, *373*, 20–23. https://doi.org/10.1016/j.jbiotec.2023.06.006

Velastegui, E., Theron, C., Berrios, J., & Fickers, P. (2019). Downregulation by organic nitrogen of *AOX1* promoter used for controlled expression of foreign genes in the yeast *Pichia pastoris*. *Yeast*, *36*(5), 297–304. https://doi.org/10.1002/yea.3381

Vemuri, G. N., Eiteman, M. A., McEwen, J. E., Olsson, L., & Nielsen, J. (2007). Increasing NADH oxidation reduces overflow metabolism in *Saccharomyces cerevisiae*. *Proceedings of the National Academy of Sciences*, *104*(7), 2402–2407. https://doi.org/10.1073/pnas.0607469104

Vogl, T., & Glieder, A. (2013). Regulation of *Pichia pastoris* promoters and its consequences for protein production. In *New Biotechnology* (Vol. 30, Issue 4, pp. 385–404). https://doi.org/10.1016/j.nbt.2012.11.010

Vogl, T., Kickenweiz, T., Pitzer, J., Sturmberger, L., Weninger, A., Biggs, B. W., Köhler, E. M., Baumschlager, A., Fischer, J. E., Hyden, P., Wagner, M., Baumann, M., Borth, N., Geier, M., Ajikumar, P. K., & Glieder, A. (2018). Engineered bidirectional promoters enable rapid multi-gene co-expression optimization. *Nature Communications*, *9*(1). https://doi.org/10.1038/s41467-018-05915-w

Vogl, T., Ruth, C., Pitzer, J., Kickenweiz, T., & Glieder, A. (2014). Synthetic core promoters for *Pichia pastoris*. *ACS Synthetic Biology*, *3*(3), 188–191. https://doi.org/10.1021/sb400091p

Vogl, T., Sturmberger, L., Kickenweiz, T., Wasmayer, R., Schmid, C., Hatzl, A. M., Gerstmann, M. A., Pitzer, J., Wagner, M., Thallinger, G. G., Geier, M., & Glieder, A. (2016). A Toolbox of Diverse Promoters Related to Methanol Utilization: Functionally Verified Parts for Heterologous Pathway Expression in *Pichia pastoris*. *ACS Synthetic Biology*, *5*(2), 172–186. https://doi.org/10.1021/acssynbio.5b00199

Wang, J., Wang, X., Shi, L., Qi, F., Zhang, P., Zhang, Y., Zhou, X., Song, Z., & Cai, M. (2017). Methanol-Independent Protein Expression by *AOX1* Promoter with trans-Acting Elements Engineering and Glucose-Glycerol-Shift Induction in *Pichia pastoris*. *Scientific Reports*, *7*. https://doi.org/10.1038/srep41850

Wang, J., Wang, X., Shi, L., Zhang, Y., Zhou, X., & Cai, M. (2018). Reduced methanol input induces increased protein output by *AOX1* promoter in a *trans* -acting elements engineered *Pichia pastoris*. *Journal of Industrial Microbiology and Biotechnology*, *45*(1), 25–30. https://doi.org/10.1007/s10295-017-1988-y

Wang, L., Li, Y., Cui, S., Xu, X., Liu, Y., Li, J., ... & Liu, L. (2024). Engineering a transport pathway to boost extracellular production of human lactoferrin in *Komagataella phaffii*. *Food Bioscience*, *59*, 104057. https://doi.org/10.1016/j.fbio.2024.104057

Wang, X., Cai, M., Shi, L., Wang, Q., Zhu, J., Wang, J., Zhou, M., Zhou, X., & Zhang, Y. (2016). PpNrg1 is a transcriptional repressor for glucose and glycerol repression of *AOX1* promoter in methylotrophic yeast *Pichia pastoris*. *Biotechnology Letters*, *38*(2), 291–298. https://doi.org/10.1007/s10529-015-1972-4

Wang, X., Wang, Q., Wang, J., Bai, P., Shi, L., Shen, W., Zhou, M., Zhou, X., Zhang, Y., & Cai, M. (2016). Mit1 transcription factor mediates methanol signaling and regulates the alcohol oxidase 1 (*AOX1*) promoter in *Pichia pastoris*. *Journal of Biological Chemistry*, *291*(12), 6245–6261. https://doi.org/10.1074/jbc.M115.692053

Xu, H., Wang, S., Li, K., Bai, Z., & Yang, Y. (2025). Optimization of Multiple Combinations of Early Secretion Pathways to Enhance Extracellular Protein

Secretion in *Komagataella phaffii*. Journal of Agricultural and Food Chemistry, 73(28), 17750-17758. https://doi.org/10.1021/acs.jafc.5c03402

Yu, S., Miao, L., Huang, H., Li, Y., & Zhu, T. (2020). High-level production of glucose oxidase in *Pichia pastoris*: Effects of Hac1p overexpression on cell physiology and enzyme expression. *Enzyme and Microbial Technology*, *141*, 109671. https://doi.org/10.1016/j.enzmictec.2020.109671

Zavec, D., Gasser, B., & Mattanovich, D. (2020). Characterization of methanol utilization negative *Pichia pastoris* for secreted protein production: New cultivation strategies for current and future applications. *Biotechnology and Bioengineering*, *117*(5), 1394–1405. https://doi.org/10.1002/bit.27303

Zhan, C., Yang, Y., Zhang, Z., Li, X., Liu, X., & Bai, Z. (2017). Transcription factor Mxr1 promotes the expression of Aox1 by repressing glycerol transporter 1 in *Pichia pastoris*. *FEMS Yeast Research*, *17*(4). https://doi.org/10.1093/femsyr/fox015

Zhang, C., Ma, Y., Miao, H., Tang, X., Xu, B., Wu, Q., Mu, Y., & Huang, Z. (2020). Transcriptomic Analysis of *Pichia pastoris* (*Komagataella phaffii*) GS115 During Heterologous Protein Production Using a High-Cell-Density Fed-Batch Cultivation Strategy. *Frontiers in Microbiology*, *11*. https://doi.org/10.3389/fmicb.2020.00463

Zhang, P., Zhang, W., Zhou, X., Bai, P., Cregg, J. M., & Zhang, Y. (2010). Catabolite Repression of Aox in *Pichia pastoris* is dependent on hexose transporter PpHxt1 and pexophagy. *Applied and Environmental Microbiology*, *76*(18), 6108–6118. https://doi.org/10.1128/AEM.00607-10

Zhou, H., Wang, Z., & Qian, J. (2023). Engineering of the hypoxia-induced *Pichia stipitis ADH2* promoter to construct a promoter library for *Pichia pastoris*. *Journal of Biotechnology*, *376*, 24–32. https://doi.org/10.1016/j.jbiotec.2023.09.002

Žitkus, E., Čiplys, E., Žiaunys, M., Sakalauskas, A., & Slibinskas, R. (2025). Development of an efficient expression system for human chaperone BiP in *Pichia pastoris*: production optimization and functional validation. *Microbial Cell Factories*, *24*(1), 66. https://doi.org/10.1186/s12934-025-02679-z

Zou, C., Lu, L., Wang, S., Zhang, C., Chen, X., Lin, Y., & Huang, Y. (2022). The α-mating factor secretion signals and endogenous signal peptides for recombinant protein secretion in Komagataella phaffii. *Biotechnology for biofuels and bioproducts*, *15*(1), 140. https://doi.org/10.1186/s13068-022-02243-6